Constrained Allocation Flux Balance Analysis

Matteo Mori[1,2,3], Terence Hwa[3,4], Olivier C. Martin[5], Andrea De Martino[1,6,7,8‡¶], Enzo Marinari[1,6,9 ‡]

[1] Dipartimento di Fisica, Sapienza Università di Roma, Rome, Italy, [2] Departamento de Bioquímica y Biología Molecular I, Universidad Complutense de Madrid, Madrid, Spain, [3] Department of Physics, University of California at San Diego, La Jolla, California, USA, [4] Institute for Theoretical Studies, ETH Zurich, Switzerland, [5] GQE - Le Moulon, INRA, Univ. Paris-Sud, CNRS, AgroParisTech, Université Paris-Saclay, Gif-sur-Yvette, France, [6] Soft and Living Matter Lab, Istituto di Nanotecnologia (CNR-NANOTEC), Consiglio Nazionale delle Ricerche, Rome, Italy, [7] Center for Life Nano Science@Sapienza, Istituto Italiano di Tecnologia, Rome, Italy, [8] Human Genetics Foundation, Turin, Italy, [9] INFN, Sezione di Roma 1, Rome, Italy

‡Authors contributed equally to this work
¶andrea.demartino@roma1.infn.it

arXiv:1607.00128v1 [q-bio.MN] 1 Jul 2016

Abstract

New experimental results on bacterial growth inspire a novel top-down approach to study cell metabolism, combining mass balance and proteomic constraints to extend and complement Flux Balance Analysis. We introduce here Constrained Allocation Flux Balance Analysis, CAFBA, in which the biosynthetic costs associated to growth are accounted for in an effective way through a single additional genome-wide constraint. Its roots lie in the experimentally observed pattern of proteome allocation for metabolic functions, allowing to bridge regulation and metabolism in a transparent way under the principle of growth-rate maximization. We provide a simple method to solve CAFBA efficiently and propose an "ensemble averaging" procedure to account for unknown protein costs. Applying this approach to modeling *E. coli* metabolism, we find that, as the growth rate increases, CAFBA solutions cross over from respiratory, growth-yield maximizing states (preferred at slow growth) to fermentative states with carbon overflow (preferred at fast growth). In addition, CAFBA allows for quantitatively accurate predictions on the rate of acetate excretion and growth yield based on only 3 parameters determined by empirical growth laws.

Author Summary

The intracellular protein levels of exponentially growing bacteria are known to vary strongly with growth conditions, as described by quantitative "growth laws". This work introduces a computational genome-scale framework (Constrained Allocation Flux Balance Analysis, CAFBA) which incorporates growth laws into canonical Flux Balance Analysis. Upon introducing 3 parameters based on established growth laws for *E. coli*, CAFBA accurately reproduces empirical results on the growth-rate dependent rate of carbon overflow and growth yield, and generates testable predictions about cellular energetic strategies and protein expression levels. CAFBA therefore provides a simple, quantitative approach to balancing the trade-off between growth and its associated biosynthetic costs at genome-scale, without the burden of tuning many inaccessible parameters.

Introduction

The coupling between the physiology of cell growth and cellular composition has been actively investigated since the 1940s. In exponentially growing bacteria, whose growth state is conveniently associated to a single parameter, namely their growth rate, such interdependence is best expressed in a quantitative way by the bacterial 'growth laws' that directly relate the protein, DNA and RNA content of a cell to the growth rate. Many such laws have been experimentally characterized [1–4] and many more are currently being probed at increasingly high resolution [5, 6]. The emerging scenario suggests that proteome organization in bacteria is actively regulated in response to the growth conditions. Recent experiments have in particular provided validation to the picture according to which, as the growth rate changes, bacteria adjust the relative amounts of ribosome-affiliated, nutrient scavenging and metabolic proteins (enzymes), so as to optimize their growth

performance and energy production strategy [6–8]. At present, several phenomenological models explain the origin of different growth laws at a coarse-grained level [5, 7]. In contrast, genome-scale approaches probing such relationships at molecular levels are less developed.

Constraint-based models (CBMs) are powerful in silico tools that can be used to examine metabolic networks at genome scale. Starting from a non-equilibrium steady state assumption for metabolic fluxes, CBMs define the space of feasible reaction profiles through simple physico-chemical constraints like mass-balance. Once physiologically or thermodynamically motivated bounds of variability are assigned to fluxes, the solution space is essentially determined by the stoichiometry of the network alone. On the other hand, in genome-scale models stoichiometric constraints usually generate high-dimensional solution spaces in which physiologically relevant flux patterns may be hard to isolate. In many cases, optimal flux patterns can be defined through the maximization of specific objective functions. Flux Balance Analysis (FBA) [9–15] allows for instance to compute optimal flux configurations by means of linear programming (LP), employing biomass production as a standard objective function [16]. This approach is widely used to describe microbial growth in lab conditions.

It is clear that in order to capture the phenomenology of growth laws one needs to go beyond the basic elements of CBMs, and incorporate the costs associated with gene expression and protein synthesis into models of cellular metabolism. Resource Balance Analysis (RBA) [17, 18] and ME-models [19, 20] have taken important steps in this direction. These approaches propose a data-based optimization scheme to predict the growth-maximizing metabolic flux configurations under a variety of constraints, including stoichiometric mass-balance, 'demand functions' characterizing how the amounts of cellular components change with the growth rate, and specific prescriptions that relate fluxes to enzyme levels. The resulting schemes are more involved than FBA (resulting in nonlinear optimization problems) and require a large number of parameters. It is therefore important to devise a theoretical framework with the conceptual appeal and computational simplicity of FBA, in particular one that is more resilient to the choice of parameters and in which the interplay between metabolism and regulation is expressed through a more intuitive and transparent framework.

In this work we present a generalized FBA scheme, called Constrained Allocation FBA or CAFBA, in which (optimal) regulation is accounted for effectively through a single additional global constraint on fluxes that encodes for the relative adjustment of proteome sectors at different growth rates. In a nutshell, the CAFBA-specific constraint describes the tug-of-war in the allocation of cellular resources across ribosomal, transport and biosynthetic proteins that has been observed in experiments. By imposing that the ribosomal share of the proteome behaves in accordance with empirically established growth laws [5, 21, 22], CAFBA is able to reproduce observed behaviors without requiring parameter tuning. In addition, CAFBA generates a variety of testable predictions, including about the usage of metabolic pathways, despite lacking the level of biochemical detail that characterizes ME-models or RBA.

Cellular strategies for energy production are the central focus of CAFBA. It is well known that fast-growing microorganisms tend to avoid using high-yield respiratory pathways to generate ATP even in the presence of oxygen, relying instead on aerobic fermentation [23–28]. The preference for low-yield pathways is manifested in the secretion of fermentation products like acetate for *E. coli* or ethanol for *S. cerevisiæ* [23, 25, 26, 29]. This phenomenon, known as 'overflow metabolism', is captured by standard FBA schemes at a qualitative level when additional capacity constraints on respiratory pathways [30] or density constraints for soluble [31, 32] or membrane-bound [33] enzymes are included. However, certain quantitative aspects of potential interest for industrial applications, like the rate of metabolic overflow and the growth rate at which it occurs, have so far eluded comprehensive mechanistic models. By effectively modeling the trade-off between growth and its biosynthetic costs, CAFBA naturally produces cellular states with suboptimal growth yields, where carbon overflow is obtained with quantitative accuracy.

This paper focuses on the scenario obtained by CAFBA for carbon-limited growth of *E. coli*. We find in particular that acetate secretion appears in *E. coli* at fast growth rates, whereas yield-maximizing FBA-like solutions dominate at slow growth rates. In spite of the nominal need for a large number of uncharacterized parameters in genome-wide models, CAFBA solutions remarkably depend only on a few global parameters. In particular, overflow metabolism is obtained consistently with quantitative accuracy, while all results are robust against 10-fold changes in the values of the enzymatic efficiency parameters. From a technical viewpoint, CAFBA effectively turns out to be an LP problem even when one accounts for growth-rate dependent biomass composition. This, together with its simple conceptual framework, makes CAFBA a very convenient scheme to analyze the interplay of metabolism and gene expression at genome scale.

Model

Proteome sectors

Phenomenological studies of bacterial growth physiology suggest that the bacterial proteome is organized into "sectors" whose mass fractions adjust linearly with the growth rate in response to specific environmental and intracellular changes, including carbon limitation, anabolic limitation and translational inhibition [5, 6, 8]. Proteome organization and optimal growth constitute in essence an intertwined allocation problem, with the cell trying to optimally partition its proteome so as to maximize its growth performance. Based on empirical evidence on *E. coli* growth in carbon-limited media, CAFBA posits a 4-sector partitioning of the proteome in

- ribosome-affiliated proteins (R-sector);
- biosynthetic enzymes (E-sector);
- proteins devoted to carbon intake and transport (C-sector);
- core housekeeping proteins whose expression level is independent of the growth rate (Q-sector).

The corresponding proteome fractions (denoted by ϕ_X for the X-sector) should sum up to 1, i.e.

$$\phi_C + \phi_E + \phi_R + \phi_Q = 1 \quad . \tag{1}$$

We shall now provide an explicit characterization of the different terms in the above sum.

The ribosomal sector. ϕ_R is experimentally found to be linearly dependent on the growth rate λ when growth is nutrient-limited [3–5], namely

$$\phi_R = \phi_{R,0} + w_R \lambda \quad , \tag{2}$$

where $\phi_{R,0}$ is a strain-dependent constant representing the extrapolated ribosomal proteome fraction at zero growth rate, and w_R is a strain-independent constant related to the ribosome's translational efficiency [5, 6]. Phenomenologically, w_R describes the proteome fraction allocated to ribosomal proteins per unit of growth rate. At the molecular level, the linear relation (2) is enforced by a regulatory mechanism involving the alarmone ppGpp [34–37]. When focusing on carbon-limited growth, one can set w_R equal to the empirical value $w_{R,0} \simeq 0.169$ h [5]. The effects of translational inhibition can instead be studied by increasing w_R from the value $w_{R,0}$, so as to model the increasingly slowed-down translation induced by antibiotics [22]. As will soon become clear, the value of the offset $\phi_{R,0}$ is immaterial for the formulation of CAFBA.

The carbon catabolic sector. We focus on balanced growth in a minimal medium containing a single carbon source (e.g. glucose). Based on experimental findings [6, 8], we assume that ϕ_C depends linearly on the carbon intake flux v_C, i.e.

$$\phi_C = \phi_{C,0} + w_C v_C \quad , \tag{3}$$

where, by analogy with (2), $\phi_{C,0}$ is a λ-independent offset and w_C characterizes the proteome fraction allocated to the C-sector per unit of carbon influx. Recent proteomic studies [8, 38] suggest that the C-sector should include not only the specific transport system taking up the sugar, but also other proteins that are co-expressed in response to carbon limitation through mediation by the pleiotropic regulator cAMP-Crp [6], like intake proteins for other nutrients, motility proteins, etc. Therefore, (3) should be seen as an effective prescription accounting for the fact that several types of proteins intended for nutrient scavenging and intake are co-expressed in carbon limitation. All of these should be expected to contribute to ϕ_C, even if certain proteins, like motility proteins, may not be required for growth in laboratory conditions. The offset $\phi_{C,0}$ thus represents a basal level of proteins not due to carbon intake only.

In order to better characterize w_C (i.e. the carbon-intake dependent part of ϕ_C), we assume that the carbon influx v_C at a given extracellular sugar level $[g]$ is described by a Michaelis-Menten kinetics of the form

$$v_C = \frac{V}{M_{\rm DW}} k_{{\rm cat},g} [E_g] \frac{[g]}{[g] + K_{M,g}} \quad , \tag{4}$$

where $[E_g]$ stands for the level of the intake protein(s) specific to g that are not in $\phi_{C,0}$, $k_{{\rm cat},g}$ and $K_{M,g}$ are kinetic constants, and V and $M_{\rm DW}$ represent the cell volume and dry weight, respectively. (The ratio

$V/M_{\rm DW}$ is introduced so that the flux units are mmol/$g_{\rm DW}$h.) Denoting the total protein mass by M_{TP} and the enzyme's molecular weight by μ_g, and letting α_g be the mass fraction of enzyme E_g in the C-sector, we can express $[E_g]$ in terms of the C-sector's proteome fraction ϕ_C as $[E_g] = (\phi_C - \phi_{C,0})\alpha_g M_{TP}/(\mu_g V)$. In turn, (4) can be rewritten as

$$v_C = \kappa_{{\rm cat},g}(\phi_C - \phi_{C,0})\frac{[g]}{[g] + K_{M,g}} \quad , \tag{5}$$

where $\kappa_{{\rm cat},g} \equiv \alpha_g(k_{{\rm cat},g}/\mu_g)(M_{TP}/M_{\rm DW})$. The factor $M_{TP}/M_{\rm DW} \simeq 60\%$ is roughly constant for a wide range of growth rates [39, 40], $k_{{\rm cat},g}/\mu_g$ is instead an enzyme-specific property, while the proportion α_g is determined genetically by the expression level of the enzyme E_g relative to those of the other co-expressed C-sector proteins. Comparing (5) to (3), one sees that w_C can be represented as

$$w_C = w_{C,0}\left(1 + \frac{K_{M,g}}{[g]}\right) \quad , \tag{6}$$

with $w_{C,0} \equiv 1/\kappa_{{\rm cat},g}$.

The above analysis suggests that w_C can be conveniently used to control the carbon influx: it takes on a sugar-specific value $w_{C,0}$ at saturating sugar concentrations (i.e. for $[g] \gg K_{M,g}$) and the effect of reducing extracellular sugar levels can be modeled by simply increasing its value. Hence, as a proxy of varying the abundance of the carbon source, we will simply dial w_C. The importance of using w_C as control parameter, as opposed to varying the maximum nutrient intake capacity, is discussed in Note B in the Supporting Text. Note that the maximal growth rate achievable in the medium we consider (referred to as $\lambda_{\rm max}$ below, and obtained for $w_C = 0$ or, equivalently, $w_{C,0} = 0$) is experimentally determined by the extrapolated growth rate at which C-sector protein expression vanishes [6, 41].

The biosynthesis sector. The flux through enzymatic reactions involved in biosynthesis (E-sector) can be generally written in the form

$$v_i = \frac{V}{M_{\rm DW}} k_{{\rm cat},i}[E_i]\, f_i([s_i], [p_i]) \quad , \tag{7}$$

where $[E_i]$ denotes the concentration of enzyme i and we considered explicitly an additional dependence on the concentrations of the substrates ($[s_i]$) and products ($[p_i]$) through the function f_i. For an elementary irreversible reaction with a single substrate and a single product, f_i is a Michaelis-Menten function of $[s_i]$, while for reactions close to thermodynamic equilibrium $f_i \simeq [s_i] - [p_i]/K_{\rm eq}$ [42]. In full analogy with the previous case, we can express $[E_i]$ in terms of the proteome fraction ϕ_i of enzyme E_i as $[E_i] = \phi_i M_{TP}/(\mu_i V)$. Defining $\kappa_{\rm cat} \equiv (k_{{\rm cat},i}/\mu_i)(M_{TP}/M_{\rm DW})$, we then have

$$v_i = \kappa_{\rm cat}\phi_i\, f_i([s_i], [p_i]) \quad . \tag{8}$$

Motivated by the observed linear dependence between enzyme abundance and growth rate in carbon-limited growth [6, 8] and assuming the generic linear dependence between biosynthetic flux and growth rate, we set

$$\phi_i = \phi_{i,0} + w_i|v_i| \quad , \tag{9}$$

with a fixed offset $\phi_{i,0}$. The "weight" w_i represents the proteome fraction to be invested in enzyme E_i per unit flux of reaction i. The absolute value instead reflects the fact that, for a reversible process, a protein cost has to be faced independently of the net direction. Note that, in principle, the values of the weights w_i can be determined experimentally by fitting, for each reaction, proteomic and flux measurements at different growth rates to (9).

The linear relation (9) can be directly obtained from (8) assuming that reaction i is irreversible and that the enzyme E_i is operating in the saturated regime. In this case, $\phi_{i,0} = 0$ and $w_i = 1/\kappa_{{\rm cat},i}$. However, such reactions would be incapable of balancing flux in the event of transient changes, leading to the accumulation of intermediate metabolites. Therefore, most intracellular reactions in physiological conditions should not be expected to operate in the saturated regime. Reactions carrying a flux proportional to the substrate level (as in flux sensors [5, 43] and charged tRNAs [35]) can again be described by (9), albeit with an offset $\phi_{i,0}$; see Note A in the Supporting Text. In this view, the offset $\phi_{i,0}$ provides a mathematically simple way to capture the fact that, at slow growth, the flux approaches zero due to adjustments in metabolite pools while enzyme levels remain finite. As for the other sectors, the values of these offsets play no role in CAFBA (see below).

Summing up the contributions of each reaction, the proteome fraction of the E-sector $\phi_E \equiv \sum_i \phi_i$ can be written as

$$\phi_E = \phi_{E,0} + \sum_i w_i |v_i| \quad , \tag{10}$$

where the sum runs over all enzyme-catalyzed reactions and $\phi_{E,0} \equiv \sum_i \phi_{i,0}$ contributes to a core, λ-independent proteome fraction for baseline expression levels [6, 8].

Proteome-wide constraint

Putting the different terms together, the sum rule (1) for proteome fractions can be recast as

$$w_C v_C + \sum_i w_i |v_i| + w_R \lambda = \phi_{\max} \quad , \tag{11}$$

where $\phi_{\max} = 1 - \phi_Q - \phi_{C,0} - \phi_{E,0} - \phi_{R,0}$ denotes the proteome fraction accessible to growth-rate dependent components of the protein sectors, which was estimated to be of the order of 50% for *E. coli* [5]. The linear constraint (11) encodes for the tug-of-war that ultimately determines optimal growth and proteome allocation, as depicted in Fig 1A: as λ increases, so does the proteome fraction of the R-sector, and the E- and C-sectors will concomitantly have to adjust their shares so as to satisfy (11), forcing in turn a remodeling of the underlying flux and nutrient intake patterns.

Formally, the proteome allocation constraint (11) resembles the molecular crowding constraint defined in [31, 32], which essentially enforces a global upper bound on fluxes due to finite solvent capacity and was also adopted in RBA [17, 18]. However, the intracellular density is empirically known to be (roughly) constant across different growth conditions [44], suggesting that cells can adapt their volume to accommodate additional metabolites and macromolecules when necessary. In this respect, a hard constraint on solvent capacity is not fully justified. The CAFBA constraint (1) is instead derived from the normalization of protein fractions, due ultimately to the limited translational capacity of the ribosomes [5]. Note that the growth rate λ is explicitly involved in (11).

Constrained allocation FBA

Summing up, CAFBA is defined by the following optimization problem:

$$\begin{aligned} \max_{\mathbf{v}} \lambda \quad \text{subject to} \quad & \text{(i)} \quad \sum_i S_{\mu i} v_i = 0 \quad \forall \mu \\ & \text{(ii)} \quad \ell_i \le v_i \le u_i \quad \forall i \\ & \text{(iii)} \quad w_C v_C + \sum_i w_i |v_i| + w_R \lambda = \phi_{\max} \end{aligned} \tag{12}$$

where $S_{\mu i}$ stands for elements of the metabolic network's stoichiometric matrix (with μ indexing metabolites and i indexing reactions), ℓ_i and u_i denote lower and upper bounds for the flux v_i, while the value of λ is defined by the flux of the biomass reaction [16].

Results

We have studied CAFBA solutions for the *E. coli* iJR904 GSM/GPR reconstruction [45] assuming growth limited by a single carbon source (glucose). (See Note C in the Supporting Text for details about CAFBA in different growth-limiting conditions.) We started from the case of λ-independent biomass composition, in which CAFBA can be solved exactly by LP (see Materials and Methods), and then considered the more general case of growth-rate dependent biomass. Throughout this study, we set the parameters w_R and $\phi_{\max}$ to the values $w_{R,0} = 0.169$ h and $\phi_{\max} = 48.4\%$ found empirically for *E. coli* K-12 MG1655 [5]. A nearly identical $w_{R,0}$ and a slightly smaller $\phi_{\max}$ have been reported in [6, 29] for *E. coli* K-12 strain (NCM3722). (The values of $w_{R,0}$ and $\phi_{\max}$ need not be fine-tuned. In fact, variations in one of these parameters can be compensated by rescaling the weights of reactions in the E-sector. The dependence of the fluxes on $w_{R,0}$ and $\phi_{\max}$ is described in detail in Note D in the Supporting Text.) Carbon limitation is enforced by increasing the value of w_C from its minimum $w_{C,0}$, corresponding to saturating glucose concentrations. (Likewise, translational limitation can be studied by increasing the value of w_R from its minimum, $w_{R,0}$ [22].) For each choice of w_C and w_R (and of the set of w_i's), we solve (12) for the fluxes v_i that maximize the growth rate λ.

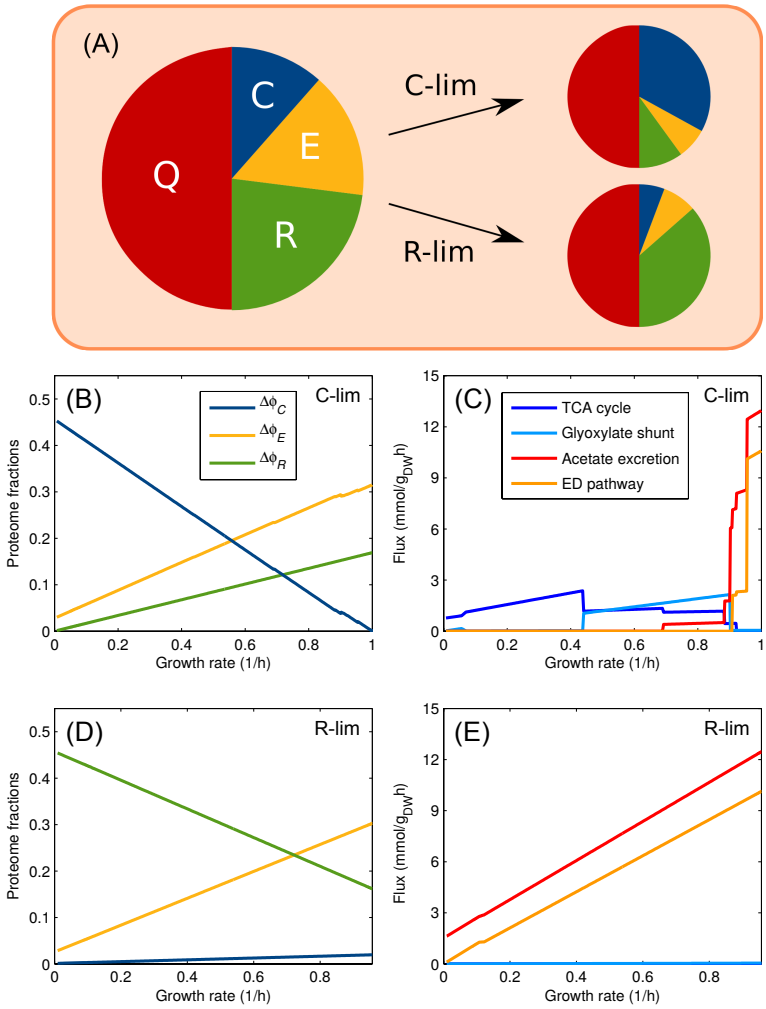

Figure 1. CAFBA solutions for *E. coli* in the homogeneous case for carbon limitation and translational limitation. (A) Proteome organization in CAFBA: R-sector of ribosome-affiliated proteins (growth rate dependent), E-sector of "enzymes" (flux-dependent), C-sector of catabolic proteins (dependent on the carbon influx), and a fixed Q-sector of "housekeeping" proteins. The fractions in these four sectors sum up to one. C-, E- and R- sectors adjust their size depending on the environmental conditions, while the Q-sector accounts for roughly 50% of the proteome. We model the three growth-dependent sectors as a constant plus a variable part, i.e. $\phi_X = \phi_{X,0} + \Delta\phi_X$ with $X \in \{C, E, R\}$. $\Delta\phi_C = w_c v_C$ is proportional to the carbon intake flux; $\Delta\phi_E = \sum_i w_i|v_i|$ is a weighted sum of non-catabolic fluxes; $\Delta\phi_R = w_R\lambda$ is proportional to the growth rate λ. (B) Growth rate-dependent parts of proteome sectors plotted versus λ in carbon limitation (C-lim). As the external glucose concentration is reduced, more catabolic proteins are needed per unit of carbon influx. The cell allocates a larger share to C-proteins, while reducing the E- and R-sector shares. (C) CAFBA fluxes as a function of λ, obtained by varying the degree of carbon (glucose) limitation (C-lim). A transition from fermentation to respiration appears when growth rate is in the range 0.7–0.9/h. The Embden-Doudoroff pathway and the glyoxylate shunt are both operated at high growth rates. (D) The λ-dependent parts of the proteome sectors plotted against growth rate in translational limitation (R-lim). This is obtained by keeping w_C constant while increasing w_R, thereby simulating increasing levels of translation-inhibiting antibiotics. The cell allocates more proteins to the ribosomal sector while reducing the proteome share devoted to carbon metabolism and biosynthesis. (E) CAFBA fluxes as a function of λ obtained in R-limitation for increasing values of w_R, at constant w_C. Acetate is secreted at low growth rates if the extracellular carbon level is large enough. Fluxes through the TCA cycle, the glyoxylate shunt and the Entner-Doudoroff pathway are represented by αKG dehydrogenase, malate synthase and 6-phosphogluconate dehydratase fluxes, respectively. In panels B and C, corresponding to C-limitation, w_R was set to $w_{R,0} = 0.169$ h, while R-limitation (panels D and E) was obtained using $w_C = 1.4 \times 10^{-3}$ gh/mmol, corresponding to a carbon source with high nutritional capacity. In both cases we set all weights in the E-sector to $w_E = 8.3 \times 10^{-4}$ gh/mmol and $\phi_{\max} = 48.4\%$.

As said above, the weights w_i could in principle be determined by combining proteomic studies [8,37,46] with direct flux measurements taken in the appropriate growth conditions. However, the coverage by mass spectroscopy is still limited, and the accuracy of protein abundance is often no better than 2-fold. Much better estimates of protein abundances have been obtained recently using ribosome profiling [47], which also provides a near complete coverage of *E. coli* proteins. This method is however much less versatile compared to proteomics and only a few conditions have been probed so far. Given the lack of reliable empirical estimates, we have focused on two limiting situations allowing us to characterize intrinsic properties of CAFBA for *E. coli* in the most transparent manner.

- The homogeneous case: here, w_i's are uniformly set to the same value, denoted by w_E, for each reaction i. w_E is chosen so that the fastest growth rate achievable $\lambda_{\max}$, corresponding to $w_C = 0$, matches the corresponding empirical value.

- The heterogeneous case: here, w_i's are taken at random, to reflect one's lack of knowledge of their specific value. More precisely, w_i is drawn from a prescribed probability distribution independently for each reaction i. The mean value $\langle w \rangle$ of the distribution essentially plays the role played by w_E in the homogeneous case, in that it sets the average growth rate obtained for $w_C = 0$ to $\lambda_{\max}$. Clearly, the quantitative details of CAFBA solutions will depend on the specific values taken by the w_i's. However, as there is no reason to concentrate on a single set of weights, we will focus our analysis on two aspects, namely (i) the "average" behaviour obtained by averaging solutions over different realizations of the w_i's, and (ii) the fluctuations of solutions around this average.

Homogeneous weights and patterns of flux

We set w_E so that the extrapolated maximal growth rate in unlimited carbon supply, corresponding to $w_C = 0$, is close to the value $1.1 - 1.2$/h found in [6, 41]. In the case of glucose as the sole carbon source, as well as for a number of other glycolytic carbon sources (see Table A in the Supporting Text), the value $w_E = 8.3 \times 10^{-4}$ gh/mmol turned out to yield $\lambda_{\max} = 1$/h. (Slightly larger growth rates are obtained with phosphorylated carbon sources due to the fact that the extra energy carried by these carbon sources allow for a reduced flux in the E-sector.) To capture the effects of changing the glucose level, we simply increased the value of w_C from zero. For the sakes of completeness, the values of w_C leading to empirically observed growth rates for *E. coli* growth on different carbon sources are reported in Table B in the Supporting Text.

Fig 1 reports results obtained for growth on glucose with this choice of parameters, while results for growth on other carbon sources are shown in Fig A in the Supporting Text. One sees in Fig 1B that the growth-dependent fraction of C-proteins ($\Delta\phi_C$, blue line) increases almost linearly with decreasing λ as the carbon concentration is limited, in line with the experimentally observed expressions of catabolic proteins [6, 8] and PTS activity [20]. Both the proteome fractions of the E- and R-sectors ($\Delta\phi_E$ and $\Delta\phi_R$, yellow and green lines, respectively) instead decrease linearly with growth rate. CAFBA therefore confirms the findings from a coarse grained model of proteome allocation [7]: in the optimal state, the cell invests more and more of its proteomic resources in intake systems as nutrient becomes limiting, while translational machinery and biosynthetic pathways are favored at high growth rates.

Fig 1C displays the main fluxes of central carbon metabolism. The rate of acetate secretion and the flux through the Entner-Doudoroff pathway (red and orange colors, respectively) both drop fast as the growth rate decreases. Respiration, represented by the flux through the TCA cycle (blue color) is the predominant energy-producing pathway at small growth rates, while at high growth rates fermentation is preferred and acetate is secreted. Note that the acetate onset point is within 10% of the one observed experimentally for NCM3722 [29] roughly independently of the specific carbon source (see Fig A in the Supporting Text) – a remarkable result given the simplicity of the homogeneity assumption for the w_i's.

Translational limitation [5] is modeled by increasing w_R from the value of $w_{R,0}$ while keeping all other parameters fixed, including w_C. In this case (see Fig 1D), the ribosomal proteome fraction ($\Delta\phi_R$) increases as translation is increasingly inhibited, while the other growth-dependent sectors ($\Delta\phi_C$ and $\Delta\phi_E$) shrink almost linearly. Acetate secretion extends to the slowest growth rates in accordance with experimental findings [29], while the respiratory flux (see Fig 1E) is negligible.

It is interesting to compare CAFBA results with the phenomenological proteome allocation model introduced in [5], which describes how proteome is allocated in different environments. There, the growth rate was predicted to be a Michaelis-Menten function of the "nutritional capacity" κ_n and "translation capacity" κ_t, independent phenomenological parameters that can be estimated from empirical growth laws. CAFBA

recovers this result within a genome-scale model, with $1/w_C$ playing the role of κ_n and $1/w_R$ acting as κ_t (see Fig B in the Supporting Text and Note D in the Supporting Text for a detailed discussion).

It transpires from Fig 1C and Fig A in the Supporting Text that the optimal flux configurations in carbon limitation vary discontinuously with the growth rate. This is due to the fact that the control parameter is not a flux (as in standard FBA), but, rather, the weight of the C-sector w_C, which, as discussed above, is a proxy for either the external carbon concentration or the amount of glucose intake proteins [6]. Even though w_C is varied continuously, growth-rate maximization can induce large rearrangements of the active pathways in response to small changes of the control parameter. This behavior is ultimately a mathematical feature due to the way in which the optimal solution in constraint-based models like CAFBA changes as one modifies w_C.

Heterogeneous weights and patterns of average flux

For the heterogeneous case, for each value of w_C we generated 1000 models, each with a random set of weights w_i independently drawn from the same probability density

$$p(w) \propto 1/w \quad , \quad w_{\min} \leq w \leq w_{\max} \quad , \tag{13}$$

which corresponds to a uniform density for the logarithm of w. $p(w)$ is fully determined by its average $\langle w \rangle$ and width $\delta \equiv \log_{10}(w_{\max}/w_{\min})$. We set $\langle w \rangle$ so that the average value of the maximum achievable growth rate $\lambda_{\max}$ (obtained for $w_{C,0} = 0$) equals 1/h. This fixes $\langle w \rangle = 8.8 \times 10^{-4}$ gh/mmol, a value that is remarkably close to $w_E = 8.3 \times 10^{-4}$ gh/mmol as determined in the homogeneous case. δ was instead fixed to 1, implying that the weights are assumed to span one order of magnitude (results obtained for different values of δ are discussed in Note E in the Supporting Text).

Each set of weights $\{w_i\}$ leads to a corresponding optimal flux pattern, growth rate, acetate secretion rate, etc. The distribution of growth rates obtained from many realizations of the weights is shown in Fig 2A. Note that in spite of the 10-fold variability of the weights, the growth rate remains within a modest range of $\pm 20\%$. The distribution for acetate secretion rates is instead conveyed in Fig 2B: it is rather heterogeneous, with a marked peak for phenotypes with very low acetate secretion. While individual fluxes can fluctuate significantly across solutions, average fluxes are strikingly well-behaved. This phenomenon is illustrated in Fig 2C where we show a set of average fluxes plotted against the average growth rate. The average acetate secretion rate (red symbols) has an approximate linear dependence on the growth rate starting from $\lambda_{\rm ac} \simeq 0.79$/h. Average fluxes through TCA and the glyoxylate shunt (blue up- and down- triangles) reach their respective maxima close to $\lambda_{\rm ac}$. Notice that a smooth transition from a predominantly fermentative to a predominantly respiratory mode of energy production clearly emerges, in full agreement with empirical evidence. It is especially remarkable that this scenario does not seem to depend on the specific choice of $p(w)$. For instance, a log-normal distribution gives qualitatively similar results (see Fig C in the Supporting Text).

Despite the crude approximations, CAFBA solutions appear to reproduce experimental findings with surprising accuracy. Fig 3A shows how the average acetate excretion rate compares with data from different experiments [29, 48–51]. Secretion rates from experiments using the MG1655 strain are consistent among each other (open triangles), as are results obtained with the NCM3722 and ML308 strains (open circles). CAFBA predictions are shown as solid circles for the two classes of strains. Data obtained with NCM3722 and ML308 were compared with CAFBA solutions obtained by setting $\lambda_{\max} = 1$/h and hence $\langle w \rangle = 8.8 \times 10^{-4}$ gh/mmol. Instead, based on experimental evidence suggesting that MG1655 cells grow about 1/3 slower than the other two strains (see Fig D in the Supporting Text), for MG1655 we set $\lambda_{\max} = 0.67$/h, leading to $\langle w \rangle = 1.55 \times 10^{-3}$ gh/mmol. With this choice, CAFBA quantitatively reproduces the growth-rate dependence of acetate secretion. Growth yields, instead, are less consistent across different experiments and/or strains, see Fig 3B. Without any further parameter tuning, CAFBA solutions capture the growth yields for NCM3722 and MG1655 at a quantitative level, although they fail for ML308. It should be noted that the differences in yield among experiments done on the same strain (MG1655) suggest that other factors beyond the scope of this simple model might be at play, such as differences in growth conditions and/or maintenance requirements.

We have also analyzed how the flux patterns of various intracellular pathways are modulated by the growth rate. Results for the central carbon pathways are summarized in Fig E in the Supporting Text, with the fluxes through the TCA cycle and glyoxylate shunt consistently increasing in proportion as glucose is limited. A similar behavior has been observed in measured expression levels of the corresponding enzymes [8, 51]. Glycolytic fluxes are heterogeneously regulated, due to the interplay between the EMP pathway, the ED pathway and the switch between glyoxylate shunt and the phosphoenolpyruvate carboxylase (PPC) reaction. The redox balance of the cell appears to be affected, as described in Fig F in the Supporting

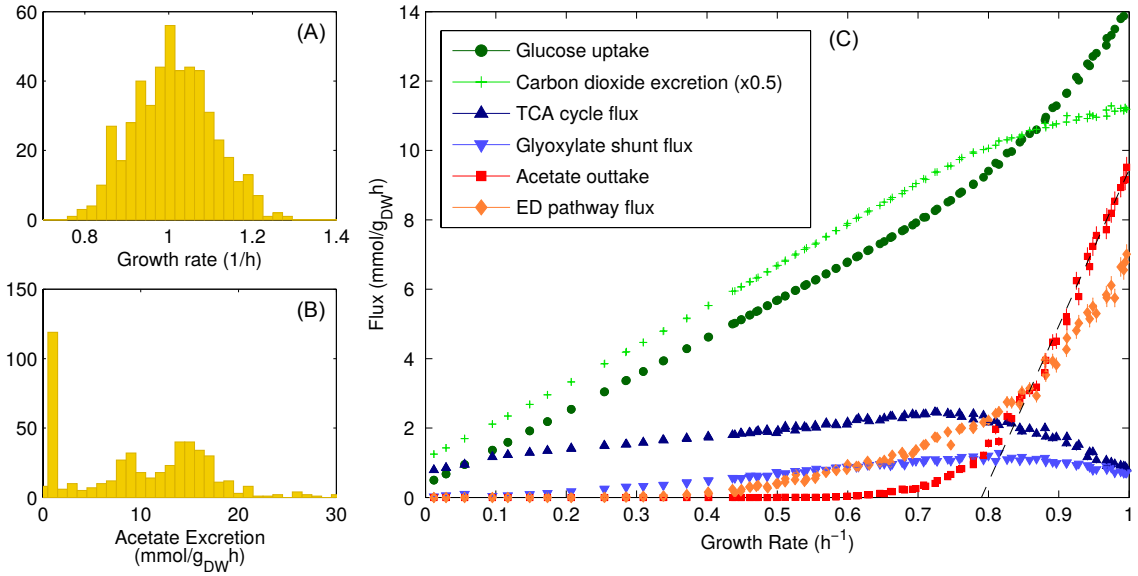

Figure 2. CAFBA solutions for *E. coli* in the heterogeneous case in carbon limitation. Fluxes in glucose minimal medium computed at fixed $w_C \geq 0$ for different realizations of the E-sector weights, using $\langle w \rangle = 8.8 \times 10^{-4}$ gh/mmol and $w_{\max}/w_{\min} = 10$ ($\delta = 1$). (A) Histogram of the growth rates obtained from 1000 CAFBA solutions obtained using different randomly drawn weights for reactions in the E-sector and $w_C = 0$. λ peaks around $\lambda_{\max} = 1$/h. (B) Histogram of the acetate secretion rates in the same conditions. Two classes of solutions are clearly visible, with roughly 25% of states excreting less than 0.5 mmol/g_{DW}h of acetate. The average secretion flux is close to 10 mmol/g_{DW}h. (C) Average fluxes (glucose intake, carbon excretion, TCA, glyoxylate shunt, acetate excretion and ED pathway) versus the average growth rate. Each point represents the average of 1000 CAFBA solutions obtained with the same w_C and different realizations of the weights of reactions in the E-sector. Both x and y error bars are shown. Different points are obtained by using different w_C values. Acetate secretion is approximately linear at large values of λ. A line $v_{\rm ac} = s \times (\lambda - \lambda_{\rm ac})$ with $s = 45$ mmol/g_{DW} and $\lambda_{\rm ac} = 0.79$/h is shown for comparison.

Text. Indeed we find that NADP transhydrogenase switches on at high growth rates, oxidizing NADH and reducing $NADP^+$, in agreement with the different roles of the two transhydrogenases, UdhA and PntA, as quantified by transcription data [52]. Moreover we observe a switch between two separate ubiquinol oxidase reactions, characterized by different abilities to generate proton-motive force, in agreement with studies focused on the crowding of the cell's membrane [33].

Patterns of average flux for different carbon sources

We further tested CAFBA's ability to describe *E. coli* growth on carbon sources other than glucose. For illustration purposes, for each carbon source studied we have varied w_C from zero to high values, so as to produce result in the entire range of growth rates $0 \leq \lambda \leq \lambda_{\max}$, even though growth rates measured on individual carbon sources are always smaller than $\lambda_{\max}$ due to non-zero values of $w_{C,0}$ (see Table B in the Supporting Text).

The typical behaviour of CAFBA solutions with different glycolytic carbon sources is remarkably consistent (see Fig 4). For each of the nutrients we tested, as the carbon supply becomes limiting, acetate excretion (Fig 4A) decreases almost linearly with growth rate, extrapolating to zero roughly at $\lambda_{\rm ac} \simeq 0.79$/h (continuous black line). By contrast, fluxes through TCA and glyoxylate shunt (Fig 4B and 4C) rise linearly with decreasing growth rate at fast growth, reaching a maximum close to $\lambda_{\rm ac}$ before decreasing at slower growth. The secretion rate of CO_2 (Fig 4D) almost always diminishes as λ is reduced. For $\lambda < \lambda_{\rm ac}$ the decrease is linear, while it is non-linear for $\lambda > \lambda_{\rm ac}$. Altogether, for all carbon sources, results point to two distinct types of behaviors arising, respectively, below and above $\lambda_{\rm ac}$.

The Entner-Doudoroff (ED) pathway, an alternative to the Embden-Meyerhoff-Parnass (EMP) pathway, is used in *E. coli* for glucose catabolism at high growth rates [53, 54]. CAFBA solutions reproduce this feature, relying on the ED pathway from medium ($\lambda \simeq 0.3$/h) to high growth rates as shown in Fig 4E.

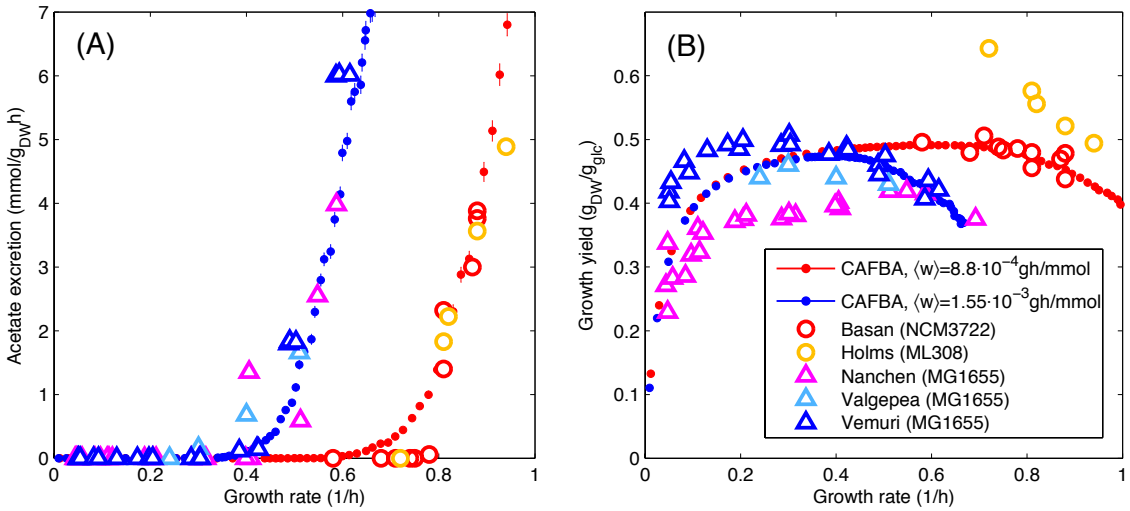

Figure 3. Comparison between CAFBA predictions and experimental data. (A) Acetate secretion rates for *E. coli* cells grown in minimal glucose media, with data obtained from different datasets [29, 48–51]. Full dots represent average CAFBA solutions (heterogeneous case) obtained with different degrees of carbon limitation (different w_C, averages over 500 solutions). Results were obtained with two different values for the average E-sector weight, namely $\langle w \rangle = 8.8 \times 10^{-4}$ gh/mmol (red) and $\langle w \rangle = 1.55 \times 10^{-3}$ gh/mmol (blue). These choices reproduce the acetate secretion rates of NCM3722 and ML308 (open circles) and MG1655 (open triangles) strains, respectively. (B) Same as panel (A), but for the growth yield. CAFBA predictions (red and blue filled circles) are obtained by averaging the ratio of the growth rate to the glucose intake flux, divided by the molecular weight of glucose $\mu_{glc} = 0.18$ g/mmol. Data points from [29] have been converted using 1 mM/OD$_{600}/h = 2$ mmol/g$_{\rm DW}$h. x- and y-error bars for the average CAFBA solutions are too small to be visible.

Interestingly, average fluxes are consistent for lactose, glucose and maltose on the one hand, and for fructose, sorbitol and mannose on the other. The reason is that, in the former group of substrates, the carbon source enters glycolysis as glucose-6P, which can be processed either by upper glycolysis or by the ED and pentose phosphate pathways. In the latter group, instead, carbon is transformed into fructose-6P, which is more conveniently processed into fructose biphosphate. A similar behavior is observed for phosphatated carbon sources or other substrates of the glycolytic or pentose pathways, see Fig G in the Supporting Text. The ED pathway, despite having a smaller ATP yield, requires a much smaller number of enzymes than the EMP pathway. Therefore, the use of ED over EMP may be the result of a proteome-saving strategy. Our findings thus agree with the conclusions of [42, 54, 55]. The switch between the EMP and ED pathways sets in at a growth rate close to 0.3/h, well below $\lambda_{\rm ac}$, suggesting that it is independent of acetate secretion. Nonetheless, both features appear in CAFBA in order to cope with increasingly expensive proteins, in agreement with quantitative proteomics data [46].

On the other hand, CAFBA shows that a variety of strategies exist for cells growing on carbon substrates belonging to the lower part of glycolysis or to the TCA cycle, see Fig H in the Supporting Text. What these strategies share is an increased production of CO_2 at faster growth, and a vanishing activity of the ED pathway. The latter is of course due to the intrinsic glycolytic, as opposed to gluconeogenic, nature of the ED pathway.

Comparison between CAFBA and FBA solutions

Standard FBA optimizes the growth yield subject to constraining the carbon intake flux. It is useful to compare CAFBA solutions with solutions obtained by FBA at the same growth rate and with glucose as the sole carbon source for both models. To do so, we have first solved Parsimonius Enzyme Usage FBA (pFBA, see [56]) varying the bounds on glucose intake so as to obtain FBA solutions as a function of the growth rate. We shall denote them as $\mathbf{z}(\lambda) = \{z_i(\lambda)\}$. CAFBA solutions found upon varying w_C lead instead to w_C-dependent mean growth rates $\overline{\lambda}(w_C)$. We shall denote CAFBA solutions obtained for a value of w_C such that $\overline{\lambda}(w_C) = \lambda$ by $\mathbf{v}(\lambda) = \{v_i(\lambda)\}$. We have then computed, for a given set $\mathcal{R}$ of reactions of interest, the

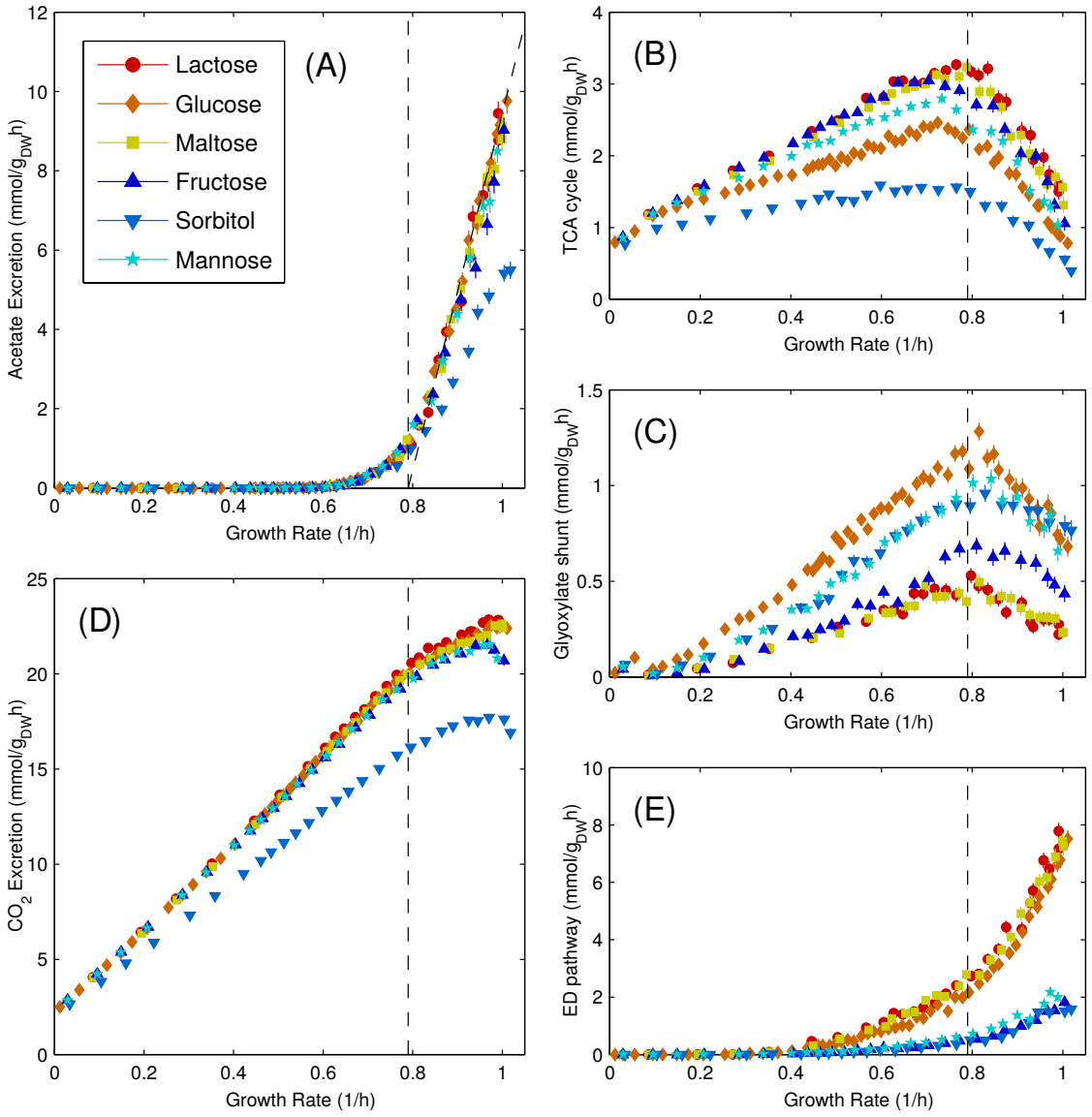

Figure 4. Average CAFBA solutions (heterogeneous case) for six different glycolytic carbon sources. Each plot shows a different average flux, specifically: (A) Acetate secretion, (B) TCA cycle flux (represented by αKG dehydrogenase), (C) Glyoxylate shunt flux (malate synthase), (D) CO2 secretion, (E) ED pathway flux, (6-phosphogluconate dehydratase). Each point represents the average over 500 solutions obtained with the same $w_C \geq 0$ and $\langle w \rangle = 8.8 \times 10^{-4}$ gh/mmol. Vertical lines at $\lambda_{\rm ac} = 0.79$/h are shown for clarity. In panel (A), acetate secretion can be approximated, for $\lambda \geq \lambda_{\rm ac}$, with a straight line $v_{\rm ac} = s \times (\lambda - \lambda_{\rm ac})$ with $s = 45$ mmol/g$_{\rm DW}$.

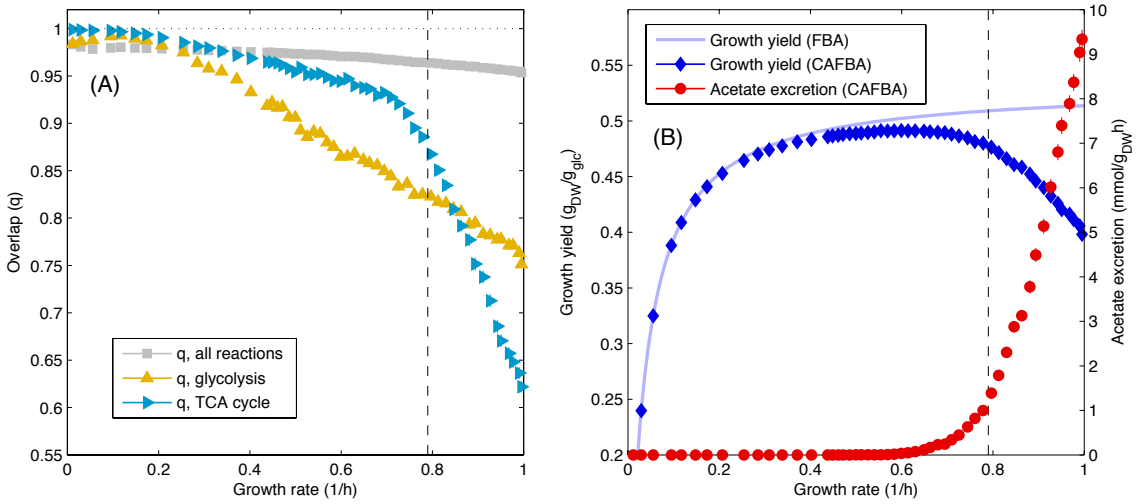

Figure 5. Overlap between FBA and CAFBA solutions. (A) Overlap q between pFBA and CAFBA solutions as a function of growth rate, computed for three different reaction sets: all reactions included in the reconstruction, reactions in the glycolysis/gluconeogenesis pathway, and reactions in the TCA cycle. FBA fluxes were computed for the same glucose influx as the CAFBA solution and then interpolated at the growth rates of CAFBA solutions in order to plot the overlap as a function of λ. (B) Growth yield and acetate secretion from CAFBA, together with the FBA-predicted growth yield. In both panels the value $\lambda_{\rm ac} = 0.79/\mathrm{h}$ is marked by a vertical dashed line.

similarity index $q_{\mathcal{R}}$ called "overlap" and defined as [57]

$$q_{\mathcal{R}}(\lambda) = \frac{1}{N_{\mathcal{R}}} \sum_{i \in \mathcal{R}} \left\langle \frac{2 v_i(\lambda) z_i(\lambda)}{v_i(\lambda)^2 + z_i(\lambda)^2} \right\rangle \quad , \tag{14}$$

where the sum is restricted to reactions in $\mathcal{R}$ and the brackets $\langle \cdots \rangle$ denote an average over 1000 different CAFBA solutions $\mathbf{v}(\lambda)$. If in each solution $v_i = z_i$ for each $i \in \mathcal{R}$, then $q_{\mathcal{R}} = 1$. Conversely, the more the two flux vectors differ, the smaller q gets. In particular, if in each solution $v_i = -z_i$ for each $i \in \mathcal{R}$, one finds $q_{\mathcal{R}} = -1$. Fig 5A shows the behavior of $q_{\mathcal{R}}$ versus λ for different choices of $\mathcal{R}$. When all reactions are accounted for, q is generally very large at low growth rates and decreases slowly as λ increases. When focusing on individual pathways, one sees that the overlap for TCA fluxes (cyan) drops abruptly above the acetate onset point $\lambda_{\rm ac} \simeq 0.79/\mathrm{h}$, where the growth yield of CAFBA solutions starts to reduce significantly compared to that of FBA solutions (Fig 5B, shown in red and blue symbols respectively). The overlap of fluxes in the glycolytic pathway instead diminishes with λ in a more gradual way, corresponding to the smooth increase in the activity of the ED pathway, see Fig 4E. Thus, as the growth rate increases, CAFBA solutions cross over from flux distributions that maximize the growth yield (slow growth) to a regime in which low-yield fermentation, accompanied by carbon overflow and energy spilling, is favored (fast growth).

Growth rate-dependent biomass composition

In CBMs, the energetic cost of anabolic pathways is accounted for by the stoichiometry of the network. By contrast, the energetic requirements of growth (e.g. protein synthesis) and homeostasis must be included separately as an additional ATP hydrolysis flux $v_{\rm ATP}$. In metabolic models, the latter is assumed to be linearly related to the growth rate, i.e. $v_{\rm ATP} = v_{\rm ATPM} + \beta_{\rm ATP}\lambda$ [15]. The first term is a growth-rate independent maintenance flux that represents the energy required to sustain basal cellular activities. The second term, instead, accounts for λ-dependence through a coefficient $\beta_{\rm ATP}$ that fixes the moles of ATP to be hydrolyzed per gram of dry weight. The values of $v_{\rm ATPM}$ and $\beta_{\rm ATP}$ are usually fitted from growth yield curves [16], and different metabolic reconstructions of *E. coli* use different numerical values for both of them, see [45, 58, 59] and Table C in the Supporting Text. However, as the cell's composition (and specifically the amounts of RNA, DNA, proteins, fatty acids, etc.) adjusts with the growth rate, biomass coefficients, including the demand of growth-related ATP, are in general λ-dependent [39]. A natural question to ask at this point is how cellular ATP requirements impact the shift between respiration and fermentation.

Results obtained by solving CAFBA with λ-dependent biomass composition are shown in Fig 6 (open symbols), together with the solution obtained for constant biomass composition at the same $\langle w \rangle = 8.8 \times 10^{-4}$ gh/mmol (filled blue circles). We tested CAFBA predictions with three different values of $\beta_{\rm ATP}$ while keeping $v_{\rm ATPM}$ fixed: (i) the default value for iJR904 model, (ii) the default value for the iAF1260 model, which is 30% larger than (i) [58], and (iii) a value 30% smaller than (i). One sees that, for the same ATP hydrolysis parameter (open and filled blue symbols), solutions for the two versions of CAFBA nearly overlap. On the other hand, both the slope and the onset growth rate $\lambda_{\rm ac}$ for acetate secretion appear to depend on the value of $\beta_{\rm ATP}$. Likewise,the flux through TCA increases with $\beta_{\rm ATP}$ so as to satisfy energetic requirements. The growth yield and maximum growth rate $\lambda_{\rm max}$ obtained at $w_C = 0$ decrease accordingly. However, if we tune $\langle w \rangle$ to fix $\lambda_{\rm max} = 1/{\rm h}$ for each value of $\beta_{\rm ATP}$, acetate secretion starts consistently at $\lambda_{\rm ac} \simeq 0.8/{\rm h}$ (Fig J in the Supporting Text), implying that energetic costs do not affect the ratio $\lambda_{\rm ac}/\lambda_{\rm max}$.

Discussion

In this work we have introduced CAFBA, an extension of FBA inspired by the proteome allocation scenario underpinned by bacterial growth laws [3, 5, 21, 60]. By integrating a single additional global constraint in FBA, CAFBA formulates the interplay of growth and expression in metabolism as a simple and elegant growth-rate optimization problem, with the same computational complexity as standard FBA. States of optimal growth found by CAFBA therefore encode for optimality from both an energetic and a proteome allocation perspective. A most distinctive feature of CAFBA lies in the extremely simple empirical inputs required to make quantitatively accurate predictions. The 3 parameters on which the proteome allocation constraint relies, namely $w_{R,0}$, $\phi_{\rm max}$ and $\lambda_{\rm max}$, can be easily obtained in experiments [5, 6]. All other parameters can be set based on these 3 numbers.

CAFBA predictions obtained for *E. coli* by averaging solutions over protein costs are found to be close to growth-yield maximizing solutions at slow growth. As growth gets faster, a continuous switch to a regime characterized by carbon overflow occurs. The onset of carbon overflow (at a growth rate denoted as $\lambda_{\rm ac}$) turns out to be largely independent of the nature of the glycolytic substrate. The ratio $\lambda_{\rm ac}/\lambda_{\rm max}$, with $\lambda_{\rm max}$ the fastest achievable growth rate, is indeed a remarkably robust quantity, that is roughly independent of the empirical parameters that characterize the proteome allocation constraint. Rather, it is mainly influenced by the weights of the biosynthetic reactions, $\{w_i\}$. These results strongly support the picture according to which acetate secretion is part of an optimal strategy to cope with increasing protein costs at high growth rates [7, 8, 29, 46].

CAFBA easily allows to model cellular metabolic activity in a variety of conditions, including translational limitation [8,22] and protein overexpression [5]. As more growth laws are being characterized in different organisms [61–63], CAFBA's application range is likely to expand significantly. Note C in the Supporting Text details how to port CAFBA to growth conditions and/or bacterial species different from those considered here. Other growth-maximizing organisms may also be studied by CAFBA if the required ingredients (network structure, biomass composition, empirical inputs) are available. Going beyond cell-autonomous models, CAFBA may prove highly effective for characterizing trophic interactions (e.g. cross-feeding) in microbial communities by treating excreted metabolites as potential nutrients [64]. CAFBA therefore provides a conceptually simple and computationally efficient platform that can be easily adapted and calibrated to describe the metabolism and growth of different organisms, making it a versatile tool for the computational modelling of interacting species in complex environments.

Comparison of CAFBA to other models

Under carbon limitation, solutions of CAFBA are obtained by varying the parameter w_C, a proxy for the extracellular carbon level representing the proteome cost of the C-sector (carbon intake). In essence, for any given substrate level, CAFBA allocates the C-sector proteins per unit flux by simultaneously optimizing the allocation of the proteome fractions required to sustain biosynthesis and translation in order to maximize growth. The use of w_C as a control parameter as opposed to directly dialing the nutrient intake flux is one of the elements that distinguish CAFBA from closely related CBMs like FBA [15], FBAwMC [31, 32] and ME-models [19, 20]. In fact, the CAFBA constraint effectively reduces to a finite capacity constraint similar to the one that characterizes FBAwMC when an upper bound on the glucose intake flux is used to modulate growth at fixed $w_C = 0$ (see Note B in the Supporting Text). (Note however that tuning nutrient levels as opposed to nutrient influx was employed in RBA to model the substitution between low affinity and high affinity cysteine transporters in *B. subtilis* [18].)

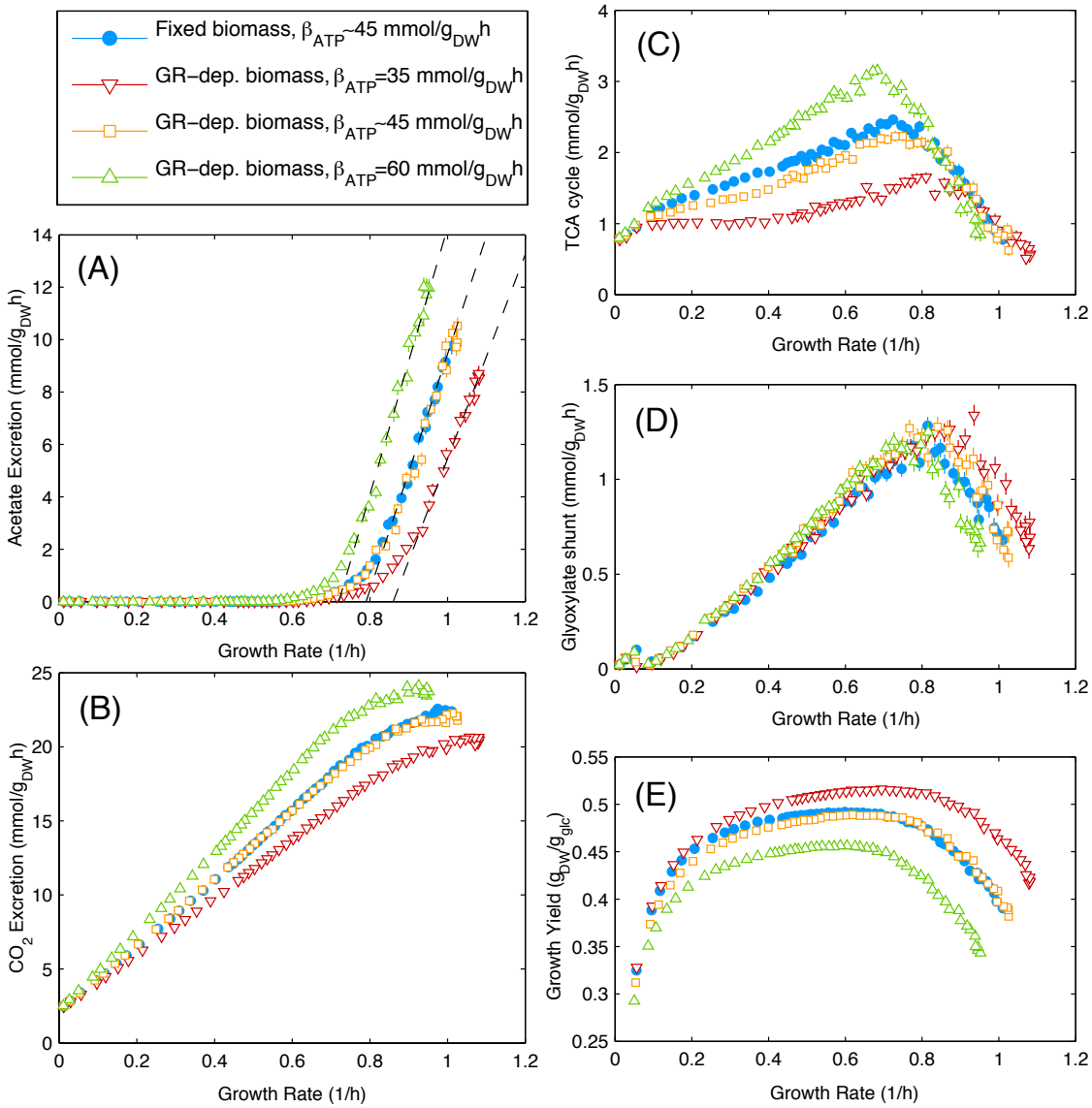

Figure 6. CAFBA solutions with growth rate-dependent biomass composition. Representative fluxes obtained by CAFBA for *E. coli* growth in glucose minimal medium with fixed (blue points) and variable biomass composition (in open red, yellow and green markers for three different values of the λ-dependent ATP hydrolysis rate $\beta_{\rm ATP}$). (A) Acetate secretion rate, (B) CO_2 secretion rate, (C) flux through TCA cycle (αKG dehydrogenase), (D) flux through glyoxylate shunt (Malate synthase), (E) growth yield. No significant differences are observed between the constant and λ-dependent cases for $\beta_{\rm ATP} = 45.5608$ mmol$_{\rm ATP}$/g$_{\rm DW}$, corresponding to the default value for the iJR904 model. We also show, for comparison, results obtained for larger and smaller values of $\beta_{\rm ATP}$. The acetate secretion rate can always be fitted by a linear function of λ, i.e. $v_{\rm ac} = s \times (\lambda - \lambda_{\rm ac})$, albeit with different slopes and intercepts. The three dashed lines correspond to $s = 39, 45, 51$ mmol/g$_{\rm DW}$, respectively, while $\lambda_{\rm ac} = 0.86, 0.79, 0.72$/h, respectively. We also indicate $\lambda_{\rm ac} = 0.79$/h with a vertical dashed line in all panels. In all cases we set $\langle w \rangle = 8.8 \times 10^{-4}$ gh/mmol, $w_C \geq 0$ and $w_{\rm max}/w_{\rm min} = 10$.

Secondly, CAFBA does not provide the detailed mechanistic description of gene expression and protein synthesis conveyed by ME-models and RBA, whose definition includes, for instance, explicit variables for macromolecular concentrations (ribosomes, DNA, RNA, etc.). Rather, it relies on an effective formulation based on empirical growth laws and (when desired) on a growth-rate dependent biomass composition. In this light, while less comprehensive than its closely related CBMs, the CAFBA scheme highlights the key biological ingredients constraining proteome allocation.

On a more technical level, both RBA and ME-models are intrinsically non-linear and handle non-linearity by approximating their underlying optimization problems through sequences of linear feasibility problems. In CAFBA, even the worst case is solved through a fast iterative algorithm involving a small number of LP problems.

Finally, the optimal proteome allocation problem posed by CAFBA can be seen as an assumption of "optimal enzymatic efficiency", close to that underlying FBA approaches based on flux minimization [65, 66].

Choice of parameters

One of the strong points of standard FBA consists in its reliance on the stoichiometric matrix and on thermodynamic reversibility constraints alone, making kinetic parameters unnecessary. CAFBA's proteome allocation constraint in principle introduces a large number of additional parameters related to reaction and/or transport kinetics that, for the most part, are either uncharacterized or inferred from in vitro studies performed in different biochemical conditions [67]. This raises the issue of parameter selection.

Two of the constants entering the proteome constraints (namely w_R and $\phi_{\max}$) are obtained directly from empirical growth laws. With w_C acting as the control variable, the only free parameters left are the weights w_i characterizing intracellular reactions. While quantitative CAFBA predictions appear to be dependent on their specific values, the qualitative behaviour of the solutions is not. Furthermore, the scenario obtained by averaging CAFBA solutions over different choices of the w_i quantitatively reproduces experimental findings for acetate secretion and growth yield. These results point to a considerable degree of robustness of the CAFBA framework against fluctuations in parameter values. Notice however that the CAFBA picture can be further improved upon tuning the weights of individual reactions. For example, by increasing the average weight of reactions involved in respiration one sees a shift in the onset of acetate secretion and the value of $\lambda_{\rm ac}/\lambda_{\max}$ changes, see Fig K in the Supporting Text. On the other hand, parameters can also be tuned according to empirical evidence so as to allow for a more thorough comparison with experiments performed on different strains and/or growth conditions, e.g. concerning intracellular fluxes (see Fig L in the Supporting Text).

In perspective, detailed flux measurements may allow to estimate typical weights for each pathway, and possibly even for individual enzymes, opening for the possibility to better calibrate the model and obtain completely quantitative predictions. Our work here has aimed at keeping the number of parameters as small as possible. In this light, many emerging features of the interplay between metabolism and gene expression appear to be mostly determined by the topology of the metabolic network. Elucidating the origin of this simplification is a foremost theoretical challenge for future studies of metabolic systems.

On using average fluxes

The need to resort to an averaging procedure in order to reproduce bulk measurements for the growth yield and the acetate excretion forces us to ask whether the CAFBA averaging may have some further meaning. We offer here two possible scenarios.

The first one is based on the fact that, even in well controlled growth conditions, cells in a population are normally heterogeneous, as transcription levels, protein abundances, reaction fluxes and instantaneous growth rates may change significantly from one to the other [68–70]. This would in turn reflect in fluctuations in the values of each w_i across cells. Averaging over different choices for the weights could then simply be interpreted as averaging over a population of heterogeneous cells (as would seem appropriate in modelling batch culture or chemostats).

The alternative scenario presupposes that, even in absence of any cell-to-cell variability, cells may not be able to perfectly adjust fluxes to the distribution maximizing the instantaneous growth rate. This may occur for different reasons. First, the regulatory machinery needed to perform protein allocation requires by itself an investment of metabolic and proteomic resources [71–73]. This burden becomes more severe as the regulatory system gets more sensitive and fine-tuned, and, clearly, CAFBA does not account for it. Secondly, environments where cells grow are always fluctuating. Any regulatory machinery implementing fast

adjustments in response to small environmental changes will necessarily come at a cost that will negatively affect the growth rate. Under such constraints, regulatory programs selected over evolutionary time scales may prefer to maximize an *average* growth rate, the average being taken over life process history. The actual regulatory programs implemented would then balance the trade-off between the costs of not being exactly in the instantaneously optimal growth state and the costs of adjusting regulation too frequently in "natural" conditions (not those provided in the laboratory). An interpretation of the CAFBA averaging prescription would then be that it is a way to implement an "average" strategy that smooths the output upon variations of the environmental conditions.

In both of the above scenarios, CAFBA points to the emergence of acetate excretion as triggered by regulatory system(s) sensing the abundance of the carbon source and the balance of biomass synthesis and energy generation [29]. We note that carbon overflow in *E. coli* has been proposed to be modulated by catabolite repression mediated ACS down-regulation [49]. Discriminating between the two scenarios we have just presented could be achieved already in bulk experiments, by changing the weight of specific enzymes over time (e.g., by expressing useless proteins specific to certain pathways) and monitoring whether the associated fluxes adjust dynamically in real time. Naturally, tests of cell-to-cell heterogeneities would also allow to favor one scenario over the other.

Finally, we address the magnitude of fluctuations of the weights w_i. The spread in the enzyme catalytic rates $k_{\mathrm{cat},i}$, as tabulated in databases, is notoriously broad, exceeding 3 orders of magnitude [32, 67]. In the absence of more refined information, it is reasonable to expect that the weights w_i should fluctuate by about the same amount. However, we have seen that unrealistic results are generated by CAFBA if weights are allowed to fluctuate more than 10-fold. Therefore, either the true width of the distribution of the weights w_i is much smaller than what is suggested by the values of $k_{\mathrm{cat},i}$ estimated in vitro, or weights are subtly distributed across pathways in such a way that strong compensatory effects occur that reduce fluctuations. With steady improvements in proteomic methods, it may soon be possible to quantitatively determine these parameters empirically and elucidate this puzzle.

Materials and Methods

Optimization problem

Given a metabolic network encoded by a stoichiometric matrix $\mathbf{S} = \{S_{\mu i}\}$, CAFBA is stated in the case of carbon limitation as

$$\max_{\mathbf{v}} \lambda \quad \text{subject to} \quad \text{(i)} \qquad \sum_i S_{\mu i} v_i = 0 \quad \forall \mu \tag{15}$$

$$\text{(ii)} \qquad \ell_i \le v_i \le u_i \quad \forall i \tag{16}$$

$$\text{(iii)} \qquad w_C v_C + \sum_i w_i |v_i| + w_R \lambda = \phi_{\max} \ , \tag{17}$$

where λ denotes the growth rate, $\mathbf{v} = \{v_i\}$ is a flux vector, and (ℓ_i, u_i) represent lower and upper bounds for each flux v_i, respectively. Condition (17) corresponds to the proteome allocation constraint $\phi_C + \phi_E + \phi_R + \phi_Q = 1$, with $v_C \ge 0$ being the active glucose intake flux and with the sum in $\sum_i w_i |v_i|$ running over all enzyme–catalyzed reactions except for transports, exchanges and carbon intake pathways. The biomass flux λ and ATP maintenance reaction are also excluded from (17).

In principle, CAFBA is a MILP (Mixed Integer-Linear Programming) problem due to the presence of absolute values in (17). However, in CAFBA they can be disposed of by splitting each flux v_i into a forward v_i^+ and a backward v_i^- component, both non-negative. Note that if either v_i^+ or v_i^- can be set to zero for each i, net fluxes $v_i = v_i^+ - v_i^-$ are univocally determined, one has $|v_i| = v_i^+ + v_i^-$ for absolute values, and CAFBA becomes equivalent to

$$\max_{\mathbf{v}^+, \mathbf{v}^-} \lambda \qquad \text{subject to} \quad \text{(i)} \quad \sum_i S_{\mu i} (v_i^+ - v_i^-) = 0 \quad \forall \mu \tag{18}$$

$$\text{(ii)} \quad 0 \le v_i^- \le -\ell_i \qquad 0 \le v_i^+ \le u_i \quad \forall i \tag{19}$$

$$\text{(iii)} \quad w_C v_C + \sum_i w_i (v_i^+ + v_i^-) + w_R \lambda = \phi_{\max} \ , \tag{20}$$

which is a simple LP problem rather than a MILP. The key observation is that, as long as λ is maximized, CAFBA actually adjusts fluxes so that either the forward or the backward component vanish for each i.

Indeed, a necessary condition for maximizing λ is that the quantity $v_i^+ + v_i^-$ is minimized for each i, which, at fixed $v_i = v_i^+ - v_i^-$, is achieved by setting either v_i^+ or v_i^- to zero. Therefore CAFBA reduces from a MILP to a LP problem.

Note that, because of the tight link between CAFBA and flux minimization, degeneracies in CAFBA solutions can only arise from the presence of (a) futile loops or (b) pathways that perform the same overall chemical conversion with the same flux at the same proteome cost, and which therefore can be used alternatively. In CAFBA with heterogeneous weights, however, the chance that two equivalent flux configurations have exactly the same total weight is negligible, since weights are i.i.d. random variables. On the other hand, futile loops only concern transports that do not involve the main carbon source and therefore are not included explicitly in the CAFBA constraint. These loops however do not affect other fluxes and are easily spotted and removed, either by manually shutting off redundant processes or by including them into the proteome allocation constraint with an arbitrarily small but non-zero weight. Therefore, each instance of the inhomogeneous CAFBA scheme has a unique solution almost surely. Because our main results are obtained in this framework, alternate optima are in practice not an issue in CAFBA.

Implementation

We implemented CAFBA on the E. coli iJR904 genome-scale model [45], comprehensive of 761 metabolites and 1075 reactions, as a Matlab® function, using the COBRA Toolbox [74] to load the network reconstruction with a minor modification. Specifically, we shut off the glucose dehydrogenase reaction, since it is only functional if the cofactor pyrroloquinoline quinone is supplied in the environment (see the Ecocyc [75] entry on the enzyme). Both GLPK- and Gurobi-compatible CAFBA solvers for Matlab are provided as additional supplementary material, along with a small set of utility functions. Running times for a single CAFBA optimization of the iJR904 network with a common laptop (single thread of an Intel Core i7–2630QM CPU @ 2.00GHz) are around 0.12 s for the GLPK (version 4.47) LP solver and 0.05 s the Gurobi Optimizer (version 5.6) solver. For comparison, the time required to compute the standard FBA solution for the same network with the COBRA toolbox using GLPK is around 0.06 s.

Case of growth-rate dependent biomass

The fact that cells adapt their composition with the growth rate [2, 4, 5] implies that biomass composition is itself λ-dependent. Growth-rate dependent biomass coefficients (see e.g. [39] for *E. coli*) indeed reflect empirical knowledge of how the amounts of RNA, DNA, proteins, fatty acids, etc. are modulated by λ. While constraint-based models such as FBA and CAFBA with growth-dependent biomass are non-linear, approximate solutions can be obtained efficiently by simple iterated LP protocols as follows: (a) starting from a given biomass vector, solve the model by optimizing the growth rate; (b) update the biomass composition to the computed optimal growth rate using the prescribed set of λ-dependent biomass coefficients; (c) iterate until a solution is reached, such that further iterations do not change the optimal growth rate within a desired precision. For CAFBA, this procedure typically converges in a very small number of iterations (see Fig I in the Supporting Text). Further details about the case of growth rate-dependent biomass composition and the iterative algorithm for computing the optimal FBA or CAFBA solutions are given in Note F in the Supporting Text.

Extension to different growth media and/or organisms

Besides the full study of the *E. coli* iJR904 model, we have tested CAFBA on the more recent reconstructions iAF1260 [58] and iJO1366 [59], obtaining very similar results. COBRA-compatible Matlab functions [74] to run CAFBA on these models are provided as additional supplementary material. Note C in the Supporting Text describes in detail how to port CAFBA to different growth media, nutrient limitations and/or bacterial species. However, provided the input coming from empirical growth laws is available together with the network structure and the biomass composition, the CAFBA framework can in principle be extended to growth-maximizing organisms other than bacteria.

Acknowledgments

MM gratefully acknowledges the hospitality for his visit to Hwa labs at UCSD. TH gratefully acknowledges the hospitality of U. Paris-Sud and Sapienza, U. Roma for his visits. The authors acknowledge members of Hwa lab

for contributing growth rate data for comparing between MG1655 and NCM3722 strains. Useful discussions with S. Hui, R. Mulet, A. Pagnani, A. Samal, A. Tramontano and Z. Yang are gratefully acknowledged.

References

1. Monod J (1949) The growth of bacterial cultures. Ann Rev Microbiol 3: 371-394
2. Schaechter M, Maaløe O, Kjeldgaard N (1958) Dependency on medium and temperature of cell size and chemical composition during balanced growth of Salmonella typhimurium. J Gen Microbiol 19: 592-606
3. Kjeldgaard N, Kurland C (1963) The distribution of soluble and ribosomal RNA as a function of growth rate. J Mol Biol 6: 341-348
4. Bremer H, Dennis PP (1996) Modulation of chemical composition and other parameters of the cell by growth rate. Escherichia coli and Salmonella: Cellular and Molecular Biology 2: 1553-1569
5. Scott M, Gunderson CW, Mateescu EM, Zhang Z, Hwa T (2010) Interdependence of cell growth and gene expression: origins and consequences. Science 330: 1099-1102
6. You C, et al. (2013) Coordination of bacterial proteome with metabolism by cyclic AMP signalling. Nature 500: 301-306
7. Molenaar D, van Berlo R, de Ridder D, Teusink B (2009) Shifts in growth strategies reflect tradeoffs in cellular economics. Mol Sys Biol 5: 323
8. Hui S, et al. (2015) Quantitative proteomic analysis reveals a simple strategy of global resource allocation in bacteria. Mol Sys Biol 11: 784
9. Papoutsakis, ET (1984) Equations and calculations for fermentations of butyric acid bacteria. Biotechnol Bioeng 26: 174-187
10. Varma A, Boesch BW, Palsson, BØ (1993) Stoichiometric interpretation of Escherichia coli glucose catabolism under various oxygenation rates. Appl Environ Microbiol 59: 2465-2473.
11. Varma A, Palsson, BØ (1994) Stoichiometric flux balance models quantitatively predict growth and metabolic by-product secretion in wild-type Escherichia coli W3110. Appl Environ Microbiol 60: 3724-3731.
12. Edwards JS, Ibarra RU, Palsson BØ (2001) In silico predictions of Escherichia coli metabolic capabilities are consistent with experimental data. Nature Biotechnol 19: 125-130
13. Ibarra RU, Edwards JS, Palsson BØ (2002) Escherichia coli K-12 undergoes adaptive evolution to achieve in silico predicted optimal growth. Nature 420: 186-189
14. Orth JD, Thiele I, Palsson BØ (2010) What is flux balance analysis? Nature Biotechnol 28: 245-248
15. Palsson, BØ (2015) Systems biology. Cambridge University Press.
16. Feist AM, Palsson BØ (2010) The biomass objective function. Curr Opin Microbiol 13: 344-349
17. Goelzer A, Fromion V (2011) Bacterial growth rate reflects a bottleneck in resource allocation. Biochimica et Biophysica Acta (BBA)-General Subjects 1810: 978-988
18. Goelzer A, Fromion V, Scorletti G (2011) Cell design in bacteria as a convex optimization problem. Automatica 47: 1210-1218
19. Lerman JA et al. (2012) In silico method for modelling metabolism and gene product expression at genome scale. Natire Comm 3: 929
20. O'Brien EJ, Lerman JA, Chang RL, Hyduke DR, Palsson BØ (2013) Genome-scale models of metabolism and gene expression extend and refine growth phenotype prediction. Mol Sys Biol 9: 693

21. Maaløe O (1979) Regulation of the protein-synthesizing machinery - ribosomes, tRNA, factors, and so on. In Biological regulation and development. Springer, pp. 487-542

22. Deris JB, et al. (2013) The innate growth bistability and fitness landscapes of antibiotic-resistant bacteria. Science 342: 1237435

23. Gottschalk G (1986) Bacterial Metabolism, chap. 8. Springer Science & Business Media, pp. 208-282

24. Clark DP (1989) The fermentation pathways of Escherichia coli. FEMS Microbiol Rev 5: 223-234

25. Wills C (1990) Regulation of sugar and ethanol metabolism in Saccharomyces cerevisiae. Critical Reviews Biochem Mol Biol 25: 245-280

26. Wolfe AJ (2005) The acetate switch. Microbiol Mol Biol Rev 69: 12-50

27. Diaz-Ruiz R, Rigoulet M, Devin A (2011) The Warburg and Crabtree effects: On the origin of cancer cell energy metabolism and of yeast glucose repression. Biochimica et Biophysica Acta (BBA)-Bioenergetics 1807: 568-576

28. Dashko S, Zhou N, Compagno C, Piškur J (2014) Why, when, and how did yeast evolve alcoholic fermentation? FEMS Yeast Res 14: 826-832

29. Basan M, et al. (2015) Efficient allocation of proteomic resources for energy metabolism results in acetate overflow. Nature 528: 99-104

30. Majewski R, Domach M (1990) Simple constrained-optimization view of acetate overflow in *E. coli*. Biotechnol Bioeng 35: 732-738

31. Beg Q, et al. (2007) Intracellular crowding defines the mode and sequence of substrate uptake by Escherichia coli and constrains its metabolic activity. Proc Natl Acad Sci USA 104: 12663-12668

32. Vazquez A, et al. (2008) Impact of the solvent capacity constraint on *E. coli* metabolism. BMC Syst Biol 2: 7

33. Zhuang K, Vemuri GN, Mahadevan R (2011) Economics of membrane occupancy and respiro-fermentation. Mol Syst Biol 7

34. Paul BJ, Ross W, Gaal T, Gourse RL (2004) rRNA transcription in Escherichia coli. Annu Rev Genet 38: 749-770

35. Klumpp S, Scott M, Pedersen S, Hwa T (2013) Molecular crowding limits translation and cell growth. Proc Natl Acad Sci USA 110: 16754-16759

36. Potrykus K, Cashel M (2008) (p)ppGpp: Still Magical? Annu Rev Microbiol 62: 35-51

37. Scott M, Klumpp S, Mateescu EM, Hwa T (2014) Emergence of robust growth laws from optimal regulation of ribosome synthesis. Mol Sys Biol 10(8): 747

38. Li Z, Nimtz M, Rinas U (2014) The metabolic potential of Escherichia coli BL21 in defined and rich medium. Microb Cell Fact 13: 45

39. Pramanik J, Keasling J (1998) Effect of Escherichia coli biomass composition on central metabolic fluxes predicted by a stoichiometric model. Biotechnol Bioeng 60: 230-238

40. Taymaz-Nikerel H, Borujeni AE, Verheijen PJ, Heijnen JJ, van Gulik WM (2010) Genome-derived minimal metabolic models for Escherichia coli MG1655 with estimated in vivo respiratory ATP stoichiometry. Biotechnol Bioeng 107: 369-381

41. Hermsen R, Okano H, You C, Werner N, Hwa T (2015) A growth-rate composition formula for the growth of *E. coli* on co-utilized carbon substrates. Mol Sys Biol 11: 801

42. Noor E, et al. (2014) Pathway thermodynamics highlights kinetic obstacles in central metabolism. PLoS Comput Biol 10: e1003483

43. Kochanowski K, et al. (2013) Functioning of a metabolic flux sensor in Escherichia coli. Proc Natl Acad Sci USA 110: 1130-1135

44. Woldringh C, Binnerts J, Mans A (1981) Variation in Escherichia coli buoyant density measured in Percoll gradients. J Bacteriol 148: 58-63

45. Reed JL, Vo TD, Schilling CH, Palsson BØ (2003) An expanded genome-scale model of Escherichia coli K-12 (iJR904 GSM/GPR). Genome Biol 4: R54

46. Peebo K, et al. (2015) Proteome reallocation in Escherichia coli with increasing specific growth rate. Mol BioSyst 11: 1184-1193

47. Li GW, Burkhardt D, Gross C, Weissman JS (2014) Quantifying absolute protein synthesis rates reveals principles underlying allocation of cellular resources. Cell 157: 624-635

48. Holms H (1996) Flux analysis and control of the central metabolic pathways in Escherichia coli. FEMS Microbiol Rev 19: 85-116

49. Nanchen A, Schicker A, Sauer U (2006) Nonlinear dependency of intracellular fluxes on growth rate in miniaturized continuous cultures of Escherichia coli. Appl Environ Microbiol 72: 1164-1172

50. Valgepea K, et al. (2010) Systems biology approach reveals that overflow metabolism of acetate in Escherichia coli is triggered by carbon catabolite repression of acetyl-CoA synthetase. BMC Syst Biol 4: 166

51. Vemuri G, Altman E, Sangurdekar D, Khodursky A, Eiteman M (2006) Overflow metabolism in Escherichia coli during steady-state growth: transcriptional regulation and effect of the redox ratio. Appl Environ Microbiol 72: 3653-3661

52. Sauer U, Canonaco F, Heri S, Perrenoud A, Fischer E (2004) The soluble and membrane-bound transhydrogenases UdhA and PntAB have divergent functions in NADPH metabolism of Escherichia coli. J Biol Chem 279: 6613-6619

53. Fuhrer T, Fischer E, Sauer U (2005) Experimental identification and quantification of glucose metabolism in seven bacterial species. J Bacteriol 187: 1581-1590

54. Flamholz A, Noor E, Bar-Even A, Liebermeister W, Milo R (2013) Glycolytic strategy as a tradeoff between energy yield and protein cost. Proc Natl Acad Sci USA 110: 10039-10044

55. Stettner AI, Segrè D (2013) The cost of efficiency in energy metabolism. Proc Natl Acad Sci USA 110: 9629-9630

56. Lewis NE, et al. (2010) Omic data from evolved *E. coli* are consistent with computed optimal growth from genome-scale models. Mol Sys Bio, 6: 390

57. Martelli C, De Martino A, Marinari E, Marsili M, Perez Castillo I (2009) Identifying essential genes in Escherichia coli from a metabolic optimization principle. Proc Natl Acad Sci USA 106: 2607-2611

58. Feist AM, et al. (2007) A genome-scale metabolic reconstruction for Escherichia coli K-12 MG1655 that accounts for 1260 ORFs and thermodynamic information. Mol Syst Biol 3: 121

59. Orth JD, et al. (2011) A comprehensive genome-scale reconstruction of Escherichia coli metabolism. Mol Sys Biol 7: 535

60. Scott M, Hwa T (2011) Bacterial growth laws and their applications. Current Opin Biotechnol 22: 559-565

61. Fisher SH (1999) Regulation of nitrogen metabolism in Bacillus subtilis: vive la difference! Mol Microbiol 32: 223-232

62. Levy S, Barkai N (2009) Coordination of gene expression with growth rate: a feedback or a feed-forward strategy? FEBS Letters 583: 3974-3978

63. Wegener KM, et al. (2010) Global proteomics reveal an atypical strategy for carbon/nitrogen assimilation by a cyanobacterium under diverse environmental perturbations. Mol Cell Proteomics 9: 2678-2689

64. Harcombe WR, et al. (2014). Metabolic resource allocation in individual microbes determines ecosystem interactions and spatial dynamics. Cell Rep 7: 1104-1115

65. Holzhütter HG (2004) The principle of flux minimization and its application to estimate stationary fluxes in metabolic networks. Eur J Biochem 271: 2905-2922

66. Tarlak F, Sadıkoğlu H, Çakır T (2014) The role of flexibility and optimality in the prediction of intracellular fluxes of microbial central carbon metabolism. Mol BioSyst 10: 2459

67. Schomburg I, et al. (2012) BRENDA in 2013: integrated reactions, kinetic data, enzyme function data, improved disease classification: new options and contents in BRENDA. Nucleic Acids Research 41: D764-D772

68. Labhsetwar P, Cole JA, Roberts E, Price ND, Luthey-Schulten ZA (2013) Heterogeneity in protein expression induces metabolic variability in a modeled Escherichia coli population. Proc Natl Acad Sci USA 110: 14006-14011

69. Kiviet DJ, et al. (2014) Stochasticity of metabolism and growth at the single-cell level. Nature 514: 376-379

70. Solopova A, et al. (2014) Bet-hedging during bacterial diauxic shift. Proc Natl Acad Sci USA 111: 7427-7432

71. Lan G, Sartori P, Neumann S, Sourjik V, Tu Y (2012). The energy-speed-accuracy trade-off in sensory adaptation. Nat Phys 8: 422-428

72. Mehta P, Schwab, DJ (2012) Energetic costs of cellular computation. Proc Natl Acad Sci USA, 109: 17978-17982

73. Govern CC, ten Wolde, PR (2014). Optimal resource allocation in cellular sensing systems. Proc Natl Acad Sci USA, 111: 17486-17491

74. Schellenberger J, et al. (2011) Quantitative prediction of cellular metabolism with constraint-based models: the COBRA Toolbox v2.0. Nature Protoc 6: 1290-1307

75. Keseler IM, et al. (2011) EcoCyc: a comprehensive database of Escherichia coli biology. Nucleic Acids Res 39: D583-D590

Constrained Allocation Flux Balance Analysis

Supporting Text

M. Mori, T. Hwa, O.C. Martin, A. De Martino, E. Marinari

Contents

Note A. The linear enzyme–flux relation **2**

Note B. The choice of the control parameter **3**

Note C. Extension to different growth media and/or bacterial species **5**
CAFBA for E. coli growth in a generic medium with a set of limiting nutrients 5
Application to different *E. coli* strains or bacterial species 5

Note D. Translational inhibition and protein over–expression in CAFBA solutions **7**
Growth rate 7
Proteome fractions 8
Fluxes and Q–limitation 9

Note E. Case of inhomogeneous proteome costs **11**
Sample to sample fluctuations and fluctuations in the weights 11

Note F. Growth-dependent biomass composition **14**
Implementation of a growth-dependent biomass composition in CAFBA 15

Supplementary Tables **20**

Supplementary Figures **21**

Supplementary References **32**

Note A. The linear enzyme–flux relation

One of our basic assumptions is the following flux–enzyme relation:

$$\phi_i = \phi_{i,0} + w_i|v_i| \ . \tag{S1}$$

Eq. (S1) is our constitutive relation between proteome fractions and fluxes. Generally speaking, this relation expresses the fact that larger fluxes require a larger proteome share in order to be sustained. Here we analyze briefly its origin and detailed implementation within CAFBA. The general case is treated extensively in the Main Text, but we will repeat the derivation in this section in the specialized case of Michaelis–Menten kinetics.

Let us consider a single irreversible reaction with a flux v_i described by Michaelis-Menten kinetics. Calling $[s]$ and $[E_i]$ the substrate and enzyme concentrations, we have:

$$v_i = \frac{V}{M_{DW}} k_{cat,i}[E_i] \frac{[s]}{[s]+K_M} \quad , \tag{S2}$$

where V is the cell volume, M_{DW} is the cellular dry weight mass and K_M the Michaelis constant of the reaction. It is worth remembering that in Eq. (S2) the dilution flux $-\lambda[p]$ of the reaction product has been neglected, as usually done in steady state calculations, since the typical concentration ranges of the metabolites are such that the dilution flux is much smaller than the flux processed by the enzymes. (See however Ref. [1] for an attempt to explicity model dilution of intermediate metabolites in genome–scale networks.) The function $f([s],[p])$ introduced in the main text is given in this case by $[s]/([s]+K_M)$. Enzyme concentration and the corresponding proteome fractions are related by:

$$[E_i] = \frac{M_{TP}}{V\mu_i}\phi_i \quad , \tag{S3}$$

where M_{TP} is the total protein mass and μ_i is the enzyme molecular mass. Therefore, Eq. (S2) can be written as:

$$v_i = \kappa_{cat,i}\phi_i \frac{[s]}{[s]+K_M} \quad , \quad \text{with} \quad \kappa_{cat,i} = \frac{k_{cat,i}}{\mu_i}\frac{M_{TP}}{M_{DW}} \quad . \tag{S4}$$

If the reaction is saturating, we obtain the linear enzyme–flux relation:

$$\phi_i = \frac{1}{\kappa_{cat,i}} v_i \tag{S5}$$

This relation is Eq. (S1) with $w_i = 1/\kappa_{cat,i}$ and $\phi_{i,0} = 0$. However, this case is not very realistic, as it is known that the average saturation level in metabolic reactions varies in different growth conditions [2, 3].

We consider instead the case in which the substrate concentration is directly proportional to the flux itself, as $[s] = \alpha v_i$. As described in the main text, this is a common situation for glycolytic enzymes. In this case one obtains another linear relation between the enzyme levels and the fluxes:

$$\phi_i = \frac{K_M}{\alpha} + \frac{1}{\kappa_{cat,i}} v_i \ . \tag{S6}$$

The presence of baseline expression levels for each enzyme can be seen as the direct consequence of the presence of finite substrate concentrations. The existence of such basal level is also supported by quantitative proteomics data [4], and can be then introduced as constant offset $\phi_{i,0} > 0$.

It is interesting to express the enzyme proteome fraction as a function of substrate concentration, $[s_i]$. In this case, one obtains the simple expression:

$$\phi_i = \frac{K_M}{\alpha} + \frac{1}{\alpha\kappa_{cat,i}}[s] = \phi_{i,0}\left(1 + \frac{1}{\kappa_{cat,i}}\frac{[s]}{K_M}\right) \ . \tag{S7}$$

where $\phi_{i,0} = K_M/\alpha$. This suggests that positive regulation of the enzyme i by its own substrate may enforce the linear flux–substrate relation. This feedforward activation regulatory motif is seen in quite a number of metabolic control, e.g., the activation of lower glycolysis proteins by fructose bisphosphate (via Cra) [5], the activation of Pyruvate dehydrogenase by pyruvate via PdhR [6]; the upregulation of ribosome synthesis by amino acid (via ppGpp) also belongs to this regulatory class.

Note B. The choice of the control parameter

In standard FBA, the carbon intake flux (or, more precisely, the upper bound on the carbon intake flux) is used as a control parameter by which the growth rate can be tuned, so that, for instance, keeping all other flux specifications (upper and lower bounds, ATP maintenance, etc.) fixed one can obtain different values of λ by simply changing the glucose intake flux. Other models [7, 8] employ global constraints on fluxes as control parameters for λ, with biological rationale based e.g. on molecular crowding constraints; finally, other models use a combination of global constraints and explicit bounds on the glucose intake flux [9].

In this work control of λ is instead achieved by tuning the weight w_C, corresponding to the proteome fraction per unit flux allocated for carbon scavenging and intake. (For sakes of simplicity, we shall henceforth refer to glucose as the main carbon source.) In other words, in CAFBA the glucose intake is a free variable. The exchange fluxes of all other carbon sources have lower bound equal to 0, so that the metabolites can only be excreted. In essence, the reason for this choice is that w_C is a convenient proxy for the extracellular glucose *level*. To see this, let us assume Michaelis–Menten kinetics for the glucose transport. In this case, one can see that the proteome fraction ϕ_C of glucose transporters and the glucose flux v_C are related by

$$v_C = \kappa_{cat}\phi_C \frac{[g]}{[g] + K_M} \quad , \tag{S8}$$

where $[g]$ denotes the extracellular glucose level and κ_{cat} is a rescaled turnover, as described in the Main Text. Therefore, the proteome fraction required to sustain a glucose intake flux at least equal to v_C in presence of an extracellular glucose level $[g]$ is given by

$$\phi_C = v_C \times \frac{1}{\kappa_{cat}} \left(1 + \frac{K_M}{[g]}\right) \quad . \tag{S9}$$

Crucially, ϕ_C increases as $[g]$ is reduced, consistently with the expectation that, as the substrate levels goes down, a larger investment in terms of proteome fraction is needed to sustain the same intake flux. We can then write $\phi_C \geq w_C v_C$, with $w_C = (1 + K_M/[g])/\kappa_{cat}$. Since the relationship between w_C and $[g]$ is invertible, w_C can be used in place of $[g]$ as a control parameter: high values for w_C are associated to low substrate levels, and vice versa. Note that the largest achievable growth rate is obtained in the limit $w_C \to 0$. Fig. N1 shows how different choices of w_C affect the growth rate in CAFBA with a fixed glucose influx v_C. λ grows linearly with v_C for small intakes, reaches a maximum, and then goes to zero for large values of v_C. Once the value of w_C is given, CAFBA returns as the optimal λ the value corresponding to the maximum in those curves, and the glucose intake corresponding to it as the actual value of v_C.

Using w_C instead of v_C as a control parameter leads to striking differences in the flux configurations observed at high growth rates. In particular, in the former case (panel (A)) one observes jump discontinuities in the fluxes as w_C is varied, see Fig. N2. These sharp transitions are due to the fact that, as w_C changes, the solutions of the optimization problem display large-scale flux rearrangements that do not occur in general upon varying v_C. Such sharp transitions are usually not observed in experiments. Acetate excretion in *E. coli* starts above a critical growth (or dilution) rate [10, 11, 12]. Sigmoidal response functions are common in regulatory system, but usually they have some crossover region. Nonetheless, the biologically significant consequence is that solutions displaying carbon overflow may be found to be optimal for growth rates well below the largest achievable. On the other hand, for $w_C = 0$, when growth is modulated by changing the upper bound on the glucose intake (panel (B)), the CAFBA constraint effectively reduces to a finite capacity constraint on the enzymatic proteome sector, similar to the molecular crowding constraint that defines FBAwMC [7, 8]. In these conditions, key transitions like that related to acetate onset shift to values of λ close to the fastest achievable rates.

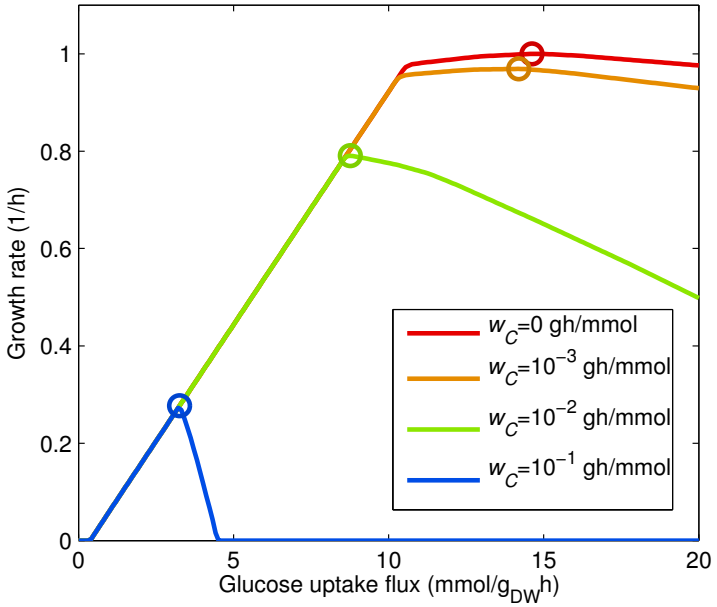

Figure N1: Growth rate of CAFBA solutions obtained as a function of the glucose uptake flux, for different degrees of carbon limitation ($w_C = 0, 10^{-3}, 10^{-2}, 10^{-1}$ $g_{DW}h/mmol$). The continuous lines show solutions obtained by directly constraining the carbon (glucose) flux; the circles indicate the CAFBA solutions when the carbon flux is not constrained.

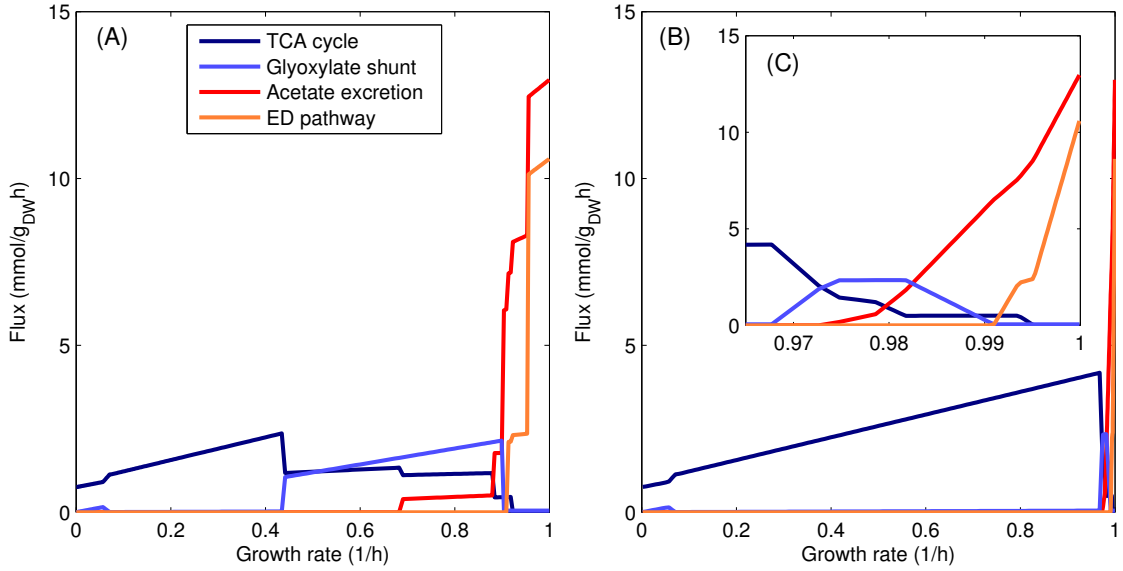

Figure N2: (**A**): CAFBA fluxes computed using w_C as the control parameter (glucose minimal medium). (**B**): CAFBA fluxes computed by imposing an upper bound on the glucose influx, at fixed $w_C = 0$. The inset (**C**) shows a detail of figure (**B**) at high growth rates.

Note C. Extension to different growth media and/or bacterial species

CAFBA for E. coli growth in a generic medium with a set of limiting nutrients

When the parameters w_R and $\phi_{\max}$, as well as the E–sector weights, are known for the strain of interest, knowledge of the substrate–specific values of the largest achievable growth rates (coming e.g. from batch culture experiments) suffices to set up CAFBA in a generic medium where different types of limitation can be analyzed. Here we describe how CAFBA can be used to study different types of limitation in *E. coli*, e.g. for growth in a rich medium or in presence of a combination of carbon sources.

The first step to set up a CAFBA (as well as standard FBA) simulation is the definition of a growth medium, that is, the list of available substrates. For each of them, the lower bound of the corresponding exchange flux v_a should be set to a large negative value, e.g. -1000 mmol/g_{DW}h, describing an in–take. As usual, the lower bound of exchange fluxes of metabolites not available in the medium should be set to zero. Then, if one wants to study growth under limitation of substrate a, the corresponding proteome fraction $\Delta\phi_a = w_a|v_a|$ should be introduced explicitly in the CAFBA–specific proteome allocation constraint. Denoting by A the set of substrates that one is interested in limiting, the proteome allocation constraint takes the form

$$\sum_{a\in A} w_a|v_a| + \sum_{i\in E} w_i|v_i| + w_R\lambda = \phi_{\max} \ . \tag{S10}$$

The empirical substrate–specific maximum growth rate can be fixed by introducing a lower bound $w_{a,0}$ for each nutrient source (see Main Text and Supplementary Table B for an example). Limitation of the nutrient source a is then obtained by fixing w_a at a value $w_a > w_{a,0}$ (or by varying it so that $w_a > w_{a,0}$ always).

Example: phosphate limitation for E. coli MG1655

The results discussed in this work concern *E. coli* growth in a carbon minimal medium. Following the previous section, we describe here the detailed procedure to set up CAFBA (in the homogeneous case) for *E. coli* MG1655 strain in minimal glucose medium subject to phosphate limitation. *E. coli* is known to possess both passive and active Pi transporters, that are up-regulated in phosphate starvation [13]. Therefore, the phosphate in-take flux can be expected to depend on the extracellular phosphate level via a relation similar to the one holding for glucose, see Eq. (5) in the Main Text.

1. As described in the main text, the values of the CAFBA–specific parameters for MG1655 are $w_E = 1.55 \times 10^{-3}$ g_{DW}h/mmol, $w_R = 0.169$/h and $\phi_{\max} = 48.4\%$. With these choices the maximum growth rate $\lambda_{\max}$ of the cells, obtained when all nutrient–specific weights are set to zero, is about 0.7/h.
2. The standard minimal medium for the *iJR*904 model contains H_2O, O_2, CO_2, $NH_4{}^+$, H^+, Na^+, K^+, Fe^{++}, $HPO_4{}^{--}$, $SO_4{}^{--}$, plus the carbon source (in this case, glucose). We set the lower bound on the corresponding exchange fluxes to -1000 g_{DW}h/mmol.
3. We introduce both a glucose–specific weight w_C and an phosphate–specific weight w_P, which are both initially set to zero.
4. CAFBA solutions are computed with increasing values of w_C, until the growth rate matches the experimental growth rate in glucose minimal medium, about 0.65/h [14]. Call $w_{C,0}$ the corresponding value for the glucose weight.
5. Phosphate limitation is finally obtained by increasing w_P at fixed $w_C = w_{C,0}$.

Other types of limitation (e.g. nitrogen or oxygen) can be easily implemented by introducing the corresponding nutrient–specific weights.

Application to different *E. coli* strains or bacterial species

When applying CAFBA to other strains or species, the starting point is the corresponding contraint–based metabolic model, such as the ones available at the BiGG database [15]. The parameters w_R, $\phi_{\max}$ and the E–sector weights have then to be defined in order to set up the CAFBA proteome allocation constraint.

Slope of the R–sector The weight w_R is the slope of the R–sector of ribosome–associated proteins. For *E. coli*, the R–sector is linearly related to growth rate as $\phi_R \simeq \phi_{R,0} + w_R\lambda$. w_R is precisely the slope of the line, i.e. $w_R = \partial\phi_R/\partial\lambda$. This value can be obtained by measuring the amount of ribosomal proteins at different growth rates. In particular, w_R has been experimentally estimated to be close to 0.169 h for MG1655 strain [14] and 0.189 h for NCM3722 [16].

Fraction of allocable proteins The proteome fraction $\phi_{\max}$ corresponding to the total fraction of growth-rate dependent ("allocable") proteins. The numerical value is obtained by measuring the maximum variation of the growth rate sectors upon different kind of growth limitation. For *E. coli*, $\phi_{\max}$ has been estimated to be around 48.4% for the MG1655 strain [14] and 43% for the NCM3722 strain [16].

Definition of the E–sector. The first step is the definition of an E–sector. In CAFBA, the E–sector includes all intracellular metabolic reactions except for those relative to the carbon uptake system. As such, it does not represent a functionally homogeneous cluster of proteins that respond coherently upon modulating the growth conditions, like those identified in [4]. To each reaction i in the E–sector one should associate a weight w_i. We distinguish two cases:

Homogeneous case – All the weights w_i of the E–sector are fixed to the same value, w_E. The value of w_E has to be fixed so that the extrapolated *E. coli* growth rate in saturating carbon sources, corresponding to $w_C \to 0$, is 1/h as found in [16].

Heterogeneous case – Each w_i is sampled randomly and independently from a given probability distribution $p(w)$. The fluxes obtained as CAFBA solutions for many independent samples are then averaged. In principle, any probability distribution $p(w)$ can be chosen (e.g. $p \sim 1/w$, or a lognormal distribution). However, we find that different choices produce quantitatively similar results as long as the mean value $\langle w\rangle$ and the standard deviation $\sigma_w = \sqrt{\langle w^2\rangle - \langle w\rangle^2}$ are similar. The latter therefore appear to be the only key parameters. Similarly to w_E in the homogeneous case, $\langle w\rangle$ is chosen so as to reproduce the growth rate in saturating glucose (1/h). σ_w, instead, has to be adjusted so as to obtain a better qualitative fit with experiments. A discussion of the results obtained with different values for the standard deviation is presented in Note E.

We conclude this note with some observations about the definition of the E–sector and the choice of the parameters.

First, in our application to carbon limitation, many catabolic reactions (e.g. carbon–specific uptake systems such as *lac*, *gal*, etc.) were not included into the E–sector, since they are empirically known to be upregulated in carbon limitation [4], which places them in the C–sector. Their inclusion in the E–sector does not affect results, as it simply generates an extra cost for the E–sector proportional to the carbon uptake, thereby being effectively equivalent to a rescaling of w_C.

Concerning the choice of the other parameters, we note finally that besides the nutrient–specific weights lower bounds $w_{a,0}$, the number of parameters in the homogeneous and the heterogeneous case is three for the homogeneous case (w_E, w_R and ϕ_{max}), while it is four for the heterogeneous case (the same parameters, plus the width of the E–sector fluctuations). Note, however, that one of these parameters can be arbitrarily fixed due to the homogeneity of the proteome allocation constraint, whereas increasing (resp. decreasing) w_R is roughly equivalent to decreasing (resp. increasing) $\phi_{\max}$. Therefore, the effective number of free parameters reduces to one for the homogeneous case and to two for the heterogeneous case.

Note D. Translational inhibition and protein over–expression in CAFBA solutions

The proteome allocation constraint in the homogeneous case $w_i = w_E$ reads

$$w_C v_C + w_E \sum_i |v_i| + w_R \lambda = \phi_{\max} \tag{S11}$$

where 4 parameters occur, namely w_C, w_E, w_R and $\phi_{\max} = 1 - \phi_{C,0} - \phi_{R,0} - \phi_Q$. Since w_E is fixed so as to ensure that $\lambda = \lambda_{\max} = 1/\text{h}$ when $w_C = 0$, and since the above condition is invariant under a re-scaling of parameters, we are left with just two free parameters, namely w_R and $\phi_{\max}$. In the Main Text, we discuss the case in which they are fixed based on experiments [14]. Here we focus instead on how CAFBA solutions depend on them. Moreover, we study in detail how CAFBA solution allow to reproduce and extend the coarse–grained theory of proteome allocation developed in Ref. [14].

Growth rate

The Michaelis-Menten dependence of the growth rate on the quality of the nutrients is a classical finding due to Monod [17]. In the proteome partition model described in Ref. [14], the growth rate λ is found to be a Michaelis-Menten function of two parameters, namely the nutritional quality k_c and the translational capacity k_r. λ is also linearly dependent on the Q–sector proteome fraction (also incorporating overexpression of unnecessary proteins. In particular,

$$\lambda = (\phi_Q^{\max} - \phi_Q) \frac{k_c k_r}{k_c + k_r} \ . \tag{S12}$$

A similar result can be obtained through a fitting procedure in CAFBA. Identifying $w_C = 1/k_c$ and $w_R = 1/k_r$, the CAFBA-predicted growth rate turns out to be described with high accuracy by the expression

$$\lambda = \mu(\phi_Q^{\max} - \phi_Q) \frac{\left(1 - \frac{k_c^{\min}}{k_c}\right)}{1 + \frac{K_M^c}{k_c} + \frac{K_M^r}{k_r}} \ , \tag{S13}$$

where μ, $k_c^{\min}$, K_M^C and K_M^R are parameters whose values are listed in Table N1. Notice that λ is a Michaelis-Menten function of k_r for fixed k_c, and reduces to a Michaelis-Menten function of k_c for fixed k_r in the $k_c^{min} \ll k_c$ limit. This approximation works well if the growth rate is not too small ($\lambda \gtrsim 0.1/h$). Furthermore, λ decreases linearly with increasing ϕ_Q. Growth rate is shown in Fig. B as a function of k_c and k_r, together with acetate expression.

Fit results

Parameter	$k_c \leq k_{c,ac}$ ($\lambda \leq \lambda_{ac}$)	$k_c \geq k_{c,ac}$($\lambda \geq \lambda_{ac}$)
μ	3.39/h	3.51 /h
$k_c^{\min}$	0.808 mmol/g_{DW}h	1.79 mmol/g_{DW}h
K_M^c	35.0 mmol/g_{DW}h	42.5 mmol/g_{DW}h
K_M^r	3.34/h	3.44/h
$\phi_Q^{\max}$	91%	91%

Table N1: Fit results, Eqs. (S14) and (S15), expressed as a function of the parameters appearing in Eq. (S13). The value of $\phi_Q^{\max}$ is obtained directly fitting growth rate as a function of ϕ_Q, see Fig. N5. The value $k_{c,ac} \sim$ 200 mmol/g_{DW}his the value at which the acetate starts to be excreted, roughtly at $\lambda_{ac} \sim 0.8$/h. All results are obtained with $w_E = 0.00083$ and $\phi_{R,0} = 6.6\%$. Note that $\phi_Q^{\max}$ is less than $(1 - \phi_{R,0}) = 93.4\%$, due to the basal enzymatic proteome fraction ϕ_E induced by the ATP mantainence flux.

The values of the parameters in Eq. (S13) are obtained by a sequence of steps. We first assume the linear relation $k_r/\lambda = f_1(k_c) \cdot k_r + f_2(k_c)$. This relation is tested for different values of k_c, thus defining the

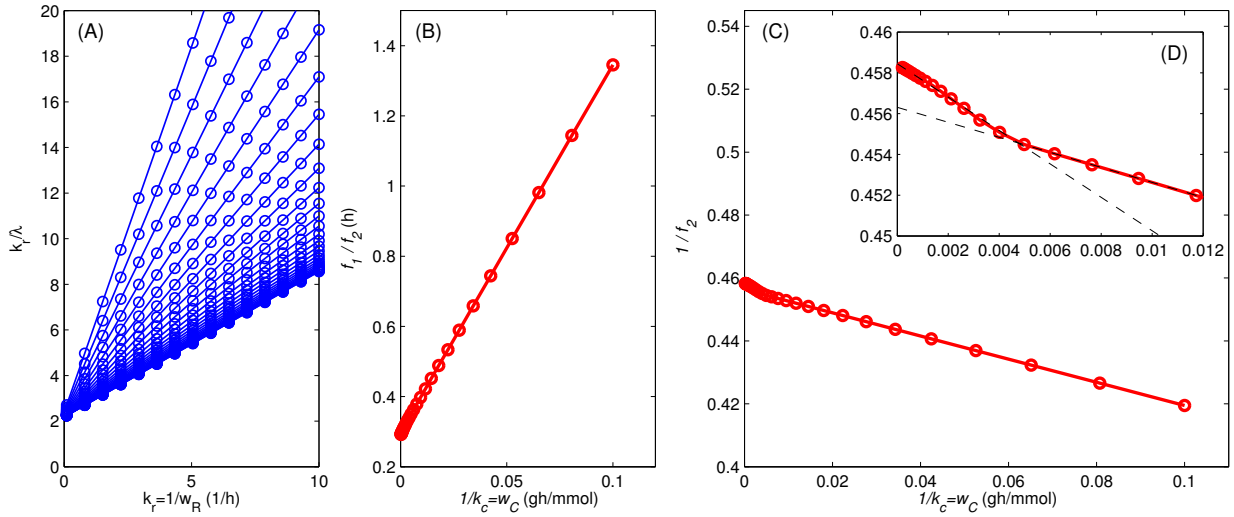

Figure N3: (**A**): k_r/λ against k_r for different values of k_c. For each k_c, k_r/λ is a linear function of k_r with slope $f_1(k_c)$ and y–intercept $f_2(k_c)$. (**B**): f_1/f_2 plotted against $1/k_c$, see Eq. (S14). (**C**): $1/f_2$ plotted against $1/k_c$, see Eq. (S15). Inset (**D**) shows a zoom on the crossover at $k_{c,ac} \sim 200$ mmol/g_{DW}h($w_{C,ac} \sim 0.005$ g_{DW}h/mmol). The dashed lines are linear fits performed on all points before or after the one at $w_{C,ac}$.

two functions f_1 and f_2. Then, we impose the following linear relations:

$$f_1/f_2 = c_1 + c_2 \frac{1}{k_c} \ , \tag{S14}$$

$$1/f_2 = c_3 - c_4 \frac{1}{k_c} \ . \tag{S15}$$

The minus sign in Eq. (S15) allows to consider positive definite constants $c_1, \ldots, c_4$. The parameters in Eq. (S13) are then obtained as $\mu(\phi_Q^{\max} - \phi_Q) = c_3/c_1$, $k_c^{\min} = c_4/c_3$, $K_M^c = c_2/c_1$ and $K_M^r = 1/c_1$. Finally, the prefactor μ is obtained by solving CAFBA for different values of ϕ_Q (see Fig. N5).

The fitting procedure is illustrated in Fig. N3. The results of the fit are impressively good from very low growth rates to the acetate switch growth rate, $\lambda_{ac} \sim 0.9/h$ ($k_{c,ac} \sim 200$).For $k_c \gtrsim k_{c,ac}$ the coefficients in Eqs. (S14) and (S15) depend on k_c. A good approximation is obtained fitting separately the parameters for $k_c < k_{c,ac}$ and $k_c > k_{c,ac}$.

The nonzero value of k_c^{min} is due to the ATP mantainence flux, which forces the carbon intake flux to be strictly positive also at zero growth rate. We see that $k_c^{\min} \ll K_M^c$, implying that the the mantainence flux only affects the growth rate at low growth rates. Most importantly, we see that when carbon overflow sets in the cell switches to a metabolism with larger maximum growth rate, $\lambda_{\max} = \mu \times (\phi_Q^{\max} - \phi_Q)$, but smaller affinity for the carbon source (that is, a larger Michaelis constant K_M^c). This is in agreement with the idea that the cell should use low-quality carbon nutrients very efficiently (with the highest possible growth yield), whereas it should grow as fast as possible in presence of high-quality nutrients.

Proteome fractions

The effect of carbon limitation and translational inhibition on the optimal proteome allocation is summarized in Main Figure 1. Results match those obtained in Ref. [14]. In particular, the ribosomal proteome fraction ϕ_R is found to anticorrelate with the growth rate upon antibiotic-induced translational limitation [14]. This is also consistent with Eq. (S13), as one can easily verify upon expressing k_r as a function of λ for fixed k_c.

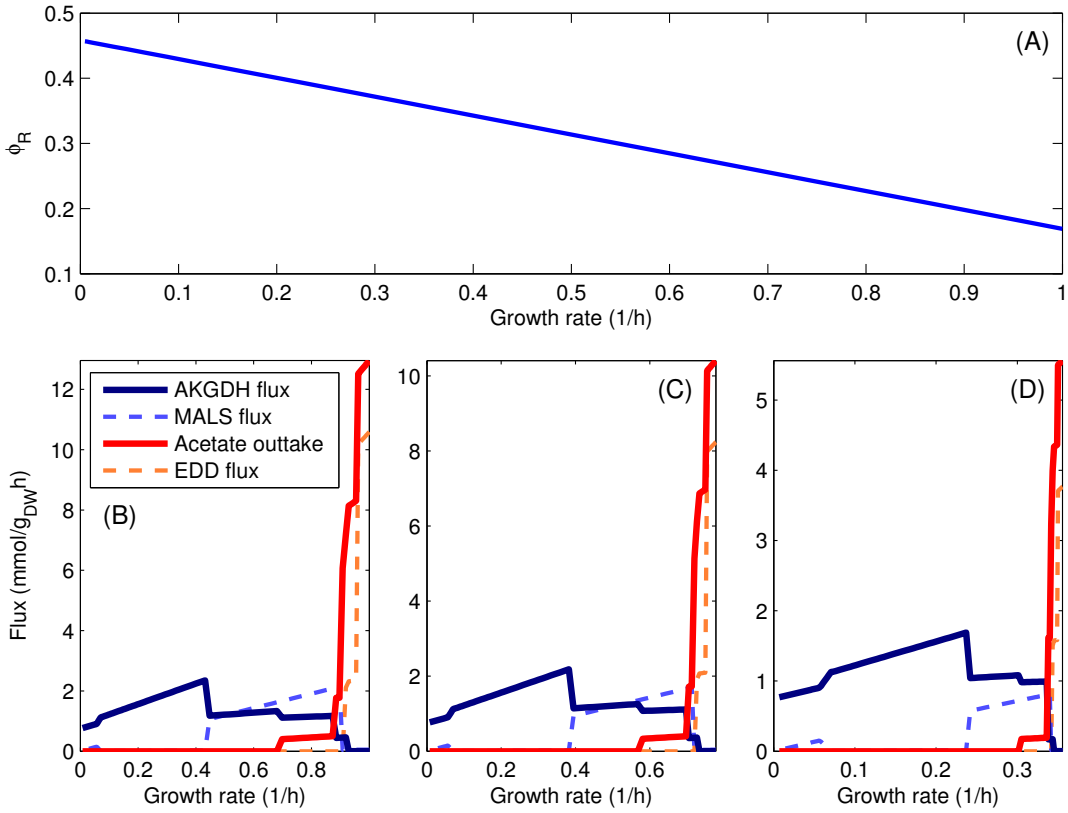

Figure N4: (**A**): ribosomal proteome fraction ϕ_R as a function of growth rate $\lambda_{\max}$, obtained by solving CAFBA with $w_C = 0$ and varying $w_R = 1/k_r$ (translational limitation). Bottom panels: fluxes as a function of λ for different values of w_R (from left to right: w_R =0.169 h (**B**), 0.3 h (**C**) and 1 h (**D**)) obtained by varying the degree of carbon limitation through w_C.

Defining $\hat{\lambda} = \lambda_{max}(k_c - k_c^{\min})/(k_c + K_M^c)$ and $\hat{K}_M^r = K_M^r k_c/(k_c + K_M^c)$ we have:

$$\lambda = \hat{\lambda}\frac{k_r}{k_r + \hat{K}_M^r} \quad \longrightarrow \quad k_r = \hat{K}_M^r \frac{\lambda}{\hat{\lambda} - \lambda} \tag{S16}$$

$$\Rightarrow \quad \phi_R = \left(\phi_{R,0} + \frac{\hat{\lambda}}{\hat{K}_M^r}\right) - \frac{\lambda}{\hat{K}_M^r} \tag{S17}$$

We see that $\hat{\lambda}/\hat{K}_M^r$ is only weakly dependent on k_c, so that the y-intercept of ϕ_R is almost constant, $\phi_R \sim \lambda_{max}/K_M^r \sim (\phi_Q^{\max} - \phi_Q)$, since $\mu \sim K_M^r$ (see Table N1). On the other hand, $\hat{K}_M^r$ increases with the nutritional quality k_c, as also shown in Ref. [14].

Fluxes and Q–limitation

Figures N4 and N5 detail how the pattern of single fluxes obtained in carbon limitation change in response to variations of w_R and $\phi_{\max}$, respectively. In both cases fluxes approximately rescale with λ, without any significant modification in the flux patterns. CAFBA predictions for both translational limitation and overexpression of unnnecessary proteins (modeled increasing ϕ_Q) therefore reduce approximatively to a rescaling of both growth rate and the fluxes with the same scaling factor, $v_i \propto (\phi_Q^{\max} - \phi_Q)$, with $\phi_Q^{\max} = 91\%$.

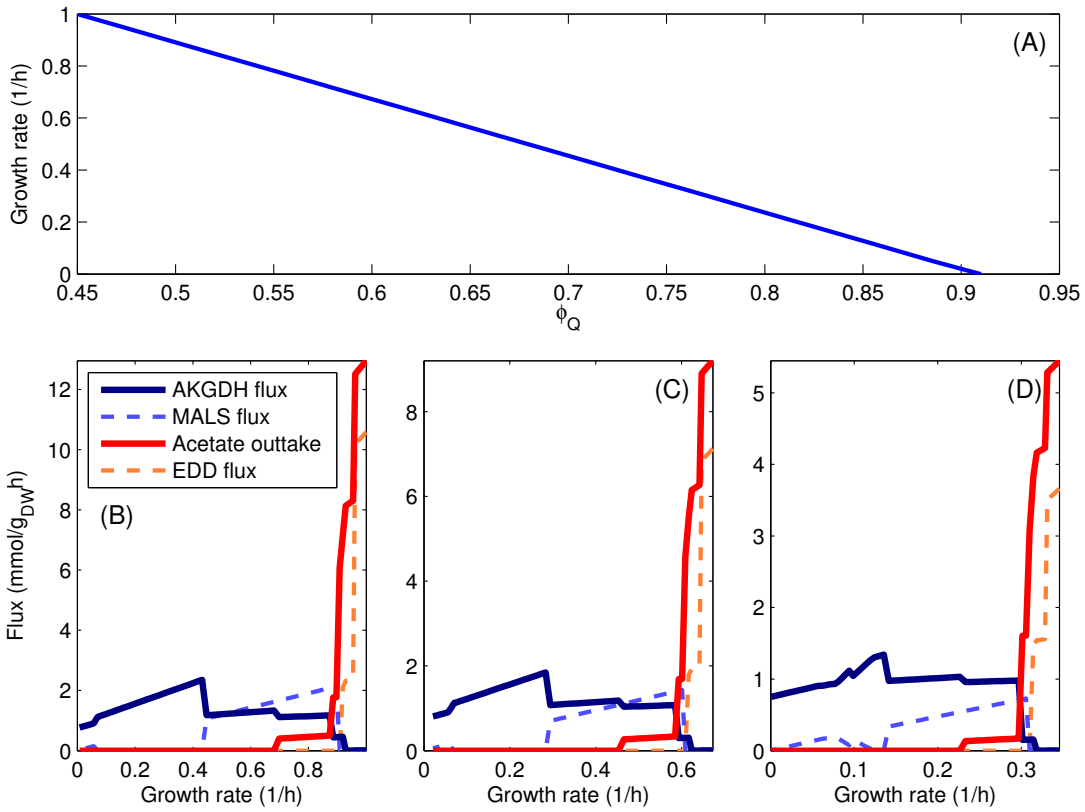

Figure N5: (**A**): growth rate λ in saturating glucose ($w_C = 0$) computed with CAFBA as a function of ϕ_Q. Note that $\lambda = 1.0$/h at $\phi_Q = 0.45$, and decreases linearly with ϕ_Q. **Bottom** panels: fluxes as a function of λ for three different values of ϕ_Q (from left to right: ϕ_Q =45% (**B**), 60% (**C**) and 75% (**D**)) obtained by varying the degree of carbon limitation through w_C.

Note E. Case of inhomogeneous proteome costs

The growth rate–dependent enzymatic proteome fraction reads

$$\Delta\phi_E = \sum_{i\in\text{int.}} w_i|v_i| \quad . \tag{S18}$$

In order to go beyond the homogeneous case $w_i = w_E \equiv 0.00083$ $\text{g}_{\text{DW}}\text{h/mmol}$ for all i, we have considered an inhomogeneous scenario in which w_i's are quenched random variables and final results are obtained by averaging over many instances of CAFBA, each with different choices of w_i's. Here we characterize this scenario more precisely.

We have chosen to draw the logarithm of each weight w_i independently from a box distribution of the form

$$p\big(\log_{10}(w_i)\big) = \begin{cases} \frac{1}{\delta} & \log_{10}(\bar{w}) - \frac{\delta}{2} \le \log_{10}(w_i) \le \log_{10}(\bar{w}) + \frac{\delta}{2} \\ 0 & \text{otherwise} \end{cases} \quad , \tag{S19}$$

where $\bar{w}$ and δ are parameters. This corresponds to a probability density function $p(w_i) \propto 1/w_i$ for $w_i \in [\bar{w}\cdot 10^{-\delta/2}, \bar{w}\cdot 10^{\delta/2}]$. δ representes therefore the number of decades spanned by the weights. The average value $\langle w\rangle$ is related to the parameters $\bar{w}$ and δ by

$$\langle w\rangle = \bar{w}\frac{10^{\delta/2} - 10^{-\delta/2}}{\delta \log_e 10} \quad . \tag{S20}$$

One can see that $\lim_{\delta\to 0}\langle w\rangle = \bar{w}$. We checked for possible biases in our analysis by comparing the results with the ones obtained using a lognormal distribution. As shown in Fig. C, the two distributions yield similar results, provided that the variance of the logarithms of the weights is the same.

Averages are computed by defining a number of replicas of the model, each one with a different realization of the coefficients $\{w_i\}$, computing the CAFBA solutions for each realization, and then averaging the resulting fluxes. This procedure will also generate a distribution for the growth rate. For small δ, it turns out to be peaked around the growth rate corresponding to $\langle w\rangle = \bar{w}$, but in general the mean growth rate will depend on δ. In practice, the parameter $\bar{w}$ is be chosen as to keep $\langle\lambda\rangle$ to a prescribed value, e.g. 1/h.

Sample to sample fluctuations and fluctuations in the weights

In this section we describe the effect of increasing the width of the fluctuations on the weights w_i. As we noted before, if we only fix the average weight $\langle w\rangle$, the average growth rate depends on δ, making CAFBA solutions more difficult to compare. Therefore, for sakes of clarity, *only in this section* we rescaled the weights w_i such that the maximum growth rate is $\lambda_{\max} = 1/\text{h}$ for all the different synthetic strains. Fig. N6 shows the sample–to–sample fluctuations in αKG dehydrogenase flux and in acetate excretion, along with the average values. The top panels (**A**) and (**B**) show the samples obtaines without rescaling the strains, while the bottom panels (**C**) and (**D**) are produced using such procedure. The results are very similar, although the rescaling reduces dramatically the variance of the growth rate at fixed w_C.

We have furthermore carried out a systematic study of how CAFBA solutions depend on the parameter δ. In particular, we have studied the averaged CAFBA solutions in glucose minimal medium, fixing the maximum growth rate to 1/h and using different values of δ, ranging from 0 (no randomization) to 4 ($w_{\max}/w_{\min} = 10^4$). Results are shown in Fig. N7 and N8. As the width δ of fluctuations is increased, transitions between pathways are progressively smoothed. For $\delta \sim 1$ the average acetate excretion grows as a linear function of growth rate, starting from $\lambda \sim 0.7/\text{h}$. As δ is increased above 1, a general decrease in growth yield is observed, with increasing average glucose uptake and excretions of intermediate metabolites (mainly dihydroxyacetone and formate). Moreover, solutions are highly heterogeneous from sample to sample, as measured by the standard deviation of the fluxes σ_v. This quantity is obtained by first computing the standard deviation of sample–to–sample fluctuations of a single flux, and then averaging over all reaction whose weight w_r is larger than zero:

$$\sigma_v = \frac{1}{N_r}\sum_{r:w_r>0}\sigma_v^r \quad \text{with} \quad \sigma_v^r = \sqrt{\left(\frac{1}{N_s}\sum_s v_{r,s}^2\right) - \left(\frac{1}{N_s}\sum_s v_{r,s}\right)^2} \tag{S21}$$

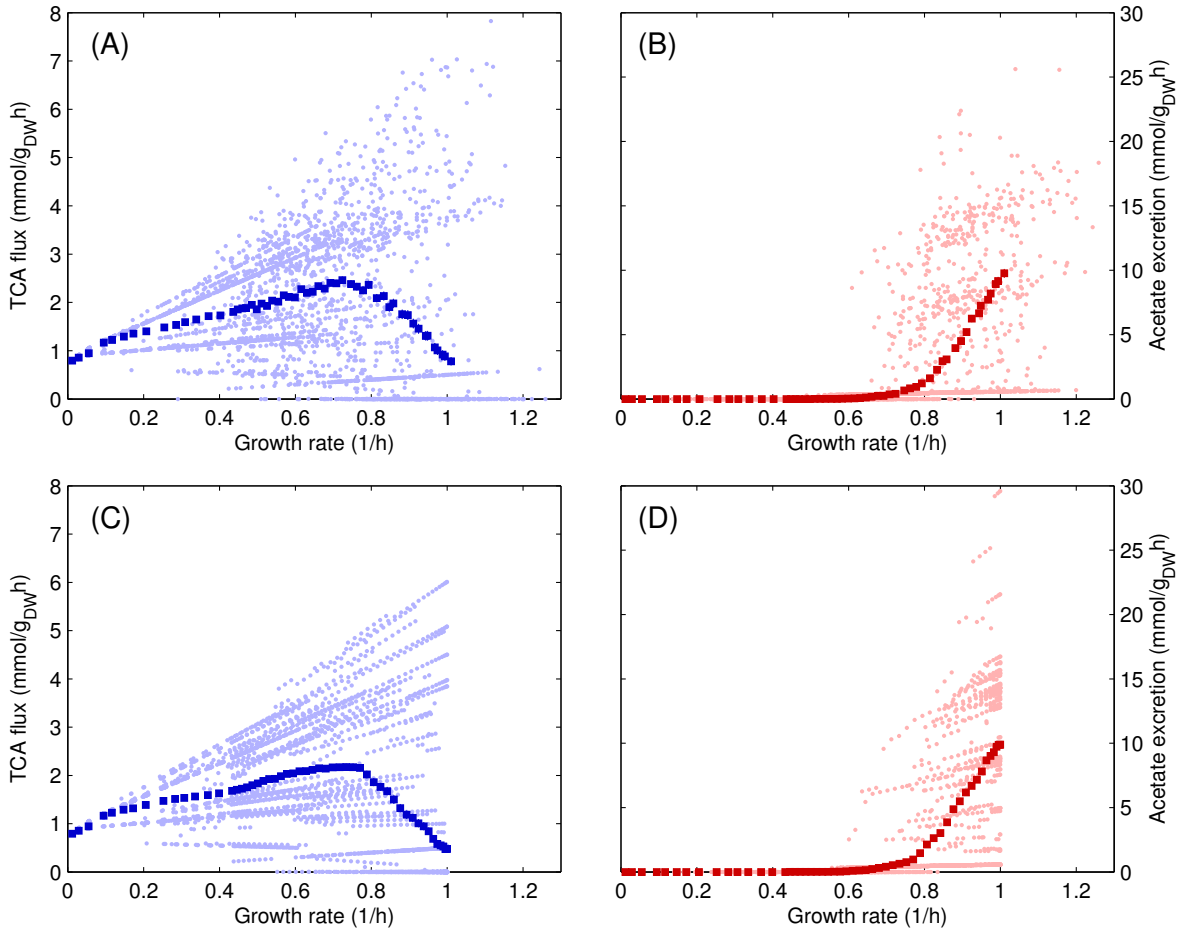

Figure N6: Sampled fluxes for the randomized models, using $\delta = 1$. The pale dots are the actual sampled fluxes, while the squares are the average of fluxes for a given w_C. Each of the $N_s = 500$ copies of the model has been sampled for 54 different values of w_C. Top panels (**A** and **B**): Indipendent extractions ($N_p \times N_s$) of the weights. Bottom panels (**C** and **D**): Each of the 500 copy of the model had the weights rescaled such that maximum growth rate is 1/h. Both procedures yield similar results, apart for the fluctuations in the growth rate. Only a subset of the sampled fluxes (50 out of 500 for each value of w_C) is shown for clarity. See text for details.

where v_r^s is the flux of reaction r in the sample s. As shown in Fig. N8, the heterogeneity of the fluxes increases with δ and with growth rate (since fluxes are generally proportional to growth rate itself).

In conclusion, we observe that exmpirical evidence is better reproduced by values of δ close to one, and we will therefore use this value throughout the rest of the study.

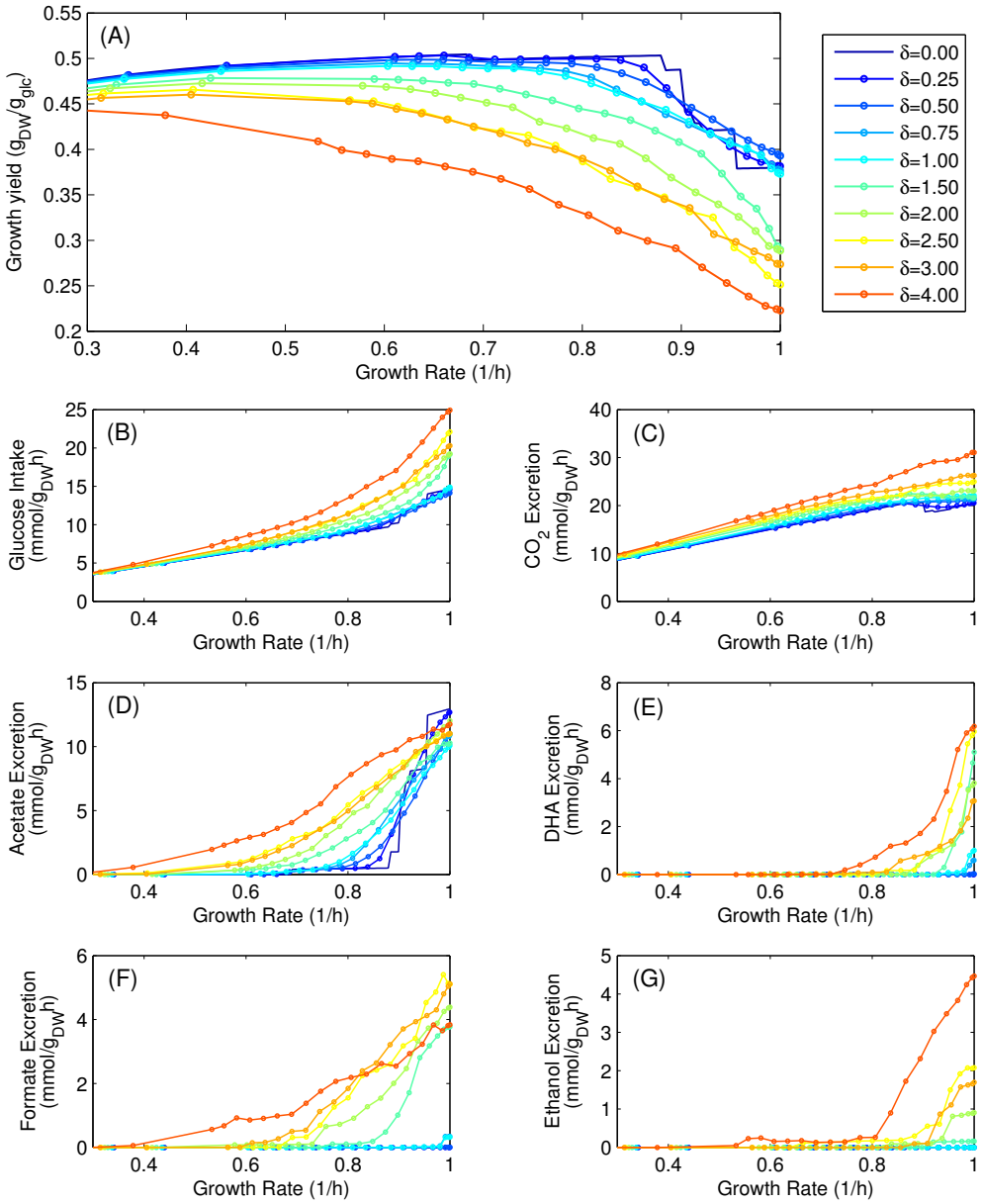

Figure N7: Average value of growth yield and exchange fluxes versus growth rate, for different values of $\delta = \log_{10}(w_{\max}/w_{\min})$, from top to bottom: (**A**) growth yield, (**B**) glucose uptake, (**C**) CO2 excretion, (**D**) acetate excretion, (**E**) formate excretion, (**F**) dihydroxiacetone (DHA) excretion and (**G**) ethanol excretion. The $\delta = 0$ case corresponds to the non-randomized case. For each value of w_C and δ, the averages fluxes (using 200 samples for each point) are indicated with circles (error bars not shown for clarity). Weights have been reascaled as to fix the maximum growth rate to 1/h.

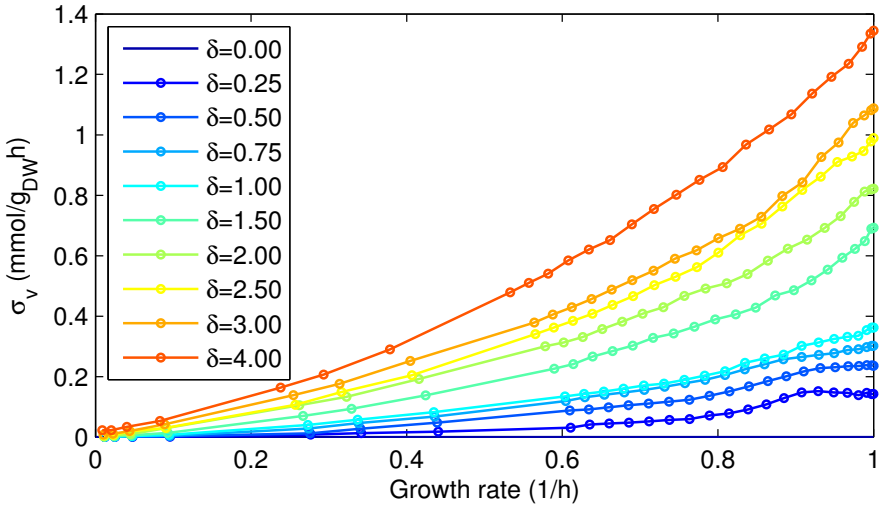

Figure N8: Average standard deviation σ_v of the fluxes, as a function of the average growth rate for different values of δ. Flux variability increases with both growth rate and δ.

Note F. Growth-dependent biomass composition

Growth rate–dependent biomass composition produces a nonlinear optimization problem, which is no longer solvable using the standard linear programming tools. We will first show how one can account for a growth–rate dependent biomass composition, and then we will describe how it can be straightforwardly implemented as a sequence of LP problems in Sect. .

A growth–rate dependent biomass composition can be easily accounted for in CAFBA and, more in general, in constraint–based metabolic models. Let us denote by β_μ the stoichiometric coefficient corresponding to the amount of metabolite μ required to build one gram of dry weight (corresponding, for instance, to the coefficients given in the iJR904 model). The mass fraction of metabolite μ, ψ_μ, is obtained multiplying β_μ by μ's molecular mass. Because the cell's composition changes with λ, β_μ's are, in general, functions of the growth rate. For sakes of simplicity, we have characterized the biomass composition by dividing biomass components and their corresponding β_μ in four classes:

- β_{AA} is the total amount of amino acids per unit of dry weight;
- β_{DNA} is the total amount of DNA nucleotides (DATP, DCTP, DGTP,DTTP) per unit of dry weight;
- β_{RNA} is the total amount of RNA nucleotides (ATP,CTP,GTP,UTP) per unit of dry weight;
- β_{LIP} denotes the amount of lipids, liposaccharides and similar biomass constituents (see Table N2).

The individual stoichiometric coefficients for metabolite μ change with λ as

$$\beta_\mu(\lambda) = \beta_{X[\mu]}(\lambda)\frac{\beta_\mu}{\sum_{\nu\in X[\mu]}\beta_\nu}\ , \tag{S22}$$

where $X[\mu] \in \{AA, RNA, DNA, LIP\}$ denotes the class to which metabolite μ belongs.

All remaining stoichiometric coefficients for biomass components are chosen as in the iJR904 model. They are mainly cofactors or other components with very small biomass fractions: 5–methyltetrahydrofolate, acetyl–CoA, CoA, FAD, NAD, NADH, NADP, NADPH, Succinyl–CoA and UDP–glucose. Together, they account for a mass M_{other} which is roughly $\sim 2.5\%$ of total dry weight mass.

In order to provide plausible β functions we have to consider two constraints. Let us define $\psi_X = M_X/M_{DW}$. These quantities are related to the β functions through the molecular masses of the biomass

components. The first one is the normalization of the total mass of the cell:

$$\psi_{AA} + \psi_{DNA} + \psi_{RNA} + \psi_{LIP} = 1 - \psi_{other} \ . \tag{S23}$$

The second constraint is the linear relation between the RNA/protein mass ratio and growth rate λ [18]. The biomass functions $\beta(\lambda)$ we choose must satisfy such empirical constraint, which can be written as [14]:

$$R(\lambda) = \psi_{RNA}/\psi_{AA} = r_0 + \lambda/\kappa_t \ , \qquad r_0 = 0.087 \pm 0.009 \ , \qquad \kappa_t = 4.5 \pm 0.2/\mathrm{h} \ . \tag{S24}$$

Therefore, we have to fix two ψ functions, for instance ψ_{DNA} and ψ_{LIP}, while the other two can be computed using using the constraints Eqs. (S23) and (S24). These four ψ–functions are listed in Table N3 and plotted against growth rate in Fig. N11.

Implementation of a growth-dependent biomass composition in CAFBA

Growth rate–dependent biomass coefficients cannot be directly included in CAFBA (or FBA), since the resulting problem is no longer linear. On the other hand, one can treat this case as a sequence of LP problems with constant biomass composition along the following lines:

1. Initiate by fixing a growth rate λ_0 and computing the biomass coefficients $\beta(\lambda_0)$, e.g. via the prescriptions shown in Table N3 for the main biomass groups and Eq. (S22) for the individual stoichiometric coefficients.

2. At each step k, compute the growth rate λ_k by solving CAFBA with biomass coefficients $\beta(\lambda_{k-1})$;

3. Iterated until $\lambda_k - \lambda_{k-1}$ is smaller than a fixed threshold (in our case, 10^{-4}/h).

This method is found to converge very rapidly to the optimal solution, see Fig. I. In particular, the difference $|\lambda_k - \lambda_{k-1}|$ decreases exponentially with the number of steps k. This procedure is performed keeping all other parameters fixed. For instance, in the case of carbon limitation, the procedure must be performed individually for each value of w_C. A good initial guess λ_0 for the growth rate can speed up the calculation, although providing an intermediate value (e.g. 0.6/h for all w_C's) works well in practice.

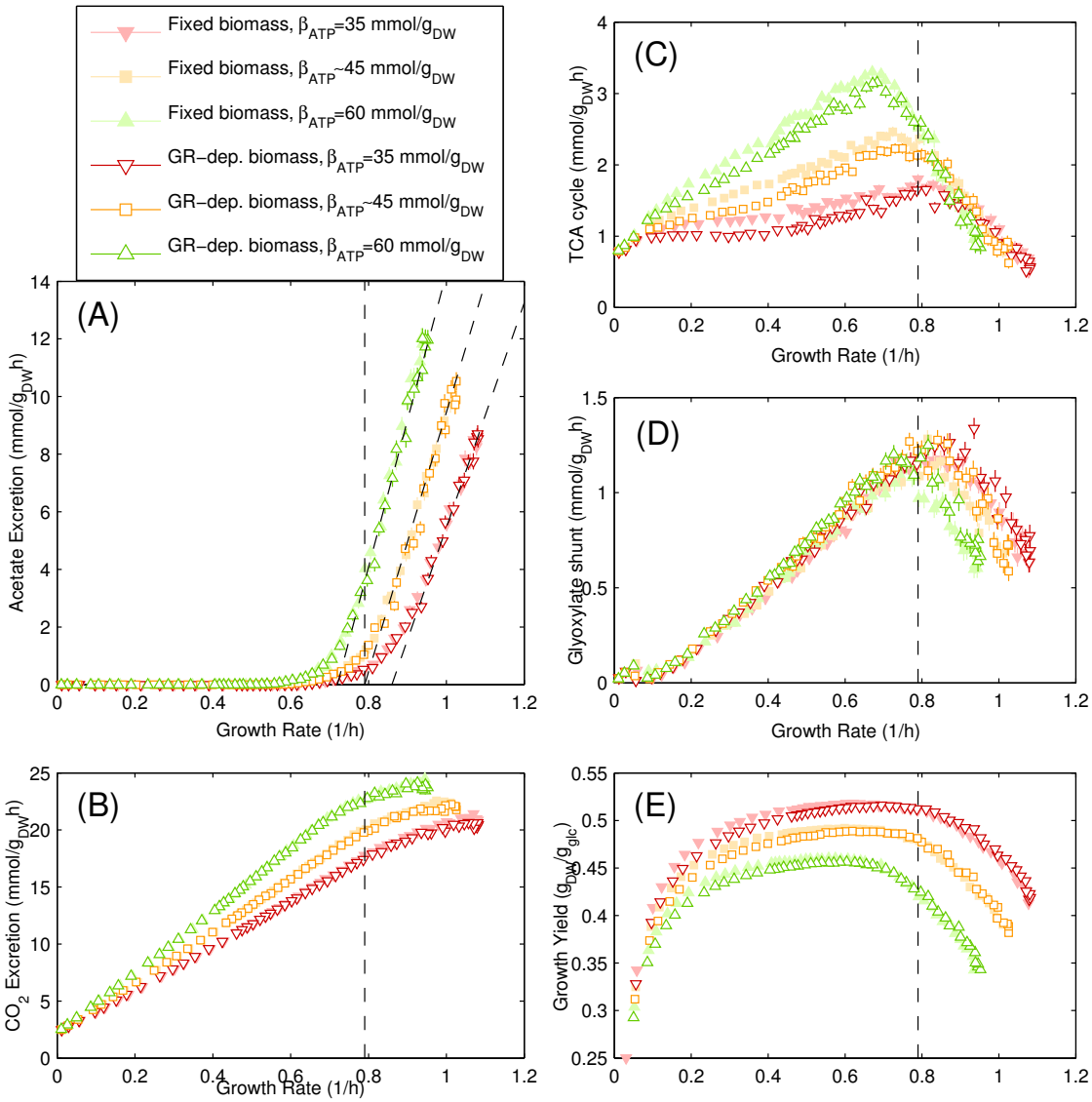

Figure N9: Representative fluxes obtained by CAFBA for *E. coli* growth in glucose minimal medium with constant (filled red, yellow and green markers) and variable (in open red, yellow and green markers) biomass composition for three different values of the λ-dependent ATP hydrolysis rate $\beta_{\rm ATP}$. (A) Acetate secretion rate, (B) CO_2 secretion rate, (C) flux through TCA cycle (αKG dehydrogenase), (D) flux through glyoxylate shunt (Malate synthase), (E) growth yield. No significant differences are observed between the constant and λ-dependent cases for $\beta_{\rm ATP} = 45.5608$ mmol$_{\rm ATP}$/g$_{\rm DW}$, corresponding to the default value for the iJR904 model. We also show, for comparison, results obtained for larger and smaller values of $\beta_{\rm ATP}$. The acetate secretion rate can always be fitted by a linear function of λ, i.e. $v_{\rm ac} = s \times (\lambda - \lambda_{\rm ac})$, albeit with different slopes and intercepts. The three dashed lines correspond to $s = 39, 45, 51$ mmol/g$_{\rm DW}$, respectively, while $\lambda_{\rm ac} = 0.86, 0.79, 0.72$/h, respectively. We also indicate $\lambda_{\rm ac} = 0.79$/h with a vertical dashed line in all panels. In all cases we set $\langle w \rangle = 8.8 \times 10^{-4}$ gh/mmol, $w_C \geq 0$ and $w_{\rm max}/w_{\rm min} = 10$.

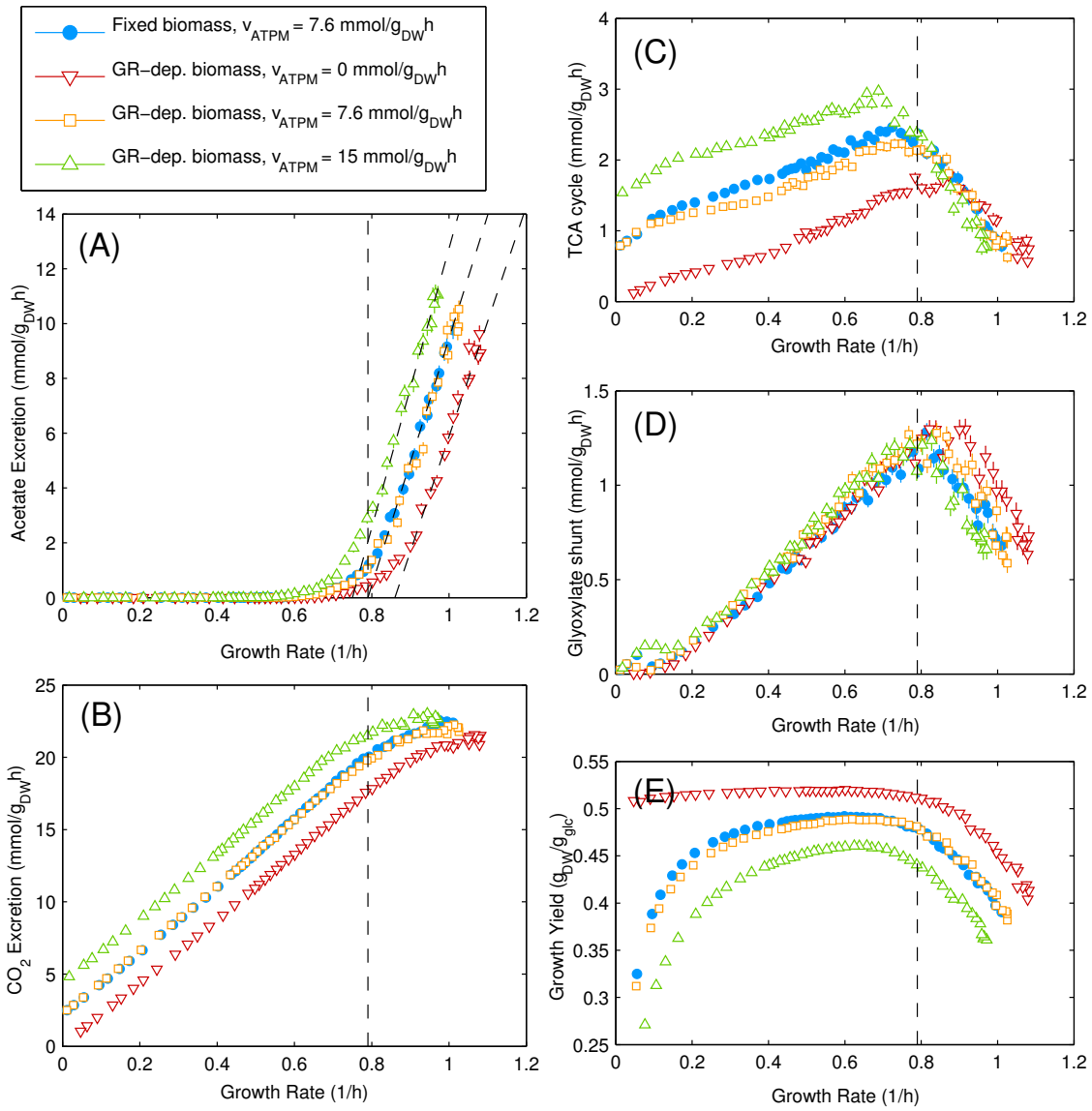

Figure N10: Representative fluxes obtained by CAFBA for *E. coli* growth in glucose minimal medium with constant (filled red, yellow and green markers) and variable (in open red, yellow and green markers) biomass composition for three different values of the λ-independent ATP hydrolysis rate $v_{\rm ATPM}$). (A) Acetate secretion rate, (B) CO_2 secretion rate, (C) flux through TCA cycle (αKG dehydrogenase), (D) flux through glyoxylate shunt (Malate synthase), (E) growth yield. Results are similar to the case shown in Fig. N9, where β_E is varied instead. The acetate secretion rate can always be fitted by a linear function of λ, i.e. $v_{\rm ac} = s \times (\lambda - \lambda_{\rm ac})$, albeit with different slopes and intercepts. The three dashed lines correspond to $s = 42, 45, 51$ mmol/g$_{\rm DW}$, respectively, while $\lambda_{\rm ac} = 0.86, 0.79, 0.75$/h, respectively. We also indicate $\lambda_{\rm ac} = 0.79$/h with a vertical dashed line in all panels. In all cases we set $\langle w \rangle = 8.8 \times 10^{-4}$ gh/mmol, $w_C \geq 0$ and $w_{\rm max}/w_{\rm min} = 10$.

#	Name	β (mmol/g_{DW})	m (g/mol)	Mass fraction (%)
227	Cardiolipin (LP)	0.000129	69708	0.9
576	Phosphatidylethanolamine (PE)	0.001935	35656	6.9
580	Phosphatidylglycerol (PG)	0.000464	37155	1.72
614	Phosphatidylserine (PS)	0.000052	37805	0.20
406	Glycogen	0.154	162	2.5
489	Lipopolisaccharide	0.0084	3877	3.25
579	Peptidoglycan subunit (murein)	0.0276	990.4	2.73
616	Putrescine	0.035	90	0.315
662	Spermidine	0.007	148	0.1

Table N2: Stoichiometric coefficients β of lipids (LP+PE+PG+PS), lipopolysaccarides, glycogen, murein, putrescine and spermidine in the iJR904 model (the first column gives the metabolite's ID in the reconstruction).

Function (mmol/g_{DW})	Reference
$\psi_{DNA}(\lambda) = 0.06\dfrac{1+\lambda^2}{1+3\lambda^2}$	See Ref. [19]
$\psi_{LIP}(\lambda) = \dfrac{0.27+0.14\lambda}{1+2\lambda}$	See Ref. [20]
$\psi_{AA}(\lambda) = \dfrac{1}{1+R(\lambda)} \times [1-\psi_{other}-\psi_{DNA}(\lambda)-\psi_{LIP}(\lambda)]$	See Refs. [20] (low growth rates) and [21] (high growth rates)
$\psi_{RNA}(\lambda) = \dfrac{R(\lambda)}{1+R(\lambda)} \times [1-\psi_{other}-\psi_{DNA}(\lambda)-\psi_{LIP}(\lambda)]$	See Refs. [20] (low growth rates) and [21] (high growth rates)

Table N3: Formulas for the mass fractions ψ of various biomass groups: proteins (AA), RNA, DNA and lipids (LIP). Here $R(\lambda)$ is the experimental RNA/protein mass ratio, Eq. (S24). In all formulas, λ is to be expressed in units of 1/h. The functions are plotted in Fig. N11. In the "Reference" column some references which were used to build the functions are shown. We also use $\psi_{other} = 2.5\%$.

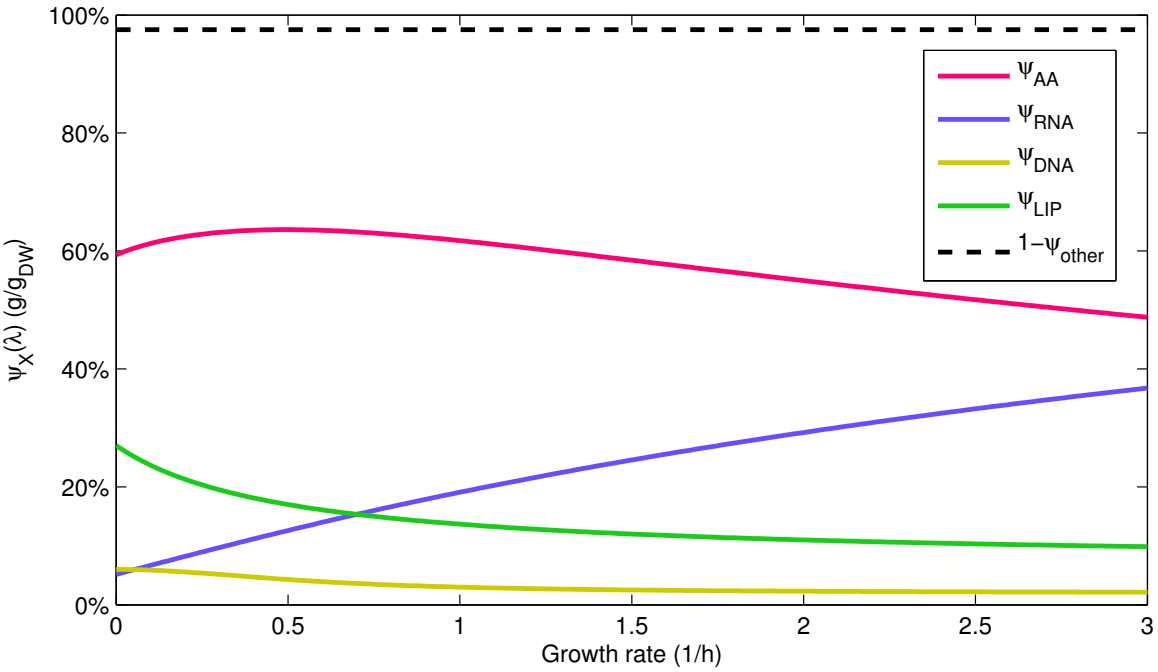

Figure N11: Plots of the four $\psi(\lambda)$ functions (ψ_{AA}, ψ_{RNA}, ψ_{DNA}, ψ_{LIP}) which fix the mass fraction of each biomass sector. The functions are further described in the text and in Table N3.

Supplementary Tables

Carbon source	$\lambda_{\max}$ (1/h)
Glucose	1.000
Lactose	0.984
Mannose	0.987
Maltose	0.991
Sucrose	1.005
Galactose	0.990
Fructose	1.000
Mannitol	1.009
Sorbitol	1.010
Glucose-6P	1.075
Mannose-6P	1.075

Table A: Extrapolated maximum growth rates $\lambda_{\max}$ for a variety of carbon sources using $w_C = 0$ and $w_E = 8.3 \times 10^{-4}$ g_{DW}h/mmol. In this conditions the proteome fraction of the C-sector is at its minimum, $\phi_C = \phi_{C,0}$ and $\Delta\phi_C = 0$, while growth is limited by the E– and R–sectors only. In this case the CAFBA constraint reads $\Delta\phi_E + \Delta\phi_R = \phi_{\max}$ with $\Delta\phi_E = \sum_r w_r|v_r|$ and $\Delta\phi_R = w_R\lambda$. $\lambda_{\max}$ is, by definition, the x–axis intercept of the C–line (see Fig. 1B). All non–phosphorylated carbon sources have similar C–lines, as seen by $\lambda_{\max}$ consistently being between 0.984 and 1.01/h. Glucose–6P and mannose–6P can provide a larger maximum growth rate due to the extra ATP they generate per flux unit. CAFBA solutions are computed using $w_i = w_E = 8.3 \times 10^{-4}$ g_{DW}h/mmol for all E–sector reactions, $w_R = 0.169$ h and $\phi_{\max} = 48.4\%$.

Carbon source	$\lambda_{\exp}$ (1/h)	$w_{C,0}$ (g_{DW}h/mmol)	$\Delta\phi_C$
Mannose	0.41	5.67×10^{-2}	26.4%
Sorbitol	0.46	5.09×10^{-2}	24.6%
Fructose	0.61	2.57×10^{-2}	17.3%
Maltose	0.67	3.8×10^{-2}	14.0%
Glucose	0.85	6.38×10^{-3}	6.0%
Lactose	0.98	2.7×10^{-4}	0.2%

Table B: Carbon limitation is modeled in CAFBA by varying the parameter w_C, which sets the C–sector fraction per carbon flux unit, or C–sector weight. We report here a set of experimental growth rates $\lambda_{\exp}$ from Ref. [16], obtained for an *E. coli* NCM3722 strain in batch culture for different carbon sources (minimal medium). For each carbon source a lower bound $w_{C,0}$ to the C-sector weight exists, so that CAFBA growth rate equals $\lambda_{\exp}$ at $w_C = w_{C,0}$. Reduced external concentrations of the nutrient are modeled by using an increased value of $w_C \geq w_{C,0}$, as described in the Main Text. In the last column we show the value of $\Delta\phi_C = w_C v_C$ at $w_C = w_{C,0}$, i.e. at the maximum growth rate allowed for the specific carbon source.

Model	Growth indep. ATP hydr. flux (v_{ATPM})	Growth dep. ATP hydrolysis (β_{ATP})
iJR904	7.6 mmol/g_{DW}h	45.5608 $\text{mmol}_{\text{ATP}}/g_{DW}$
iAF1260	8.39 mmol/g_{DW}h	59.806 $\text{mmol}_{\text{ATP}}/g_{DW}$
iJO1366	3.15 mmol/g_{DW}h	53.95 $\text{mmol}_{\text{ATP}}/g_{DW}$

Table C: *E. coli* metabolic models include an ATP hydrolysis flux $v_{ATP} = v_{ATPM} + \beta_{ATP}\lambda$ to model the energy requirements of the cell. We show here the values of v_{ATPM} and of β_{ATP} for the three models *iJR*904 [22], *iAF*1260 [23] and *iJO*1366 [24].

Supplementary Figures

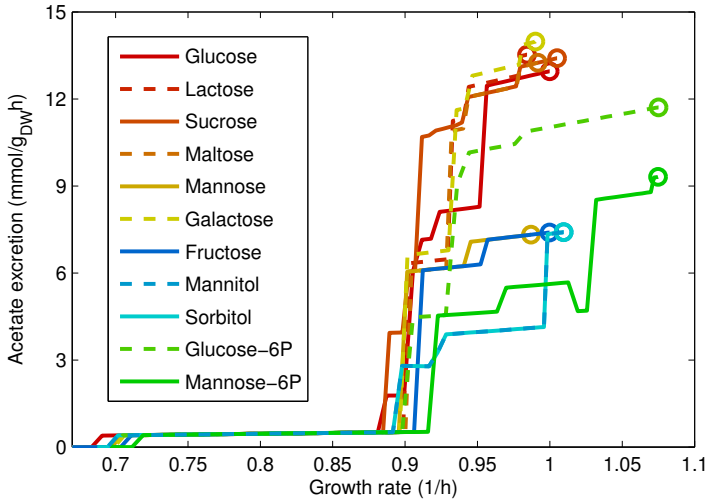

Figure A: Acetate excretion for a variety of carbon sources with uniform weights plotted against growth rate, using $w_E = 8.3 \times 10^{-4}$ $g_{DW}h/mmol$ and $w_C \geq 0$. In particular, the circles indicate the acetate production at the maximum growth rate λ_{max}, obtained for $w_C = 0$. See Table A for the numeric values of λ_{max}.

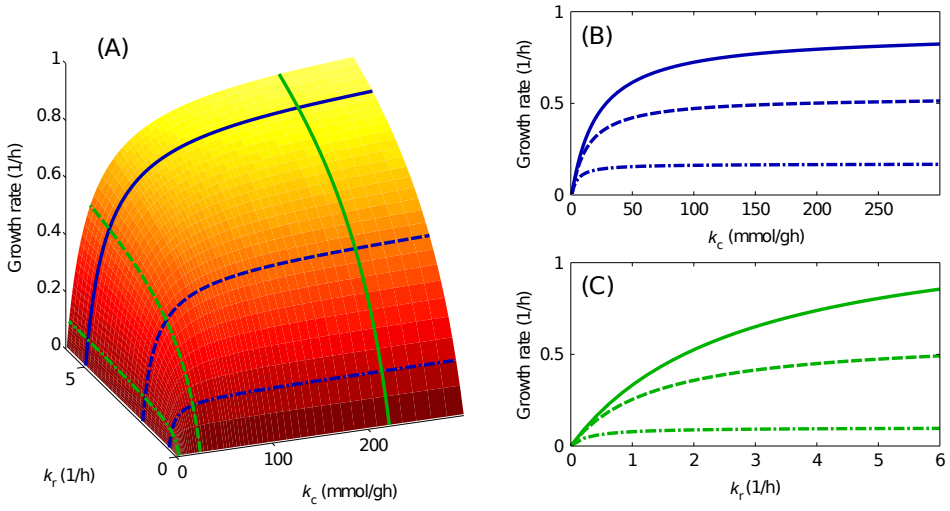

Figure B: (A) Growth rate of CAFBA solutions (minimal glucose medium, homogeneous case using $w_E = 8.3 \times 10^{-4}$ g_{DW}h/mmol) as a function of the two parameters $k_c = 1/w_C$ (*nutritional quality*) and $k_r = 1/w_R$ (*translational capacity*). Growth rate is a continuous function of both k_c and k_r, while acetate excretion presents discontinous transitions at different k_c values. Growth rate can be approximated as a Michaelis–Menten function of k_c and k_r, as described in detail in Note D. (B) Growth rate plotted as a function of k_c for three fixed values of k_r. These lines correspond to growth rates obtained in C–limitation for different, fixed, amounts of translation limiting antibiotics. The lines are also shown in panel (A) with the same colors and line style. (C) Same as panel (B), but plotting growth rate as a function of k_r for fixed k_c. In this case the lines represent the growth rates obtained in R-limitaiton for different carbon nutrient qualities.

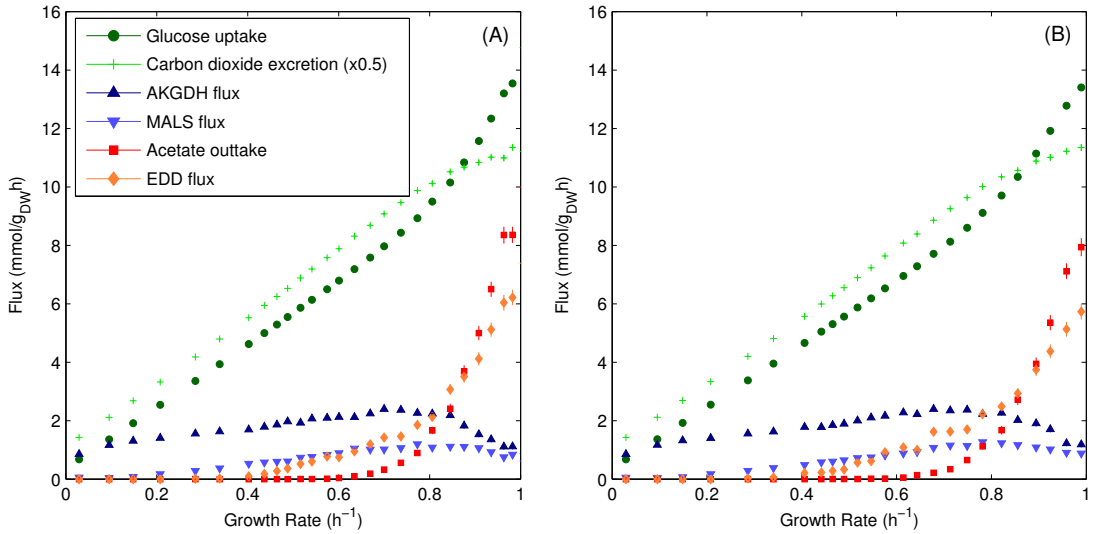

Figure C: Here we compare two sets of CAFBA solutions (500 samples per each value of w_C) computed using different distributions for the E–sector weights w_i. Panel (A): $\log_{10} w_i$ is extracted uniformly in an interval $\log_{10} w_{\min} \leq \log_{10} w \leq \log_{10} w_{\max}$, with $\delta = \log_{10} w_{\max} - \log_{10} w_{\min} = 1$, independently for each i. Note that the variance of this distribution is $\delta^2/12 = 1/12$. Panel (B): the E–sector weights w_i are independently extracted from a lognormal distribution with variance $1/12$, the same as the previous case. In both cases, the average values of the distribution have been tuned such that $\langle \lambda \rangle = 1/h$ when $w_C = 0$. The two distributions yield equivalent results.

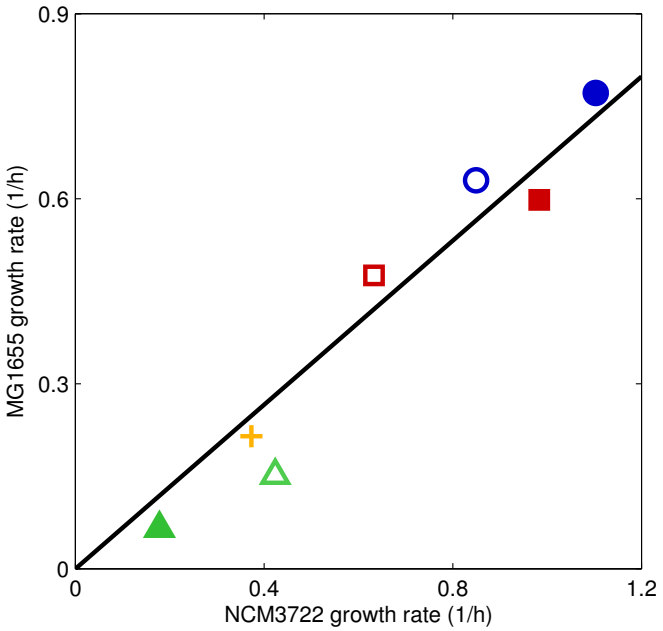

Figure D: Growth rates for *E. coli* K-12 strains NCM3722 and MG1655 in batch cultures at 37°C with vigorous shaking. N^-C^- minimal medum (see Ref. [16]) was supplemented with the following carbon and nitrogen sources (all in saturating amounts): acetate and NH_4Cl (+), lactose and NH_4Cl (■), glycerol and NH_4Cl (□), glucose-6P, gluconate and NH_4Cl (•), glucose and NH_4Cl (○), glucose and arginine (▲), glucose and aspartate (△). The best-fit line $\lambda_{MG} = s\lambda_{NCM}$ is shown in the figure, where $s = 0.6652 \sim 2/3$ is the best fit value for the slope.

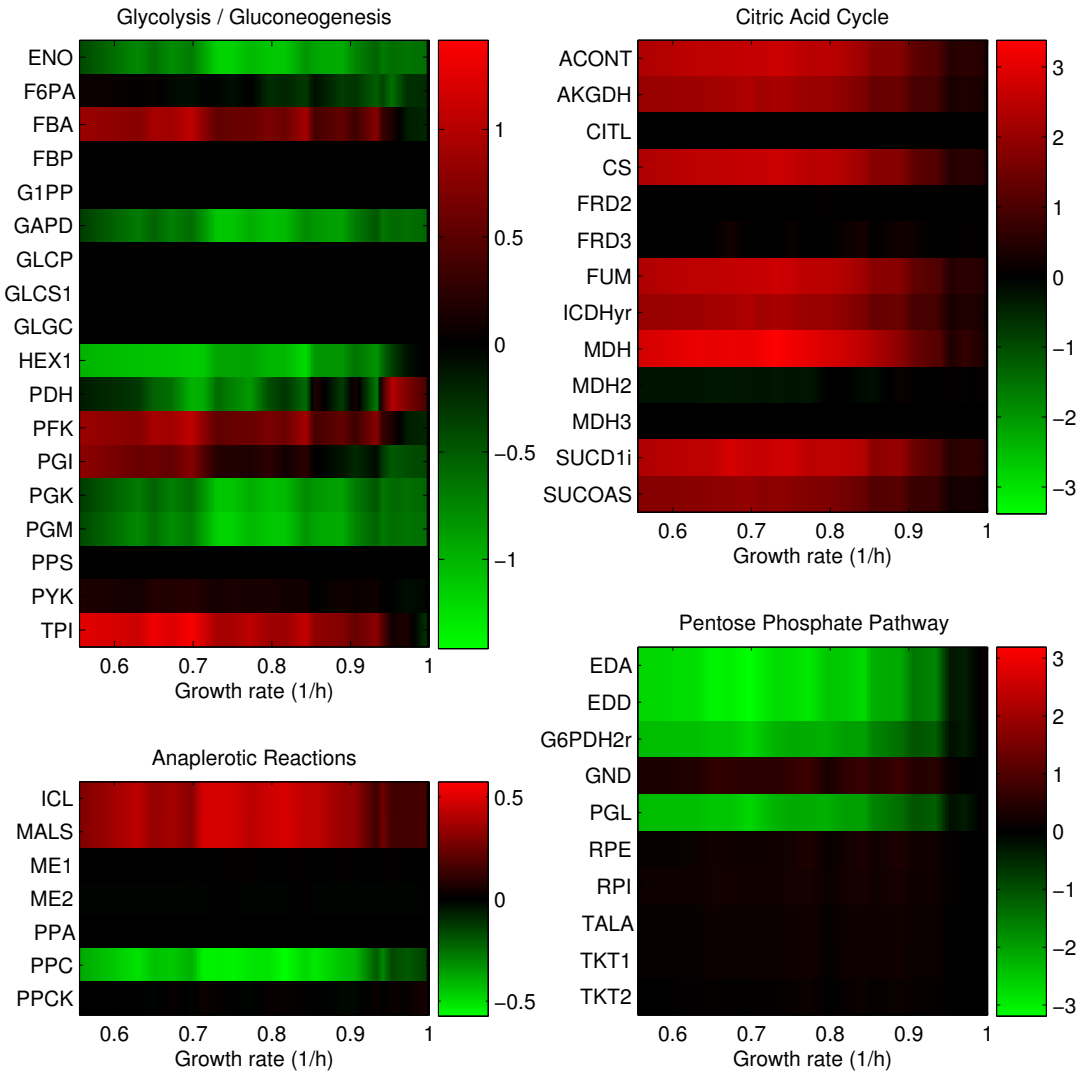

Figure E: Flux differences Δv (in mmol/g_{DW}h units) for the main catabolic pathways in glucose minimal substrate. The flux differences are computed from the average fluxes $\langle v_i \rangle$ and growth rates $\langle \lambda \rangle$ (200 samples for each value of w_C) as $\Delta v_i = \langle v_i \rangle - v_i^{\rm ref} = \langle v_i \rangle - \langle v_i \rangle (\lambda_{\rm max}) \cdot (\lambda / \lambda_{\rm max})$, so that Δv_i is zero at the maximum growth rate $\lambda_{\rm max} = 1/h$. Δv_i is larger than zero (shades of red) if the flux $\langle v_i \rangle$ is larger than the reference flux $v_i^{\rm ref} \propto \lambda$ upon carbon limitation, suggesting an upregulation of the corresponding enzymes.

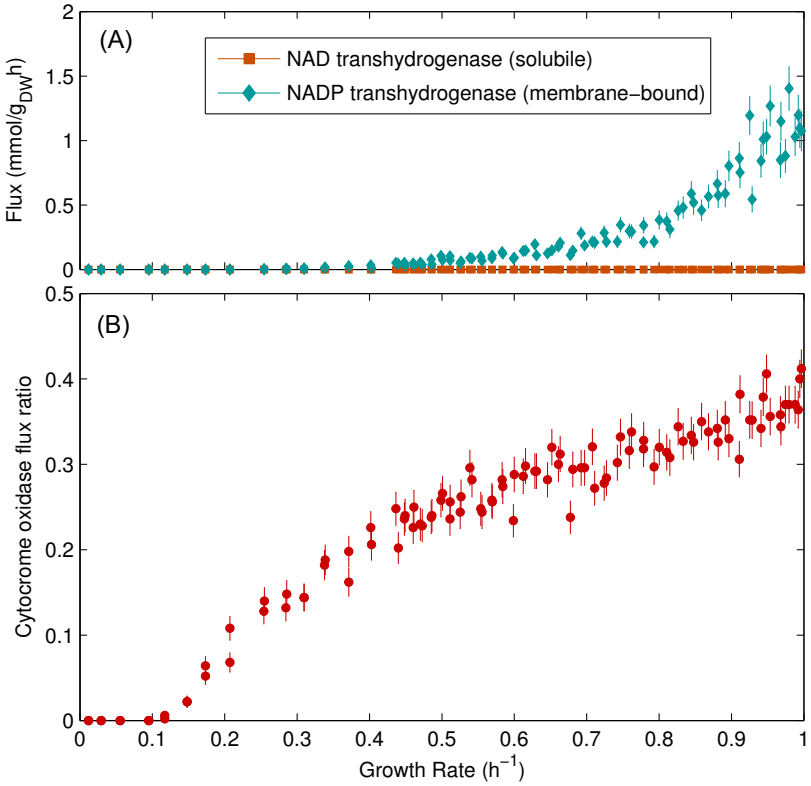

Figure F: (A): The *iJR*904 *E. coli* model contains two distinct NAD(P)H transhydrogenase reactions, whose labels in the model are NADTRHD (NAD transhydrogenase) and THD2 (energy-dependent, membrane-bound, NADP transhydrogenase). The two enzymes are found to be differently regulated, depending on the redox state of the cell [25]. CAFBA solutions show an activation of the THD2 flux at high growth rates, in agreement with experiments. (B): The *iJR*904 *E. coli* model contains two distinct ubiquinol oxidase reactions, CYTBD (*bd*–I enzyme) and CYTBO3 (bo_3 enzyme). The two reactions differ in the proton stoichiometry, as CYTBO3 generates a larger proton–motive force. The ratio $v_{BD}/(v_{BD} + v_{BO3})$ is shown as a function of growth rate. At low growth rates, only the CYTBO3 reaction is active, while the fluxes of the two reactions are comparable at large growth rates. In both panels we show average fluxes obtained from 1000 independent realizations of the weights w_i for each value of w_C in glucose minimal medium.

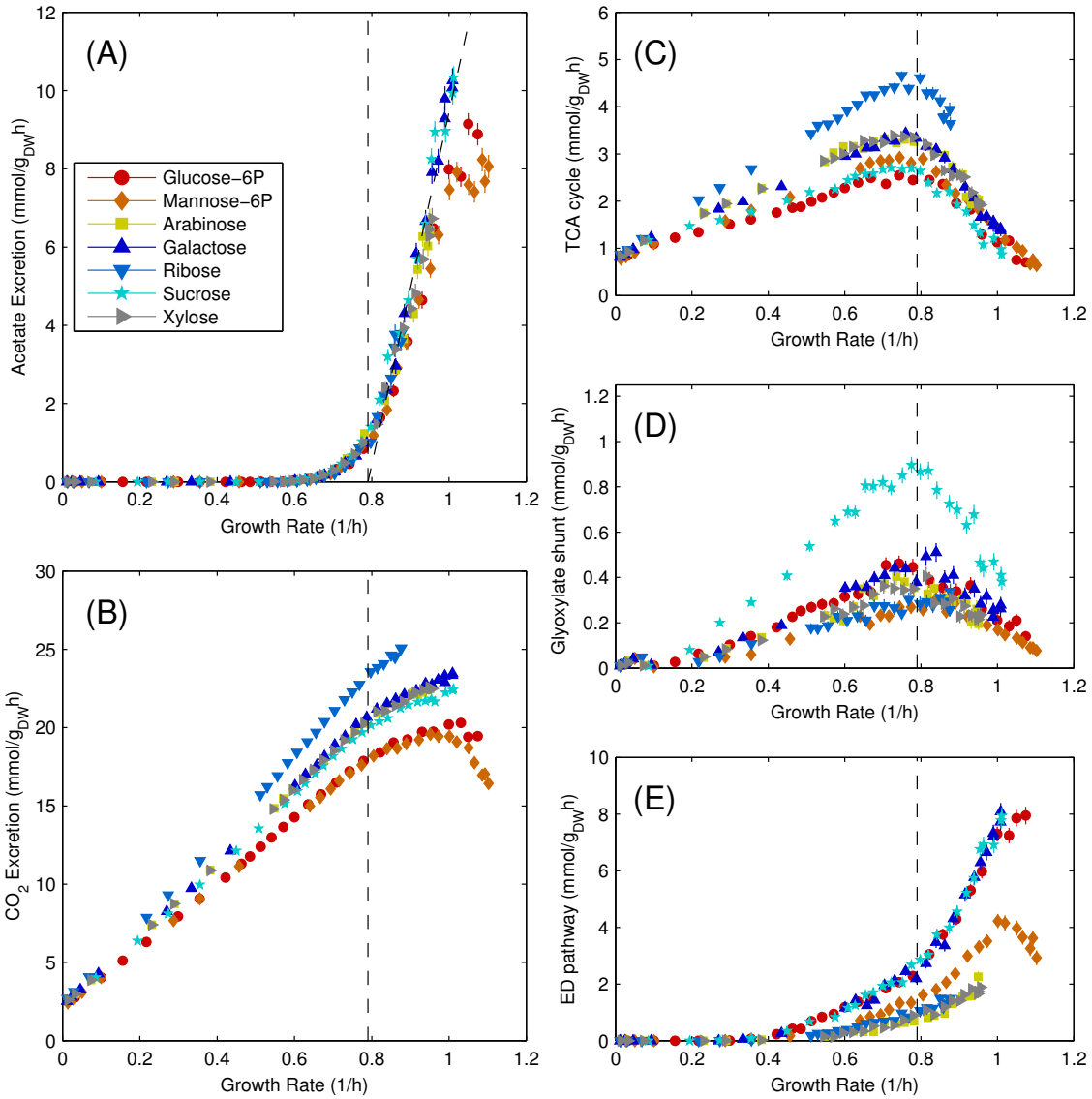

Figure G: CAFBA solutions for seven different glycolitic carbon sources (glucose-6P, mannose-6P, arabinose, galactose, ribose, sucrose, xylose). Acetate excretion rate is consistent for all carbon sources, with slight deviations in the case of phosphorylated carbon sources. The flux through the ED pathway is also heterogeneous, although showing similar trends from carbon to carbon. In all panels the values $\langle w \rangle = 8.8 \times 10^{-4}$ $\mathrm{g_{DW}h/mmol}$ and $\delta = 1$ are used. The averages are computed using 500 samples for each value of w_C.

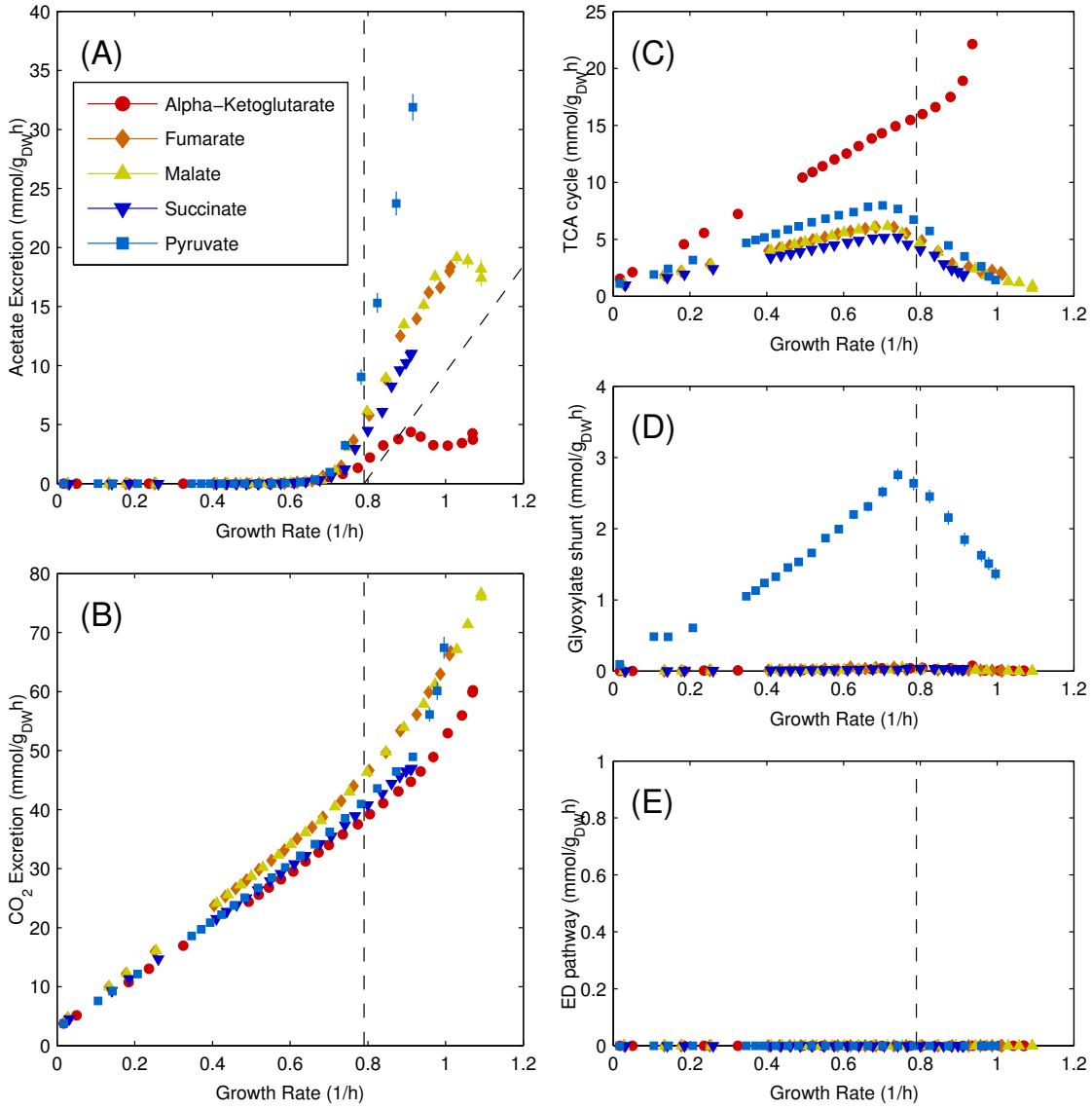

Figure H: CAFBA solutions for five different TCA carbon sources (α-ketoglutarate, fumarate, malate, succinate, pyruvate). Carbon dioxide production is much higher for these non-glycolytic carbon sources, although acetate excretion is still present for growth rates larger than $\lambda_{ac} = 0.79/\mathrm{h}$. In all panels the values $\langle w \rangle = 8.8 \times 10^{-4}$ $\mathrm{g_{DW}h/mmol}$ and $\delta = 1$ are used. The averages are computed using 500 samples for each value of w_C.

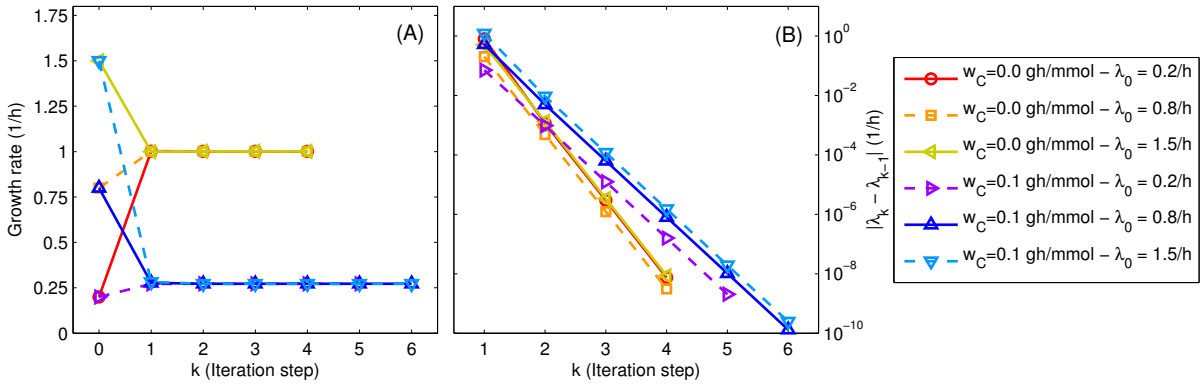
(A)
(B)
Growth rate (1/h)
k (Iteration step)
k (Iteration step)
$|\lambda_k - \lambda_{k-1}|$ (1/h)
w_C=0.0 gh/mmol – λ_0 = 0.2/h
w_C=0.0 gh/mmol – λ_0 = 0.8/h
w_C=0.0 gh/mmol – λ_0 = 1.5/h
w_C=0.1 gh/mmol – λ_0 = 0.2/h
w_C=0.1 gh/mmol – λ_0 = 0.8/h
w_C=0.1 gh/mmol – λ_0 = 1.5/h

Figure I: Growth-rate dependent biomass composition can be handled in CAFBA (and also in standard FBA) by means of an iterative procedure, in which the growth rate λ_k at step k is obtained by computing the optimal CAFBA solution using the biomass composition obtained at the previous step, $\beta(\lambda_{k-1})$. (A): Growth rate λ_k at each step k of the iterative procedure, for different values of w_C and the initial growth rate guess λ_0. (B): differences between growth rates at two consecutive steps (same as panel A). We stopped the algorithm when $|\lambda_k - \lambda_{k-1}| < 10^{-8}$/h, even if thresholds as large as 10^{-4}/h can be used in practice.

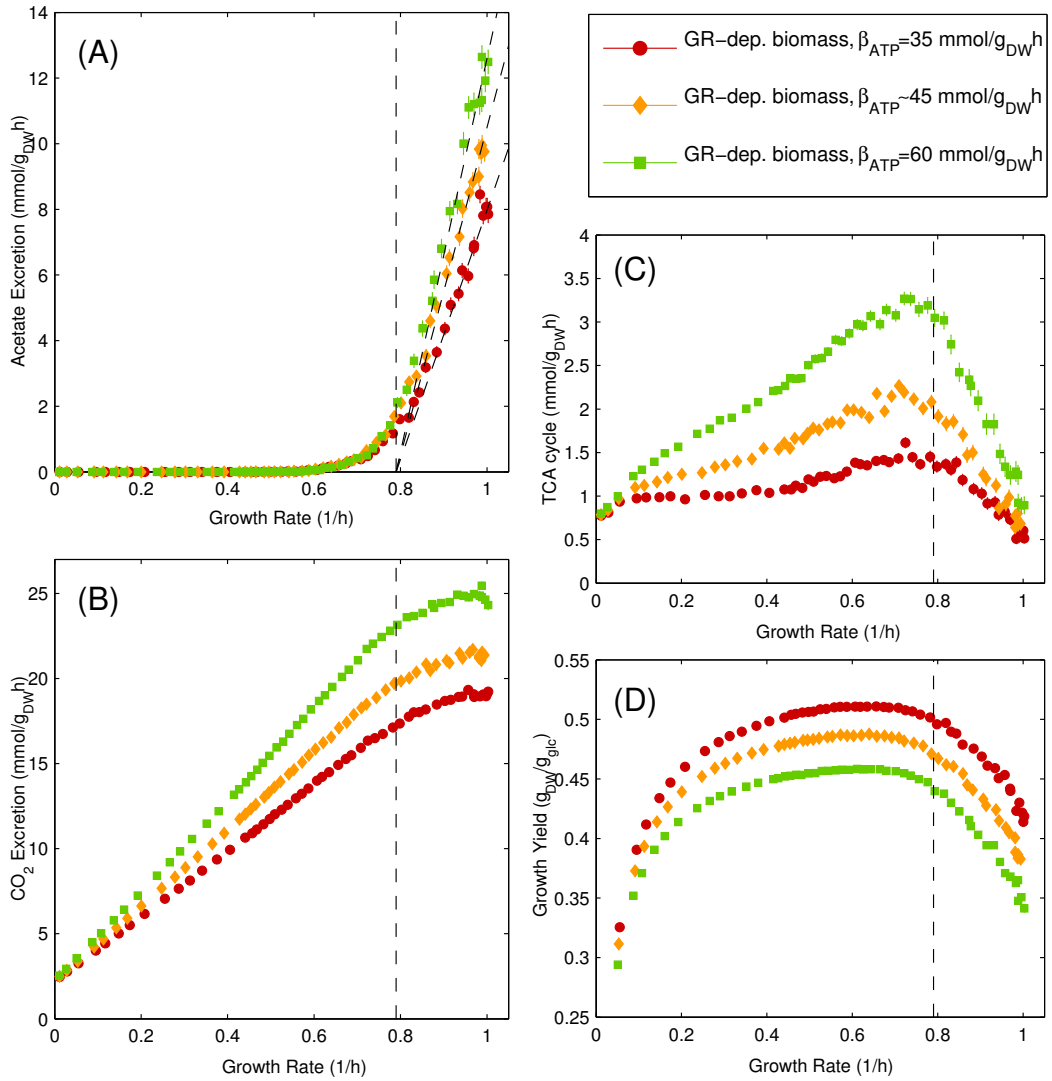

Figure J: As in Fig. 6, we show here fluxes and growth yields obtained by CAFBA in glucose minimal medium with variable biomass composition for three different growth-dependent ATP hydrolysis rates: 35, 45.5608 (as in the *iJR*904 *E. coli* model) and 60 mmol ATP/g_{DW}. The panels show (A) acetate excretion, (B) carbon dioxide excretion, (C) TCA (AKG dehydrogenase) flux, (D) growth yield. In this case, however, the value of $\langle w \rangle$ was tuned as to ensure that the average maximum growth rate is 1/h. This time the slope of acetate excretion flux depends on the growth-rate dependent ATP hydrolysis rate, β_{ATP}, attaining the values 60, 50 or 38 mmol/g_{DW}. However, the x–intercept is independent on β_{ATP}, being $\lambda_{ac} = 0.79$/h in all cases. We used $\langle w \rangle = 9.9 \times 10^{-4}$ g_{DW}h/mmol for $\beta_{ATP} = 35$ $mmol_{ATP}/g_{DW}$, $\langle w \rangle = 9.2 \times 10^{-4}$ g_{DW}h/mmol for $\beta_{ATP} = 45.5608$ $mmol_{ATP}/g_{DW}$, and $\langle w \rangle = 8.2 \times 10^{-4}$ g_{DW}h/mmol for $\beta_{ATP} = 60$ $mmol_{ATP}/g_{DW}$, while in all cases $w_C \geq \langle w \rangle$ and $w_{max}/w_{min} = 10$ (i.e. $\delta = 1$).

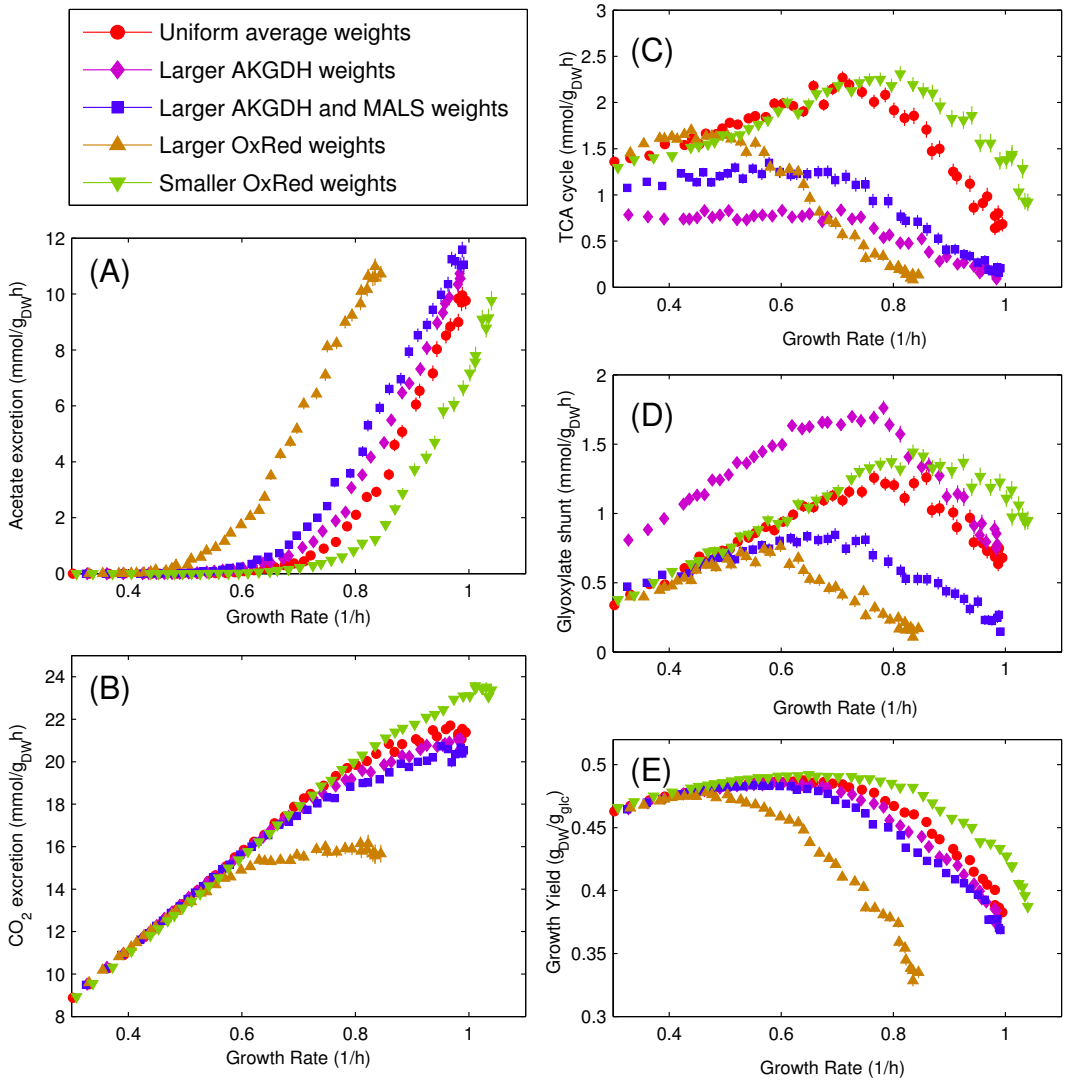

Figure K: Fluxes and growth yields obtained by CAFBA in glucose minimal medium with variable biomass composition for different fine-tunings of single weights. (A) Acetate excretion, (B) carbon dioxide excretion, (C) TCA flux, (D) glyoxylate shunt flux and (E) growth yield. Instead of extracting all weights of the E-sector from the same probability distribution, we used a different average value for single reactions, while keeping the average weight for all other reactions to the value $\langle w \rangle = 9.2 \times 10^{-4}$ $g_{DW}h/mmol$. Red dots (●): all reactions have the same average weight. Purple diamonds (♦): αKG–dehydrogenase weight is multiplied by a factor 5; Blue squares (■): both αKG–dehydrogenase and malate synthase weights have been multiplied by 5; Up–pointing gold triangles (▲): Oxidative phosphorilation reactions (ubiquinol oxidases) weights have been multiplied by 5; Down–pointing green triangles (▼): Oxidative phosphorilation reactions weights have been divided by 5.

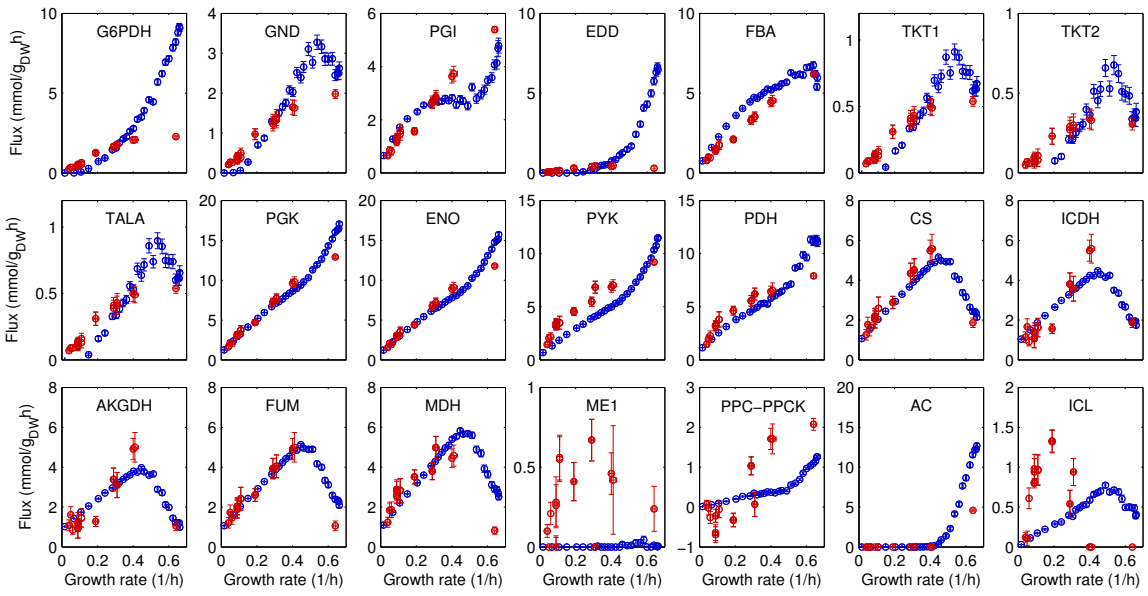

Figure L: Comparison between CAFBA fluxes (blue markers) and experimental fluxes for the *E. coli* MG1655 strain (red markers). All data are derived from chemostat experiments with glucose minimal medium [26] except for the points at $\lambda = 0.64$/h, obtained from batch culture experiments [27]. To match the low growth yield found in [26] (see Fig. 3B therein), we set the ATP maintenance flux at $v_{ATPM} = 9$ mmol ATP/g_{DW}h and the growth-dependent ATP hydrolysis rate at $\beta_{ATP} = 90$ $mmol_{ATP}/g_{DW}$. Correspondingly, the average weight of the E-sector was set to $\langle w \rangle = 1.15 \cdot 10^{-3}$ g_{DW}h/mmol in order to keep the maximum growth rate close 0.7/h, consistently with data. CAFBA obtains a good agreement for most of the fluxes. The qualitative behaviour of the flux through the glyoxylate shunt is captured, whereas the largest discrepancy is found for the ED pathway (G6PDH and EDD fluxes). Note that the optimal CAFBA flux through this pathway, which is computed assuming growth on a single carbon source, depends strongly on the specific substrate (see Fig. 4 in the Main Text). However, it is unlikely that metabolic fluxes *in vivo* are optimized for growth on a single carbon source.

Supplementary References

1. Benyamini T, Folger O, Ruppin E, Shlomi T (2010) Method flux balance analysis accounting for metabolite dilution. *Genome Biol* 11(4):R43.

2. Boer VM, Crutchfield CA, Bradley PH, Botstein D, Rabinowitz JD (2010) Growth-limiting intracellular metabolites in yeast growing under diverse nutrient limitations. *Mol Biol Cell* 21(1):198–211.

3. Valgepea K, Adamberg K, Seiman A, Vilu R (2013) Escherichia coli achieves faster growth by increasing catalytic and translation rates of proteins. *Mol Biosyst* 9(9):2344–2358.

4. Hui S et al. (2015) Quantitative proteomic analysis reveals a simple strategy of global resource allocation in bacteria. *Molecular systems biology* 11(2).

5. Chubukov V, Gerosa L, Kochanowski K, Sauer U (2014) Coordination of microbial metabolism. *Nature Reviews Microbiology* 12(5):327–340.

6. Ogasawara H, Ishida Y, Yamada K, Yamamoto K, Ishihama A (2007) Pdhr (pyruvate dehydrogenase complex regulator) controls the respiratory electron transport system in escherichia coli. *Journal of bacteriology* 189(15):5534–5541.

7. Beg Q et al. (2007) Intracellular crowding defines the mode and sequence of substrate uptake by Escherichia coli and constrains its metabolic activity. *Proc Natl Acad Sci USA* 104(31):12663–12668.

8. Vazquez A et al. (2008) Impact of the solvent capacity constraint on E. coli metabolism. *BMC Syst Biol* 2(1):7.

9. Lerman JA, Chang RL, Hyduke DR, Palsson BØ, et al. (2013) Genome-scale models of metabolism and gene expression extend and refine growth phenotype prediction. *Mol Syst Biol* 9(1).

10. Vemuri G, Altman E, Sangurdekar D, Khodursky A, Eiteman M (2006) Overflow metabolism in escherichia coli during steady-state growth: transcriptional regulation and effect of the redox ratio. *Applied and environmental microbiology* 72(5):3653–3661.

11. Valgepea K et al. (2010) Systems biology approach reveals that overflow metabolism of acetate in escherichia coli is triggered by carbon catabolite repression of acetyl-coa synthetase. *BMC Syst Biol* 4(1):166.

12. Basan M et al. (2015) Efficient allocation of proteomic resources for energy metabolism results in acetate overflow. *Nature* 528:99–104.

13. Rao N, Torriani A (1990) Molecular aspects of phosphate transport in Escherichia coli. *Molecular Microbiology* 4:1083–1090.

14. Scott M, Gunderson CW, Mateescu EM, Zhang Z, Hwa T (2010) Interdependence of cell growth and gene expression: origins and consequences. *Science* 330(6007):1099–1102.

15. Schellenberger J, Park JO, Conrad TM, Palsson BØ (2010) Bigg: a biochemical genetic and genomic knowledgebase of large scale metabolic reconstructions. *BMC bioinformatics* 11(1):213.

16. You C et al. (2013) Coordination of bacterial proteome with metabolism by cyclic AMP signalling. *Nature* 500(7462):301–306.

17. Monod J (1949) The growth of bacterial cultures. *Annual Reviews in Microbiology* 3(1):371–394.

18. Schaechter M, Maaløe O, Kjeldgaard N (1958) Dependency on medium and temperature of cell size and chemical composition during balanced growth of salmonella typhimurium. *J Gen Microbiol* 19(3):592–606.

19. O'Brien EJ, Lerman JA, Chang RL, Hyduke DR, Palsson BØ (2013) Genome–scale models of metabolism and gene expression extend and refine growth phenotype prediction. *Mol Syst Biol* 9(1).

20. Taymaz-Nikerel H, Borujeni AE, Verheijen PJ, Heijnen JJ, van Gulik WM (2010) Genome-derived minimal metabolic models for escherichia coli mg1655 with estimated in vivo respiratory atp stoichiometry. *Biotechnol Bioeng* 107(2):369–381.

21. Pramanik J, Keasling J (1997) Stoichiometric model of *Escherichia coli* metabolism: incorporation of growth–rate dependent biomass composition and mechanistic energy requirements. *Biotechnology and bioengineering* 56(4):398–421.

22. Reed JL, Vo TD, Schilling CH, Palsson BO, et al. (2003) An expanded genome–scale model of *Escherichia coli* K–12 (*iJR*904 GSM/GPR). *Genome Biol* 4(9):R54.

23. Feist, AM ea (2007) A genome-scale metabolic reconstruction for Escherichia coli K-12 MG1655 that accounts for 1260 ORFs and thermodynamic information. *Mol Syst Biol* 3(1).

24. Orth JD et al. (2011) A comprehensive genome-scale reconstruction of *escherichia coli* metabolism. *Mol Syst Biol* 7(1).

25. Sauer U, Canonaco F, Heri S, Perrenoud A, Fischer E (2004) The soluble and membrane–bound transhydrogenases udha and pntab have divergent functions in nadph metabolism of escherichia coli. *J Biological Chem* 279(8):6613–6619.

26. Nanchen A, Schicker A, Sauer U (2006) Nonlinear dependency of intracellular fluxes on growth rate in miniaturized continuous cultures of Escherichia coli. *Appl Environ Microbiol* 72:1164–1172.

27. Perrenoud A, Sauer U (2005) Impact of global transcriptional regulation by ArcA, ArcB, Cra, Crp, Cya, Fnr, and Mlc on glucose catabolism in Escherichia coli. *Journal of Bacteriology* 187:3171–3179.